الجمهورية الجزائرية الديمقراطية الشعبية

People's Democratic Republic of Algeria

وزارة التعليم العالي و البحث العلمي

Ministry of Higher Education and Scientific Research

University MUSTAPHA Stambouli

Mascara

جامعة مصطفى أسطمبولي

معسكر

Faculty of Exact Sciences

Department of Physics

DOCTORATE THESIS OF 3ème cycle

Specialty: Physic

Option: Materials for renewable energy

Contribution to the study of the optoelectronic properties of chalcogenide-based materials for solar cells application

Presented by: Mouacher Mohammed Ryad

On: 17/05/2023

In front of the jury:

President	**S.BENTATA**	***Prof***	**University of Mascara**
Reviewer	**R.KHENATA**	***Prof***	**University of Mascara**
Reviewer	**M.ELKEURTI**	***Prof***	**University of Saida**
Reviewer	**T.DJAAFRI**	***Prof***	**University of Saida**
Supervisor	**T.SEDDIK**	***MCA***	**University of Mascara**
Co-Supervisor	**A.BELFEDAL**	***Prof***	**University of Mascara**

Academic Year: 2022-2023


بسم الله الرحمن الرحيم

Summary

This work presents a contribution to the study of the thallium substitution effect on structural, electronic, and optical properties of chalcopyrite-type materials $AgGaS_2$ and $AgGaSe_2$.

To predict these different properties, we performed simulations by applying the Linearized Augmented Planar Wave method with local orbitals (FP-APW+lo) which is based on density functional theory (DFT) using the generalized gradient approximation (WC-GGA) to treat the exchange and correlation term.

The computed band gap energy of pure $AgGaS_2$ and $AgGaSe_2$ is about 2.59 eV and 1.85eV using Tran-Blaha (TB)-modified Becke Johnson (mBJ) exchange potential, which is in good accord with experimental measurements. Those band gap values were observed to decrease when Tl is substituted into Ga site, respectively, for 25%, 50%, and 75% concentrations. This investigation establishes that Tl substitution increases both hole and electron carrier mobility of the pure $AgGaS_2$ and $AgGaSe_2$ compounds. By analyzing the band alignment diagram, it was observed that the Tl substitution increases the valence band offset (VBO) and decreases the conduction band offset (CBO), which can lead to the improvement of open-circuit voltage V_{OC}. Moreover, the optical analysis reveals that Tl substitution enhances the optical properties of $AgGaS_2$ and $AgGaSe_2$ by reducing the transparency and improving the refractive index and the absorption in the visible light region.

Based on obtained results, it is predicted that the band gap and the optical properties of the $AgGaS_2$ and $AgGaSe_2$ chalcopyrite can be effectively tuned by Tl substitution over the Ga sites, making $AgGa_{1-x}Tl_xS_2$ and $AgGa_{1-x}Tl_xSe_2$ alloys promising candidates for optoelectronic and photovoltaic applications.

Keywords: FP-LAPW; Electronic properties; Optical properties; Band alignment; Photovoltaic applications.

Résumé

Ce travail présente une contribution à l'étude de l'effet de la substitution du thallium sur les propriétés structurelles, électroniques et optiques des matériaux de type chalcopyrite $AgGaS_2$ et $AgGaSe_2$.

Pour déterminer ces différentes propriétés, nous avons effectué des simulations en appliquant la méthode Linearized Augmented Plan Wave avec des orbitales locales (FP-APW+lo) qui est basée sur la théorie de la fonction de la densité (DFT) en utilisant l'approximation du gradient généralisé (WC-GGA) pour traiter le terme d'échange et de corrélation.

L'énergie de la bande interdite calculée pour l'$AgGaS_2$ et l'$AgGaSe_2$ dans leur état pur est d'environ 2,59 eV et 1,85 eV respectivement en utilisant le potentiel d'échange Tran-Blaha (TB) - Becke Johnson (mBJ) modifié, ce qui est en bon accord avec les mesures expérimentales. On a remarqué que ces valeurs de bande interdite diminuent lorsque Tl est substitué dans le site Ga, respectivement pour des concentrations de 25%, 50% et 75%. Cette étude montre que la substitution de Tl augmente la mobilité des trous et des porteurs d'électrons des composés $AgGaS_2$ et $AgGaSe_2$ purs. En analysant le diagramme d'alignement des bandes, il a été constaté que la substitution de Tl augmente le décalage de la bande de valence (VBO) et diminue le décalage de la bande de conduction (CBO), ce qui peut conduire à l'amélioration de la tension en circuit ouvert V_{OC}. De plus, l'analyse optique révèle que la substitution de Tl améliore les propriétés optiques d'$AgGaS_2$ et $AgGaSe_2$ en réduisant la transparence et en améliorant l'indice de réfraction et l'absorption dans la région de la lumière visible.

Sur la base des résultats obtenus, il est prévu que la bande interdite et les propriétés optiques de la chalcopyrite $AgGaS_2$ et $AgGaSe_2$ peuvent être efficacement ajustées par la substitution de Tl sur les sites Ga, ce qui fait des alliages $AgGa_{1-x}Tl_xS_2$ et $AgGa_{1-x}Tl_xSe_2$ des candidats prometteurs pour des applications optoélectroniques et photovoltaïques.

Mots-clés : FP-LAPW ; propriétés électroniques ; propriétés optiques ; alignement de bande ; applications photovoltaïques.

ملخص

يقدم هذا العمل مساهمة في دراسة تأثير استبدال الثاليوم على الخصائص الهيكلية والإلكترونية والبصرية للمواد من نوع الكالكوبيريت t و $AgGaSe_2$.

للتنبؤ بهذه الخصائص المختلفة ، أجرينا عمليات محاكاة من خلال تطبيق طريقة الموجة المستوية الخطية المعززة مع المدارات المحلية (FP-APW lo) والتي تستند إلى نظرية الكثافة الوظيفي (DFT) باستخدام تقريب التدرج المعمم (WC-GGA)لمعالجة مصطلح التبادل والارتباط، حيث يتم تنفيذ حزمة هذه الطريقة في التعليمات البرمجية WIEN2K.

تبلغ طاقة فجوة النطاق المحسوبة لـ $AgGaS_2$ و $AgGaSe_2$ النقي حوالي 2.59eV و1.85 eV باستخدام Tran-Blaha - تعديل Becke Johnson mBJ إمكانية التبادل, وهو يتفق بشكل جيد مع القياسات التجريبية. ولوحظ أن قيم فجوة النطاق هذه تنخفض إلى وقت استبدال Tl في موقع Ga ، على التوالي ، لتركيزات 25٪ و 50٪ و 75. إلى جانب ذلك ، تم أيضًا حساب فجوة النطاق $AgTlS_2$ ووجدت أنها 0.61eV. يثبت هذا التحقيق أن استبدال Tl يزيد من حركة الثقب وحامل الإلكترون لمركبات $AgGaS_2$ و $AgGaSe_2$ النقية. من خلال تحليل مخطط محاذاة النطاق ، لوحظ أن استبدال Tl يزيد من إزاحة نطاق التكافؤ (VBO) ويقلل من إزاحة نطاق التوصيل (CBO), مما قد يؤدي إلى تحسين الجهد الكهربائي للدائرة المفتوحة. علاوة على ذلك ، يكشف التحليل البصري أن استبدال Tl يعزز الخصائص البصرية لـ $AgGaS_2$ و $AgGaSe_2$ عن طريق تقليل الشفافية وتحسين معامل الانكسار والامتصاص في منطقة الضوء المرئي.

استنادًا إلى النتائج التي تم الحصول عليها ، من المتوقع أن يتم ضبط فجوة النطاق والخصائص البصرية لـ $AgGaS_2$ و $AgGaSe_2$ بشكل فعال عن طريق استبدال Tl عبر مواقع Ga, جعل سبائك $AgGa_{1-x}Tl_xS_2$ و $AgGa_{1-x}Tl_xSe_2$ مرشحين واعدين للتطبيقات الإلكترونية الضوئية والخلايا الكهروضوئية.

الكلمات الرئيسية: الخصائص الإلكترونية. الخصائص البصرية ؛ التطبيقات الكهروضوئية ؛ نهج المبادئ الأولى ؛ Wien2k

Credits

***F**irst of all, I thank the Lord Almighty for giving me the courage, will and patience to complete this work.*

***I** would like to express my sincere gratitude to **Mr. Seddik Taieb**, MCA at University of Mascara, for leading my researches and for the faith he has shown in me throughout the years of my doctoral studies and for all his advices and constructive remarks. His impact has been very fruitful both on a human and scientific level. Words won't express the room he has taken in my heart so a massive thanks for him.*

***I** also address my warm thanks to my co-director of thesis **Mr. BELFEDAL Abdelkader**, Professor at university of Mascara, for his constant attention to my research work, for his judicious councils and his listening which were prevailing for the good success of this work.*

***I** would like to express my warmest thanks to **Mr.BENTATA Samir**, Professor at the University of Mascara, for the honour he has bestowed on me by chairing the jury of this thesis.*

***I** would like to express my gratitude to **Mr.KHENATA Rabah**, Professor at the University of Mascara, **Mr.ELKEURTI Mohammed**, Professor at the University of Saida, **Mr. DJAAFRI Tayeb**, Professor at the University of Saida, for their approval of my work and their honourable membership of my thesis jury.*

*I thank **Mr. KHENATA Rabah**, Professor at University of Mascara and director of the laboratory LPQ3M of the University of Mascara for welcoming me in his laboratory*

***I** would like to thank Mrs. **F.Dahou** my beloved teacher and my first thesis supervisor who helped me through all my pathway Mrs. **Messekine.S** Mrs. **A.Siad** Mrs. **F.Dahou** Mrs. **H.Riane** Mrs. **Bouhani.H** for their care and tolerance their assistance throughout my entire university career.*

***I** would also like to thank my dear friends **M.Battouche**, **A.El goutni**, **B.Rezzini**, **K.Djellid**, **Fouad D.Hamidi**, **M.Khenata**, **K.Bettir** for their daily support and help as well as the good atmosphere they provide every day in the laboratory.*

***I**n the hope that no one will be forgotten, I would like to thank all those who have contributed in any way to the realization of this thesis.*

Dedication

I would like to warmly thank my mom **Mehalhal Zouina** *who has surrounded me with love, affection, never stopped supporting me and doing everything for my success, and my father* **Mouacher Noureddine** *who made me the person I am today, may God watch over them and preserve them.*

I also thank my elder sister **Mouacher Leila** *and I wish her all the best in her emotional and professional life.*

I would like to thank my fiancée **Merzoug Bouchra** *for her endless patience, encouragement and confidence, as well as her moral support and advice throughout my work.*

I dedicate this work to my daytime friend **Mahi Ali** *and all my football teammates.*

In order not to forget anyone, I would like to thank all those who have contributed in any way to the realisation of this thesis.

Mouacher Ryad

Index

Chapter II: Overview on chalcopyrite family

Chapter IV: Investigation of the structural and optoelectronic properties of the compound $AgGa_{x-1}Tl_xSe_2$

LIST OF FIGURES

LIST OF TABLES

General introduction

To overcome the decline of fossil fuel sources and to fulfill the ever-increasing need for clean energy, the production of photovoltaic energy has grown in importance, as solar cells release no toxic gases. The current solar cell industry is mostly based on monocrystalline silicon or III-V semiconductors, which have proven extremely high efficiency **[1]**, but many low-cost solar cells are needed for general and wider applications. Therefore, designing and developing new solar cell materials with desired electronic, optical, and photovoltaic properties is an important step. For example, inorganic materials based on transition metal and chalcogenides or halide materials have recently been investigated which show promising optoelectronic properties **[2,3]**. Besides, mixed organic-inorganic materials have also been suggested as promising candidates for solar cell applications due to their ideal optical properties as well as relatively low-cost preparation methods **[4–6]**.

Among these materials the chalcopyrite-based compounds of the general formula I-III-VI2, where I is usually copper (Cu) or silver (Ag), have been receiving high attention in the last decade due to its usage in detectors, light-emitting diodes (LEDs), thermoelectric, photocatalysts, nonlinear optics (NLO) applications and solar energy conversion **[7–12]**. The major characteristic of chalcopyrite semiconductors is that they possess unique electronic and optical properties, direct band gap, transparent behavior against visible and infrared radiation, a high absorption coefficient and a lifetime in outer space longer compared to that of Si and III-V compounds **[13]**.

Recently the copper (Cu-III–VI_2) based chalcopyrites have proven their efficiency for solar cell applications. For example the $CuGaSe_2$ shows efficiency of about 11.2% **[8]** while $CuInSe_2$ realizes 14.5% efficiency **[14]** via a tandem cell of ZnO/CdS/$CuInSe_2$. However, $Cu(InGa)Se_2$ (CIGS) have recorded the highest power conversion efficiency (PCE) of about 23.4% (cells), 17.4% (module) **[15–19]** which make it promising absorber materials for solar cell applications. Conversely, the silver (Ag-III–VI_2) based chalcopyrites receive much attention due to their suitability for non-linear optical and photonic applications **[20]**.

The $AgGaS_2$ and $AgGaSe_2$ are known as part of the chalcopyrite family with a direct band gap of about (2.48–2.75) eV for $AgGaS_2$ **[21–24]** and (1.86-1.90) eV for $AgGaSe_2$ **[21–24]** .Those compounds are used as commercial material for NLO applications due to its large NLO coefficient d_{36} = 39 p.m./V and excellent transparency in the mid-IR range (1–18 μm) **[25]**. Besides, the two materials were proposed as promising candidates for X-ray dosimetry **[26]**. However, its band gap values and weak absorption in the visible light region limit its use as absorber material for photovoltaic solar cells. Very recently, the best efficiency of 5.85 % was reported using $AgGaS_2$ **[27]** and 5.8 % using $AgGaSe_2$ as an absorbing layer **[28]**.

The main goal of the present work is to improve the optical and electronic properties of $AgGaS_2$ and $AgGaSe_2$ using band convergence strategy by substitution of Thallium (Tl) into the gallium (Ga) site in the $AgGaS_2$ and $AgGaSe_2$ compounds for the building of $AgGa_{1-x}Tl_xS_2$ and $AgGa_{1-x}Tl_xSe_2$ alloys. From an experimental and theoretical point of view, it has already been reported that tailoring the band gap values of $AgGaS_2$ and $AgGaSe_2$ leads to interesting optoelectronic and photocatalytic properties **[9, 29–31]**. The current work deals with the study of the structural, electronic, and optical properties of the Tl-doped $AgGaX_2$ (X = S, Se) chalcopyrite through the full potential augmented plane wave plus local orbital's method. This thesis manuscript is arranged in four chapters:

- **In the first chapter** we will briefly present an overview of the density functional density functional theory which we have used to study the properties of the chosen properties of selected materials.
- **The second chapter** gives an overview of the chalcopyrite family.
- **The third chapter** presents the structural electronic and optical properties of $AgGaS_2$ doped with Thallium.
- **The fourth chapter** will be devoted to the detailed study of the structural, optoelectronic properties of $AgGa_{1-x}Tl_xSe_2$ alloys.

We will end up this manuscript with a general conclusion on the different points discussed above and some perspectives.

Bibliography

[1] M.A. Green, K. Emery, Y. Hishikawa, W. Warta, Solar cell efficiency tables (version 36), Prog. Photovoltaics Res. Appl. 18 346–352 (2010).

[2] M. Buffiere, Dattatray S. Dhawale, F. El-Mellouhi, Chalcogenide materials and derivatives for photovoltaic applications, Energy Technol. 1900819 (2019).

[3] M. Faizan, S.H. Khan, H. Khachai, T. Seddik, S.B. Omran, R. Khenata, J. Xie, M.M. Al-Anazy, Electronic, optical, and thermoelectric properties of perovskite variants A2BX6: insight and design via first-principles calculations, Int. J. Energy Res. 45 (3) 4495–4507. (2021)

[4] A.N. Usoltsev, S.A. Adonin, A.S. Novikov, D.G. Samsonenko, M.N. Sokolova, V.P. Fedin, One dimensional polymeric polybromotellurates (IV): structural and theoretical insights into halogen···halogen contacts, CrystEngComm (2017).

[5] S.A. Adonin, M.A. Bondarenko, P.A. Abramov, A.S. Novikov, P.E. Plyusnin, M.N. Sokolov, V.P. Fedin, Bromo- and polybromoantimonates(V): structural and theoretical studies of hybrid halogen-rich halometalate frameworks, Chem. Eur. J. 24 10165 (2018).

[6] S.A. Adonin, I.D. Gorokh, A.S. Novikov, D.G. Samsonenko, P.E. Plyusnin, M.N. Sokolov, V.P. Fedin, Bromine-rich complexes of bismuth: experimental and theoretical studies, Dalton Trans. 47 2683–2689 (2018).

[7] S.F. Chichibu, T. Ohmori, N. Shibata, T. Koyama, T. Onuma, Greenish-white electroluminescence from p-type CuGaS2 heterojunction diodes using n-type ZnO as an electron injector, Appl. Phys. Lett. 85 4403 (2004).

[8] S. Ishizuka, A. Yamada, P.J. Fons, H. Shibata, S. Niki, Structural tuning of wide-gap chalcopyrite CuGaSe2 thin films and highly efficient solar cells: differences from narrow-gap Cu(In,Ga)Se2, Prog. Photovolt.22 821–829 (2014).

[9] J.S. Jang, P.H. Borse, J.S. Lee, S.H. Choi, H.G. Kim, Indium induced band gap tailoring in AgGa1_xInxS2 chalcopyrite structure for visible light photocatalysis, Chem. Phys. 128 154717 (2008).

[10] D. Lincota, J.F. Guillemolesa, S. Tauniera, D. Guimarda, J. Sicx-Kurdia, A. Chaumonta, O. Roussela, O. Ramdania, C. Huberta, J.P. Fauvarquea, N. Bodereaua, L. Parissia, P. Panheleuxa, P. Fanouillerea, N. Naghavia, P.P. Granda, M. Benfaraha, P. Mogensenb, O. Kerreca, Chalcopyrite Thin Film Solar Cells by Electro-Deposition Solar Energy, vol. 77, pp. 725–737 (2004).

[11] T. Plirdpring, K. Kurosaki, A. Kosuga, T. Day, S. Firdosy, V. Ravi, G.T. Snyder, A. Harnwunggmoung, A. Sugahara, Y. O-hishi, H. Muta, S. Yamanaka, Chalcopyrite CuGaTe2: a high-Efficiency bulk thermoelectric material, Adv. Mater.24 3622 (2012).

[12] P.C. Ricci, A. Anedda, R. Corpino, C.M. Carbonaro, M. Marceddu, I.M. Tiginyanu, V.V. Ursaki, Temperature dependence of the photoluminescence spectra in AgGaS2, J. Phys. Chem. Solid. 66 1950–1953 (2005).

[13] M.V. Yakushev, R.W. Martin, Semiconductor spectroscopy and devices. https://ssd.phys.strath.ac.uk/research-areas/chalcopyrites-for-solar-cells (2020).

[14] J.A.M. Abu Shama, S. Johnston, T. Moriarty, G. Teeter, K. Ramanathan, R. Noufi, Properties of ZnO/CdS/CuInSe2 solar cells with improved performance, Prog. Photovolt. 12 39–45 (2004).

[15] P. Chirila, F. Reinhard, P. Pianezzi, A.R. Bloesch, C. Uhl, L. Fella, D. Kranz, C. Keller, H. Gretener, D. Hagendorfer, R. Jaeger, S. Erni, S. Nishiwaki, S. Buecheler, A.N. Tiwari, Potassium-induced surface modification of Cu(In,Ga)Se2 thin films for high-efficiency solar cells, Nat. Mater. 12 1107–1111 (2013).

[16] M.A. Contreras, J. Tuttle, A. Gabor, A. Tennant, K. Ramanathan, S. Asher, A. Franz, J. Keane, L. Wang, R. Noufi, High efficiency Cu(In,Ga)Se2 based solar cells: processing of novel absorber structures, Sol. Energy Mater. Sol. Cells 119 296 (2013).

[17] A. Jager-Waldau, PV Status Report EUR 28817 EN, Publications Office of the European Union, Luxembourg, (2017).

[18] P. Reinhard, F. Pianezzi, L. Kranz, S. Nishiwaki, A. Chirila, S. Buecheler, A.N. Tiwari, Flexible Cu(In,Ga)Se2 solar cells with reduced absorber thickness, Prog. Photovoltaics Res. Appl. 23 281 (2015).

[19] Solar Frontier, Achieves world record thin-film solar cell efficiency of 23.35%. https://www.solar-frontier.com/eng/news/2019/0117press.html, (2019).

[20] P.C. Ricci, A. Anedda, R. Corpino, C.M. Carbonaro, M. Marceddu, I.M. Tiginyanu, V.V. Ursaki, Temperature dependence of the photoluminescence spectra in AgGaS2, J. Phys. Chem. Solid. 66 1950–1953 (2015).

[21] H.C. Hsu, H. Chen, S.Y. Kuo, C.S. Chang, W.F. Hsieh, Effect of annealing on the structural and optical properties of AgGaS2 thin films prepared by pulsed laser deposition, Thin Solid Films 419 237–241 (2002).

[22] H. Karaagac, M. Parlak, The investigation of structural, electrical, and optical properties of thermal evaporated AgGaS2 thin films, Thin Solid Films 519 2055–2061 (2011).

[23] J.L. Shay, J.H. Wernick, Ternary Chalcopyrite Semiconductors: Growth, Electronic Properties, and Applications, Pergamon Press, Oxford; New York, (1975).

[24] H. Xiao, J. Tahir-Kheli, W.A.Goddard, Accurate band gaps for semiconductors from density functional theory, Phys. Chem. Lett. 2 212–217 (2011).

[25] J.J. Zondy, D. Touahri, O. Acef, Absolute value of the d36 nonlinear coefficient of AgGaS2: prospect for a low-threshold doubly resonant oscillator-based 3:1 frequency divider, J. Opt. Soc. Am. B 14 (10) 2481–2497 (1997).

[26] M.M. Asadov, S.N. Mustafaeva, Xray dosimetry of an AgGaS2 single crystal, Bull. Russ. Acad. Sci. Phys. 1113–1117 (2015).

[27] M. Thirumoorthy, K. Ramesh, Materials Today: Proceedings Characteristics of pulse electrodeposited AgGaS2 thin films for photovoltaic application (2021).

[28] J. K. Larsen, O. Donzel-Gargand, K. V. Sopiha, J. Keller, K. Lindgren,C. Platzer-Bjorkman, and M. EdoffACS Appl. Energy Mater. 4, 1805−1814, (2021).

[29] N. Karunagaran, P. Ramasamy, Investigation on synthesis, growth, structure and physical properties of AgGa0.5In0.5S2 single crystals for Mid-IR application, J. Cryst. Growth 483 169–174 (2018).

[30] M. Purohit, S.K. Meena, A. Dashora, B.L. Ahuja, Bandgap engineering of AgGaS2 for optoelectronic devices: first-principles computational technique, Intellig. Comput.Techniq. Smart Energy Syst. 67–74 (2020).

[31] L.C. Tang, M.H. Lee, C.H. Yang, J.Y. Huang, C.S. Chang, Cation substitution effects on structural, electronic and optical properties of nonlinear optical AgGa(SxSe1-x)2 crystals, J. Phys. Condens.Matter 15 6043–6055 (2003).

Chapter

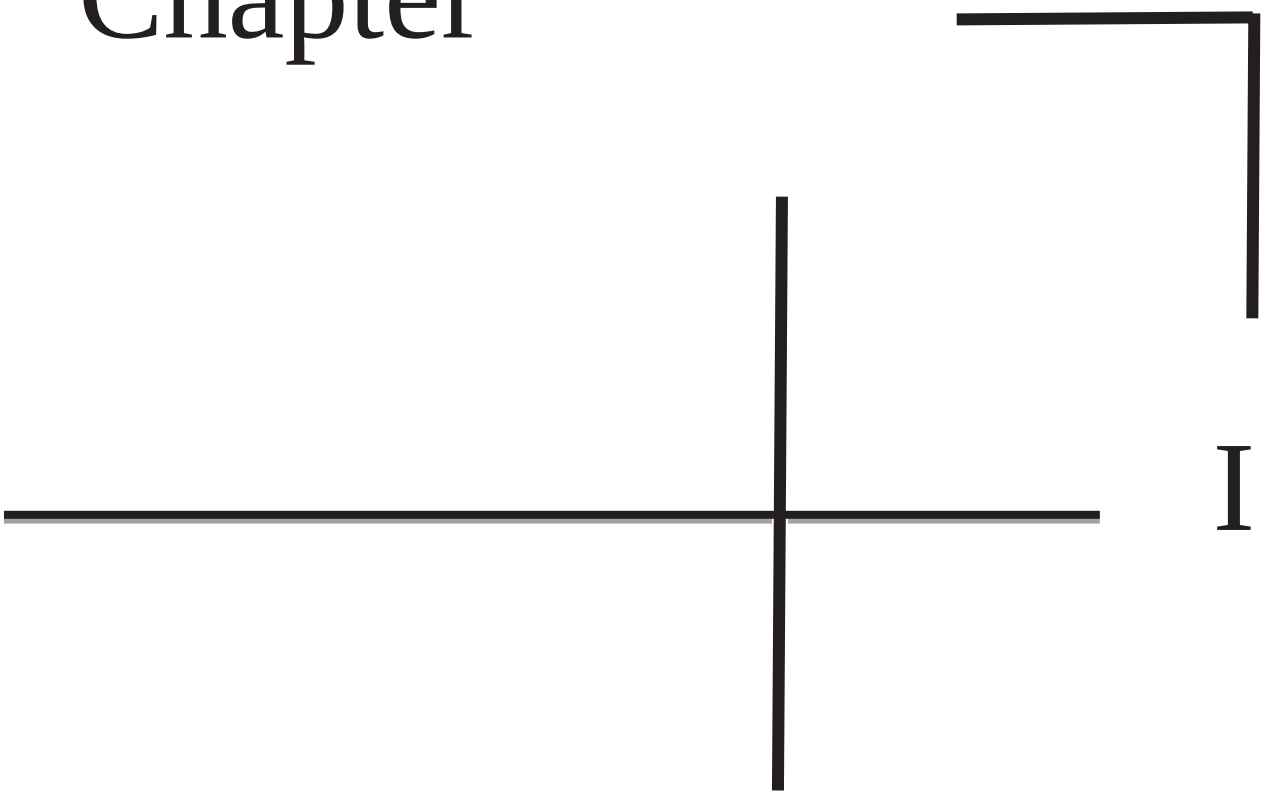

I

Density Functional Theory (DFT)

Chapter I

Density Functional Theory (DFT)

I.1.Introduction

The physical and chemical properties of matter in its atomic, liquid and solid aspects and their understanding can be described by the behavior of its constituents "electron and nucleus" and their interactions. The fundamental theoretical problem in solid state physics is to understand the inner organization of these particles which gives specific properties to the material. The calculation of its properties in the ground state of an N-electron system in a crystal is very difficult, as each particle interacts with all other particles. . The Schrödinger equation (1926) **[1]** becomes mathematically unsolvable. To overcome this difficult situation it was necessary to seek formalisms other than the traditional wave function to better describe the properties of a system.

In recent years, scientists have developed methods based on theoretical concepts known as the ab-initio methods, which attempt to predict the properties of materials by solving the quantum mechanical equations without using adjustable variables .Among the ab-initio methods, the density functional theory (DFT) **[2]**. DFT is a mean field method. It therefore proposes to replace the system of N interacting electrons by a fictitious system composed of N independent electrons, interacting with an external potential that was originally developed by Pierre Hohenberg and Walter Kohn in 1964 **[3]**.further, this theory got improved by Kohn and Lu Sham in 1965 **[4]**. They treated the N-body problem with the single-particle Schrödinger-type equations called the Kohn-Sham equations. Since then, DFT has been very successful in quantum calculations of the electronic structure of matter (atoms, molecules, solids) in both condensed matter physics and quantum chemistry.

I.2.Schrödinger's equation

Solids are made up of an association of elementary particles: nuclei and electrons. The fundamental theoretical problem of solid state physics is to understand the intimate organization of these particles at the origin of their properties **[5]**. But in this case, classical mechanics proves to be insufficient and it is necessary to call upon quantum mechanics, the basis of which is the resolution of the Schrödinger equation established by Erwin Schrödinger in 1925 and which is written in the following form **[6]**:

$$\hat{H}\,\Psi(\vec{r},\vec{R}) = E\,\Psi(\vec{r},\vec{R}) \qquad \textbf{(I.1)}$$

Where:

E Denotes the total energy of the system described by $\Psi(\vec{r},\vec{R})$

$\Psi(\vec{r},\vec{R})$ Is a function of all electronic and nuclear coordinates, which is time independent.

$\vec{r} = r_1, r_2, \ldots, r_n$ Represents the entire set of coordinates of the electrons while $\vec{R} = R_1, R_2, \ldots, R_N$ represents the full set of coordinates of the cores.

$\hat{H}$ Represents the Hamiltonian operator of the total energy of a many-body system. It form is expressed as follows:

$$\hat{H} = \hat{T}_e + \hat{T}_N + \hat{V}_{ee} + \hat{V}_{NN} + \hat{V}_{Ne} \quad \textbf{(I.2)}$$

Where $\hat{T}$ and $\hat{V}$ are the operators for kinetic and potential energy, respectively.

The general problem can be expressed as an equation of movement of all particles within the crystal. The exact Hamiltonian of the crystal (non-relativistic) results from the presence of electrostatic interaction forces (repulsion or attraction) depending on the charge of the particles (nucleus, electron) **[7]**.

$$\hat{T} = \hat{T}_e + \hat{T}_N \quad \textbf{(I.3)}$$

$$\hat{V} = \hat{V}_{ee} + \hat{V}_{NN} + \hat{V}_{Ne} \quad \textbf{(I.4)}$$

$\hat{H}$ Is a non-relativistic differential operator including all forms of energy **[6]**:

The electron kinetic energy operator $\hat{T}_e(\vec{r})$:

$$\hat{T}_e(\vec{r}) = -\frac{\hbar^2}{2m}\sum_i^n \nabla_i^2$$

The kinetic energy operator of nuclei $\hat{T}_N(\vec{R})$:

$$\hat{T}_N(\vec{R}) = -\frac{\hbar^2}{2M}\sum_I^N \nabla_I^2$$

Potential energy operator of the coulombic interaction of repulsion between electron and electron $\hat{V}_{ee}(\vec{r})$:

$$\hat{V}_{ee}(\vec{r}) = \frac{e^2}{4\pi\varepsilon_0}\sum_{i=1}^{n}\sum_{j>i}^{n}\frac{1}{\left|\vec{r}_i - \vec{r}_j\right|}$$

Operator of the potential energy of coulombic interaction of attraction between nucleus and electron $\hat{V}_{eN}(\vec{r}, \vec{R})$:

$$\hat{V}_{eN}(\vec{r}, \vec{R}) = -\frac{e^2}{4\pi\varepsilon_0}\sum_{i=1}^{n}\sum_{I=1}^{N}\frac{Z_I}{\left|\vec{r}_i - \vec{R}_I\right|}$$

Operator of the potential energy of the coulombic repulsion interaction between nucleus and nucleus $\hat{V}_{NN}(\vec{R})$:

$$\hat{V}_{NN}(\vec{R}) = \frac{e^2}{4\pi\varepsilon_0}\sum_{I=1}^{N}\sum_{J>I}^{N}\frac{Z_I Z_J}{\left|\vec{R}_I - \vec{R}_J\right|}$$

Thus, the global Hamiltonian becomes:

$$\hat{\mathbf{H}} = -\frac{\hbar^2}{2}\sum_i \frac{\nabla^2\vec{R}_i}{M_n} - \frac{\hbar^2}{2}\sum_i \frac{\nabla^2\vec{r}_i}{m_e} - \frac{1}{4\pi\varepsilon_0}\sum_{i,j}\frac{e^2 Z_i}{\left|\vec{R}_i-\vec{r}_j\right|} + \frac{1}{8\pi\varepsilon_0}\sum_{i\neq j}\frac{e^2}{\left|\vec{r}_i-\vec{r}_j\right|} + \frac{1}{8\pi\varepsilon_0}\sum_{i\neq j}\frac{e^2 Z_i Z_j}{\left|\vec{R}_i-\vec{R}_j\right|} \quad \textbf{(I.5)}$$

The calculation of the ground state energy of the system is analytically very difficult for most systems. Nevertheless, current mathematical knowledge does not yet allow the solution of equation. Knowing that with three interacting bodies it is impossible to solve this equation exactly, therefore numerous approximations have been developed to overcome this obstacle.

- The Born-Oppenheimer approximation (Frozen core approximation).
- The Hartree-fock approximation (Independent electron approximation).

I.2.1.The Born-Oppenheimer approximation

It consists in separating the movement of the electrons from that of the nuclei **[8]**. Considering the large difference in mass between electrons and nuclei, the latter can be considered as fixed compared to electrons. So the electrons move quite a bit faster than the atomic nuclei. According to Born and Oppenheimer **[9]**, electrons are always in their ground state, regardless of the position of the atomic nuclei. This approximation simplifies the Schrödinger equation, the kinetic energy terms of the nuclei and the nucleus-nucleus interactions, independent of the electrons, cancel each other out. The problem to be solved now is therefore a system of Ne electrons interacting in an external potential generated by the nuclei. The interaction term between the nuclei is only involved in the calculation of the total energy of the system, but not in the calculation of the electronic wave functions.

The Hamiltonian can thus be defined as:

$$\hat{H} = \hat{T}_e + \hat{V}_{ee} + \hat{V}_{eN} \quad \textbf{(I.6)}$$

Or:

$$\hat{\mathbf{H}} = -\frac{\hbar^2}{2}\sum_i \frac{\nabla^2\vec{r}_i}{m_e} - \frac{1}{4\pi\varepsilon_0}\sum_{i,j}\frac{e^2 Z_i}{\left|\vec{R}_i-\vec{r}_j\right|} + \frac{1}{8\pi\varepsilon_0}\sum_{i\neq j}\frac{e^2}{\left|\vec{r}_i-\vec{r}_j\right|} \quad \textbf{(I.7)}$$

The Born-Oppenheimer approximation is called adiabatic **[10]** because it separates the electronic problem from the lattice vibration problem.

Despite this reduction, the Schrödinger equation remains difficult to solve. The new total wave function of the system depends on the coordinates of all the electrons and cannot be decoupled therefore the problem cannot be solved especially using current computer resources. Therefore, further approximations are necessary.

I.2.2.Hartree-Fock approximation

In 1930 Fock **[11]** showed that Hartree **[12]** solutions infringe the Pauli Exclusion Principle as they are not antisymmetric with respect to the exchange of two random electrons. The anti-metrisation of the electronic wave function is written, for example, as follows:

$$\Phi(\vec{r}_1,\vec{r}_2,\dots\vec{r}_i.\vec{r}_{i+1},\dots\vec{r}_j,\vec{r}_{N_e})=-\Phi(\vec{r}_1,\vec{r}_2,\dots\vec{r}_i.\vec{r}_{i+1},\dots\vec{r}_j,\vec{r}_{N_e}) \qquad \textbf{(I.8)}$$

Such a description obeys the Pauli Exclusion Principle, stating that two electrons of the same quantum number cannot simultaneously occupy the same quantum state. However, in the Hartree formulation of the wave function, this is not the case, as the electron i occupies precisely the state i.

Hartree and Fock generalized this concept by showing that Pauli's principle is respected if we write the wave function **[13]** as a: <*Slater's determinant*> **[14]**

$$\Phi(\vec{r}_1\vec{\sigma}_1,\vec{r}_2\vec{\sigma}_2,\dots,\vec{r}_{Ne}\vec{\sigma}_{Ne})=\frac{1}{\sqrt{N_e\,!}}\begin{vmatrix}\Phi_1(\vec{r}_1\vec{\sigma}_1) & \Phi_1(\vec{r}_2\vec{\sigma}_2) & \dots & \Phi_1(\vec{r}_{Ne}\vec{\sigma}_{Ne})\\ \Phi_2(\vec{r}_1\vec{\sigma}_1) & \Phi_2(\vec{r}_2\vec{\sigma}_2) & \dots & \Phi_2(\vec{r}_{Ne}\vec{\sigma}_{Ne})\\ \Phi_{Ne}(\vec{r}_1\vec{\sigma}_1) & \Phi_{Ne}(\vec{r}_2\vec{\sigma}_2) & \dots & \Phi_{Ne}(\vec{r}_{Ne}\vec{\sigma}_{Ne})\end{vmatrix} \qquad \textbf{(I.9)}$$

Where $\vec{\sigma}$ is the spin.

The function Φ given by equation leads to the Hartree-Fock equations for a one-particle system:

$$\left(-\frac{1}{2}\Delta_i+V_{ext}(\vec{r})+\sum_{\substack{j=1\\(j\neq i)}}^{N_e}\int d^3\vec{r}\,\frac{\left|\Phi_j(\vec{r})^2\right|}{\left|\vec{r}-\vec{r}\right|}\right)\Phi_i(\vec{r})-\sum_{\substack{j=1\\(j\neq i)}}^{N_e}\delta_{\sigma_i\sigma_j}\int d^3\vec{r}\,\frac{\left|\Phi_{j^*}(\vec{r})\Phi_i(\vec{r})\right|}{\left|\vec{r}-\vec{r}\right|}\Phi_i(\vec{r})=\varepsilon_i\Phi_i(\vec{r}) \qquad \textbf{(I.10)}$$

Electron-electron interactions produce additional energy terms in addition to those of the Hartree approximation which are called Wigner correlation energy terms.

I.2.3.Density functional theory (DFT)

The density functional approach expresses the properties of the ground state, such as total energy, equilibrium positions and magnetic moments in terms of the electron density **ρ(r).** The basis of this theory was formulated by Hohenberg, Kohn and Sham **[8]**. In general, the Hohenberg-Kohn theorem shows that the total energy of a gas of electrons subjected to any external potential is a unique functional of the density of the gas. The ground state of the system can therefore be obtained by minimising the energy system with respect to the density. The basic principles can be expressed

according to Hohenberg and Kohn by considering a system of N_e electrons in interaction subjected to an external potential $\mathbf{V_{ext}}$

The Hamiltonian is then:

$$\mathbf{H = T + V_{ee} + \sum_{i=1}^{N_e} V_{ext}(r_i)} \quad \textbf{(I.11)}$$

Where T and V_{ee} are the kinetic energy and electron interaction terms respectively.In this case, the ground state energy of a system has several interacting electrons places in an external potential $\mathbf{V_{ext}}(r_i)$is a unique functional of $\boldsymbol{\rho}(\mathbf{r})$:

$$\boldsymbol{E[\rho] = \int V_{ext}(r)\rho(r)d^3r + F[\rho(r)]} \quad \textbf{(I.12)}$$

Where $\boldsymbol{E[\rho]}$ is a universal electron density functional $\boldsymbol{\rho}(\mathbf{r})$that contains the kinetic and coulombic contributions of energy. The functional $\boldsymbol{F[\rho(r)]}$is independent of $\boldsymbol{V_{ext}(r)}$, and is not known exactly. The term $\int \boldsymbol{V_{ext}(r)\rho(r)d^3r}$ represents the core-electron interaction.

The problem is therefore to determine $\boldsymbol{E[\rho]}$ which is expressed as follows:

$$\boldsymbol{F[\rho(r)] = T_s[\rho(r)] + E_H[\rho(r)] + E_{xc}[\rho(r)]} \quad \textbf{(I.13)}$$

Where:

$\boldsymbol{T_s[\rho(r)]}$**:** is the kinetic energy of an electrons gas without interaction

$\boldsymbol{E_H[\rho(r)]}$**:** is the classical coulomb interaction energy

$\boldsymbol{E_{xc}[\rho(r)]}$**:** is the exchange and correlation energy that describes the entire N -body contributions that are not taken into account in the Hartree approximation. This term is not known analytically. One method of solving this problem is to use the Kohn-Sham formulation and the local density approximation (LDA) or the generalized gradient approximation (GGA) explained below

I.2.4.The Kohn and Sham equations

Kohn and Sham [KS] **[9]** wrote the exact ground state energy of an interacting system in an external potential $\boldsymbol{V_{ext}}$ as a functional depending only on the electron density $\boldsymbol{\rho(\vec{r})}$,

$$\mathbf{E[\rho(r)]} = \boldsymbol{T_S[\rho(r)]} + \int \boldsymbol{d^3r V_{ext}\rho(r)} + \int \boldsymbol{d^3r d^3r \frac{\rho(r)\rho(r)}{|r-r|}} + \boldsymbol{E_{XC}[\rho(r)]} \quad \textbf{(I.14)}$$

In this case Kohn and Sham propose to solve the following system of self-consistent equations which allows to find the density $\boldsymbol{\rho(\vec{r})}$,that minimizes the energy of the system

$$\begin{cases} \boldsymbol{H_{ks}\Phi_i(r) = \left[-\frac{1}{2}\Delta_i + V_{eff}(r)\right]\Phi_i(r) = \varepsilon_i^{ks}\Phi_i(r)} \\ \boldsymbol{\rho(r) = \sum_{i=1}^{N_e} f_i|\Phi_i(r)|^2} \end{cases} \quad \textbf{(I.15)}$$

$\boldsymbol{\varepsilon i^{ks}}$ and $\Phi\mathbf{i}\boldsymbol{(\vec{r})}$ being respectively the eigenvalues and the monoelectronic (so-called Kohn-Sham) eigenwave functions from which we determine the electron density.

$\boldsymbol{\rho(\vec{r}), V_{eff}}$ is the effective potential in which the particles move:

$$\mathbf{V_{eff}(r) = V_{ext}(r) + V_H(r) + V_{xc}(r)} \quad \textbf{(I.16)}$$

Where we put: $$\boldsymbol{V_H(\mathbf{r}) = \int \mathbf{d^3 r} \frac{\rho(\mathbf{r})}{|\mathbf{r}-\mathbf{r}|}} \textbf{ et } \boldsymbol{V_{XC}(\mathbf{r}) = \frac{\delta \mathbf{E_{XC}}|\rho(\mathbf{r})|}{\rho(\mathbf{r})}} \quad \textbf{(I.17)}$$

By replacing the kinetic energy and electron density in equation (II.15) with those found by solving the system (II.15) we find the total energy of the ground state of the system:

$$\boldsymbol{E[\rho] = \sum_{i=1}^{Ne} \varepsilon_i - \int d^3\mathbf{r} d^3\mathbf{r} \frac{\rho(\mathbf{r})\rho(\mathbf{r})}{|\mathbf{r}-\mathbf{r}|} - \int d^3\mathbf{r} V_{xc}(\mathbf{r})\rho(\mathbf{r}) + E_{xc}[\rho]} \quad \textbf{(I.18)}$$

We note that the Kohn-Sham transformations are exact transformations. The problem of Ne interacting electrons is replaced by Ne independent electrons interacting with the total electron density, which simplifies the calculations considerably.

In the Kohn-Sham formulation, all the energy terms, and their associated potentials, can be evaluated, except the exchange-correlation term, which is problematic. This term $\mathbf{E_{xc}}$ **[ρ]** is not known exactly even though it appears as a corrective term. In any case, various approximations have to be used, which we will discuss next.

I.2.5.Resolution of exchange and correlation energy

There are two very common approximations for dealing with the term V_{XC}

I.2.5.1.The local density approximation (LDA)

To approximate the density functional $\boldsymbol{E_{XC}}$ **[ρ(r)]**, Kohn and Sham proposed as early as 1965 the local density approximation (LDA) **[15]**, which treats an inhomogeneous system as locally homogeneous, with exchange and correlation energy known exactly:

$$\mathbf{E[\rho(r)] = \int \rho(r)\varepsilon[\rho(r)]d^3r} \quad \textbf{(I.19)}$$

Where $\boldsymbol{\varepsilon[\rho(\mathbf{r})]}$is the exchange and correlation energy per particle of a uniform electronic gas of density $\boldsymbol{\rho}$ that is known to be in the form:

$$\mathbf{V_{XC}(r) = \frac{\delta EXC[\rho(r)]}{\delta \rho(r)} = \varepsilon[\rho(r)] + \rho(r)\frac{\delta \varepsilon_{XC}[\rho(r)]}{\delta \rho(r)}} \quad \textbf{(I.20)}$$

In the case of magnetic materials, the electron spin provides an additional degree of freedom and the LDA must then be extended to the Spin Density Approximation **[15]**. and the LDA must then be extended to the Local Spin Density Approximation (LSDA) where the exchange and correlation energy $\boldsymbol{E_{XC}}$ becomes a functional of the two high and low spin densities:

$$\mathbf{E_{XC}[\rho\downarrow \cdot \rho\uparrow] = \int \rho(r)\varepsilon[\rho\downarrow \cdot \rho\uparrow]d^3r} \quad \textbf{(I.21)}$$

The most commonly used forms for energy and exchange potential in LDA are those of Kohn-Sham and Wigner **[17]**, Von Barth-Hedin**[15]**, Gunnarson-Lundqvist **[16]**, Vosko et al.**[18]** and Perdew and Wang **[19]** .

Table. I.1: Computational performance in the LDA approximation **[13].**

Quantity	LDA error
Bond length	~1%
Vibration frequency	Some %
Elastic constant	Some %
Cohesive energy	~15%
Energy barrier	~20%

I.2.5.2.Generalized Gradient Approximation (GGA)

In several cases the (LDA) **[20]** gave reliable results, but in others it was less accurate with the experimental results. Most of the corrections that have been introduced to the LDA are based on the idea of taking into account local variations in density. For this reason the gradient of the electron density has been introduced leading to the generalized gradient approximation GGA **[21]**, in which the exchange and correlation energy is a function of the electron density and its gradient: **[22]**

$$E_{XC}^{GGA} = \int n(r)\varepsilon_{XC}[n, |\nabla_n|, \dots]d^3r \equiv \int n(r)\varepsilon_X^{hom}(n)F_{XC}[n, |\nabla_n|, \dots]d^3r \qquad \textbf{(I.22)}$$

Where $\varepsilon_X^{hom}$is the exchange energy of a non-polarized system of density $n(r)$. There are many forms of F_{XC} , the most commonly used are those introduced by Becke **[23]**, Perdew and Wang **[24]** and Perdew, Burke and Ernzerhof **[25].**

I.2.5.3.The EV-GGA approximation

The major shortcoming in both approximations (GGA and LDA) is the estimation of the energy gap value, which is essentially due to the correlation term being considered too simple, and to correct this shortcoming, Engel and Vosko **[18]** have shown that the GGA cannot improve on the second-order expansion of the generalized gradient due, most of the time, to the cancellation of local errors, hence the correction brought to the correlation term, by mixing the second-order generalized

gradient with the exact Hartree-Fock correlation term. But unfortunately it remains poor if one is interested in calculations of the fundamental energy as a function of the structural parameters [30].

I.2.5.4.Modified Becke and Johnson potential (mBJ)

A new version of the exchange potential, first proposed by Becke and Johnson [26], was published by Tran and Blaha [27]. This is the mBJ "modified Becke Johnson Potential" (also known as the TB potential: Tran-Blaha) which has been implemented in the latest versions of the ab initio Wien2k code. Tran and Blaha [28] tested the exchange potential proposed by Becke and Johnson (BJ) [26] which was designed to reproduce the shape of the exact exchange potential called the "optimised effective potential (OEP)". They noted that using the BJ potential combined with the GGA correlation potential always gives underestimated gap energies. In order to improve these results, Tran and Blaha [27] introduced a simple modification of the original BJ potential and obtained good agreement with other more expensive approaches (due to their high self-consistency) such as hybrid functional and the GW method [29-31]. The modified BJ potential (mBJ) proposed by Tran and Blaha [27] has the following form:

$$v_{x,\sigma}^{mBJ}(r) = c v_{x,\sigma}^{BR}(r) + (3c-2)\frac{1}{\pi}\sqrt{\frac{5}{12}}\sqrt{\frac{2t_\sigma(r)}{\rho_\sigma(r)}} \qquad \textbf{(I.23)}$$

$\rho_\sigma(r) = \sum_{i=1}^{n_\sigma} |\psi_{i,\sigma}(r)|^2$ is the density of electrons.

$t_\sigma(r) = \frac{1}{2}\sum_{i=1}^{n_\sigma} \nabla\psi_{i,\sigma}^*(r)$ is the density of the kinetic energy.

$$v_{x,\sigma}^{mBJ}(r) = -\frac{1}{b_\sigma(r)}\left(1 - e^{-x_\sigma(r)} - \frac{1}{2}x_\sigma(r)e^{x_\sigma(r)}\right) \qquad \textbf{(I.24)}$$

$v_{x,\sigma}^{mBJ}$ is the Becke-Roussel (BR) potential [32] which has been proposed to model the coulombic potential created by the exchange hole.

The term x_σ in equation **(I.24)** was determined from. $\rho_\sigma(r)$, $\nabla\rho_\sigma(r)$, $\nabla 2\rho_\sigma(r)$ *et* (r); while the term (r) was calculated using the following relationship:

$$b_\sigma(r) = \left[\frac{x_\sigma^3 e^{-x_\sigma}}{8\pi\rho_\sigma}\right]^{\frac{1}{3}} \qquad \textbf{(I.25)}$$

In equation (II.25), c has been chosen to depend linearly on the square root of the mean of $\frac{\nabla\rho_\sigma(r)}{\rho_\sigma(r)}$

$$c = \alpha + \beta\left(\frac{1}{V_{cell}}\int_{cell}\frac{|\nabla\rho(r')|}{\rho(r')}d^3r'\right)^{\frac{1}{2}} \qquad \textbf{(I.26)}$$

$\boldsymbol{\alpha}$ and $\boldsymbol{\beta}$ are adjustable parameters ($\boldsymbol{\alpha}$ = -0.012 (dimensionless) and ($\boldsymbol{\beta}$ = 1.023 $bohr$) and $\boldsymbol{V_{cell}}$ is the volume of the unit mesh. For $\boldsymbol{c}$ =1, we have the reproduction of the original Beck and Johnson potential.

$$v_{x,\sigma}^{BJ}(r) = v_{x,\sigma}^{BR}(r) + \frac{1}{\pi}\sqrt{\frac{5}{12}}\sqrt{\frac{2t_\sigma(r)}{\rho_\sigma(r)}} \qquad \textbf{(I.27)}$$

By varying c for a given material, it was found that for many solids the gap energy increases monotonically with respect to c **[27]**. Specifically, for solids with small gaps c_{opt} (the value of c that leads to perfect agreement with the experiment) ranges from 1.1 to 1.3 while for solids with larger gaps, c_{opt} is larger (its value varies from 1.4 to 1.7) **[28].**

I.2.6.The APW method

Slater **[36]** proposed the augmented plane wave functions (APW) as a basis for solving the one-electron Schrödinger equation, which corresponds to the DFT-based equation of Kohn and Sham. The APW method is based on the Muffin-Tin (MT) approximation to describe the crystal potential. According to this approximation the unit cell is divided into two types of regions: spheres called "Muffin-Tin" (I) which do not overlap and are centered on each atom **α** of radius $\boldsymbol{R_\alpha}$ and interstitial regions (II) (the empty space). As a consequence, the wave functions of the crystal are developed in different bases depending on the region considered: radial solutions multiplied by spherical harmonics in the MT spheres and plane waves in the interstitial region

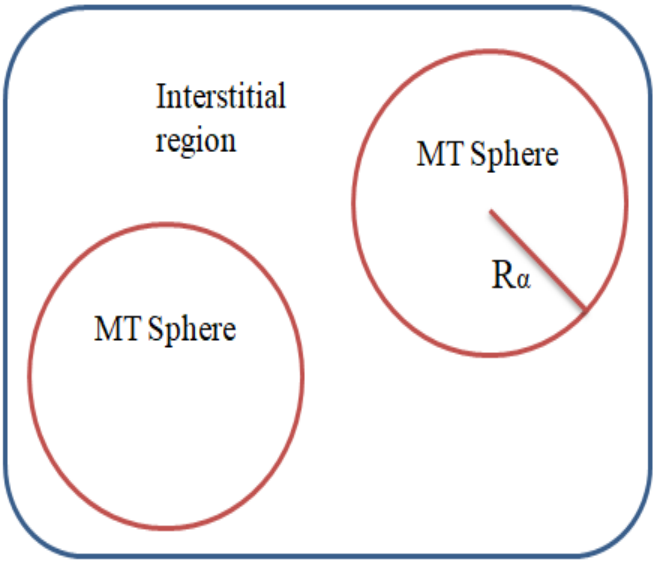

Figure I.1: Muffin-Tin" potential

Thus the wave function is of the form:

$$\varphi(r) = \begin{cases} \sum_{lm} A_{lm} U_l(r) Y_{lm}(r) & r \in I \\ \frac{1}{\Omega^{\frac{1}{2}}} \sum_G C_G e^{i(G+K)r} & r \in II \end{cases} \quad \textbf{(I.28)}$$

Where A_{lm} and C_G are the expansion coefficients, Ω is the volume of the unit cell. $U_l(r)$ is the radial solution of the Schrödinger equation which is written as :

$$\left(-\frac{\partial^2}{\partial r} + \frac{l(l+1)}{r^2} + V(r) - E_l\right) r U_l(r) = 0 \quad \textbf{(I.29)}$$

Where E_l is the linearization energy and $V(r)$ the spherical component of the potential in the sphere. The radial functions defined by equation are automatically orthogonal to any state of the same Hamiltonian that vanishes at the boundary of the sphere as the following equation shows:

$$(E_2 - E_1) r U_1 U_2 = U_2 \frac{d^2 r U_1}{dr^2} - U_1 \frac{d^2 r U_2}{dr^2} \quad \textbf{(I.30)}$$

Where U_1 and U_2 are radial solutions for the energies E_1 and E_2 .The overlap being constructed by using equation and integrating it by parts.

Slater justifies the particular choice of these functions by noting that plane waves are solutions of the Schrödinger equation when the potential is constant. As for the radial functions, they are solutions in the case of a spherical potential, when E_l is an eigenvalue.

This approximation is very good for materials with a face-centered cubic structure, and less and less satisfying as the material's symmetry decreases.

However, to ensure continuity at the sphere boundaries in the APW method, the A_{lm} have been defined in terms of the C_G coefficients of the existing plane waves in the interstitial regions. These coefficients are thus expressed by the following expression:

$$A_{lm} = \frac{4\pi i^l}{\Omega^{1/2} U_l(R_\alpha)} \sum_G C_G j(|K+g|R_\alpha) Y^*_{lm}(K+G) \quad \textbf{(I.31)}$$

R_α is the radius of the sphere, and the origin is taken as the centre of the sphere.

Thus the A_{lm} are determined by the plane wave coefficients C_G and the energy parametersE_l, as these are variational in the APW method. The individual functions which are represented by the index **G** and which consist of plane waves in the interstitial plane waves in the interstitial region and radial functions in the spheres are called augmented plane waves (APW).

The APW method, thus constructed, presents some difficulties related to the function $U_l(R_\alpha)$ which appears in the denominator of the equation. Indeed, depending on the value of the parameterE_l, the

value of $U_l(R)$ can become nil at the surface of the MT sphere, leading to a separation of the radial functions from the plane wave functions. In order to overcome this problem, several modifications to the APW method have been made, including those proposed by Koelling and Andersen **[37].**

I.2.7.The LAPW method

The LAPW (linearized Augmented Plane Wave) method developed by Andersen **[37]** is one of the most accurate bases for the calculation of crystalline solids. It corresponds to an improvement of the Augmented Plane Wave (APW) method, developed by Slater. This LAPW method provides a more flexible and accurate basis for band structure calculations of crystal lattices. This procedure uses the partition of space into two zones. The improvement of this formalism over the APW method lies in the fact that the basis functions in the MT sphere are linear combinations of the radial functions multiplied by spherical harmonics, $u_l(r)Y_{lm}(\vec{r})$ and their derivatives $\dot{u}_l(r)Y_{lm}(\vec{r})$ in relation to energy.

The functions $u_l(r)$ are defined as in the APW method and the $\dot{u}_l(r)Y_{lm}(\vec{r})$ must satisfy the following condition:

$$\left\{-\frac{d^2}{dr^2}+\frac{l(l+1)}{r^2}+V(r)-E_l\right\}r\dot{u}_l(r)=ru_l(r) \qquad \textbf{(I.32)}$$

In a non-relativistic treatment, the radial functions u_l and $\dot{u}_l$ ensure continuity with plane waves on the surface of the MT sphere. The wave functions thus augmented constitute the basic functions of the LAPW method:

$$\phi_{\underline{G}}^{\underline{i}}\left(\vec{r}\right)=\begin{cases}\frac{1}{\Omega^{\frac{1}{2}}}\sum_G C_G e^{i\left(G+E\right)r} & r>R_\alpha \\ \sum\left[A_{im}^{\alpha}u_l(r)+\mathrm{B}_{lm}^{\alpha}\dot{u}_l(r)Y_{bm}(r)\right. & r<R_\alpha\end{cases} \qquad \textbf{(I.33)}$$

Where B_{lm}^{α} are the coefficients corresponding to the $\dot{u}_l$ function and are of the same nature as the A_{im}^{α} coefficients. The LAPW functions are plane waves only in the interstitial zones as in the APW method. Within the spheres, LAPW functions are better suited than APW functions. Indeed, if E_l differs a little from the band energy$E$, a linear combination of and will reproduce the radial function better than APW functions consisting of a single radial function. Non-spherical potentials inside the "Muffin -Tin" sphere can now be treated without difficulty. The LAPW method thus ensures the continuity of the wave function on the surface of the MT sphere, but the calculations lose accuracy compared to the APW method. LAPW functions form a good basis for obtaining all valence bands in a large energy region with a single E_l. When this is not possible, the energy window can usually be split into two parts, which is a great simplification compared to the APW method.

I.2.8.The FP-LAPW method

In the Full Potentiel Linearized Augmented plane Waves (FP-LAPW) **[35]** as implemented in the wien2k code **[34]** the LAPW basis provided by equation and the APW+lo basis provided by equations and are involved and used depending on the nature of the electronic states of the system under study as explained above. However, no approximation is made for the shape of the potential nor for the charge density. Indeed, the potential describing the interactions between nuclei and electrons can be treated differently depending on whether one is inside or outside the muffin sphere. It is developed in harmonics (in each spherical muffin tin atom) and in Fourier series (in the interstitial regions):

$$\mathbf{U}(\vec{\mathbf{r}}) = \begin{cases} \sum_{\mathbf{lm}} \mathbf{U}_{\mathbf{lm}} \mathbf{Y}_{\mathbf{lm}}(\vec{\mathbf{r}}) & \mathbf{r} < \mathbf{R}_{\boldsymbol{\alpha}} \\ \sum_{\mathbf{K}} \mathbf{U}_{\mathbf{K}} \mathbf{e}^{\mathbf{ik}\vec{\mathbf{r}}} & \mathbf{r} > \mathbf{R}_{\boldsymbol{\alpha}} \end{cases} \qquad \textbf{(I.34)}$$

The potential then has an angular dependence in the interior through the intervention of spherical harmonics. The introduction of such a potential gives the FP-LAPW method the "full potential" characteristic because it takes into account the angular dependence in the whole space **[35].**

I.2.9.The LAPW+LO method

The FP-LAPW method generally gives accurate band energies in the vicinity of the linearisation energies and in most materials, it is sufficient to choose these energies in the neighbourhood of the centre of the bands. In order to improve the linearisation and make it possible to the treatment of valence and semicore states in a single energy window, so-called local orbitals (LO) are added to the LAPW database, and consist of a linear combination of two radial functions corresponding to two different energies and the derivative with respect to energy of one of these two functions. A local orbital (LO) is defined by **[40]:**

$$\boldsymbol{\varphi}(\boldsymbol{r}) = \begin{Bmatrix} \mathbf{0} & \boldsymbol{r} < \boldsymbol{R_a} \\ [\boldsymbol{A_{lm}} \boldsymbol{U_l}(\boldsymbol{r}, \boldsymbol{E_l}) + \boldsymbol{B_{lm}} \boldsymbol{U_l}(\boldsymbol{r}, \boldsymbol{E_l}) + \boldsymbol{C_{lm}}(\boldsymbol{r}, \boldsymbol{E_l}) +] \boldsymbol{Y_m^l}(\boldsymbol{r}), & \boldsymbol{r} < \boldsymbol{R_a} \end{Bmatrix} \qquad \textbf{(I.35)}$$

Where the coefficients $\boldsymbol{C_{lm}}$ are of the same nature as the coefficients $\boldsymbol{A_{lm}}$ and $\boldsymbol{B_{lm}}$defined previously.

A local orbital is defined for a given atom for each l and m. It is called local because it is null everywhere except in the muffin-tin sphere to which it refers. These local orbitals are then added to the LAPW basis. Thus the addition of local orbitals increases the size of the LAPW basis.

I.2.10.The APW + lo method

The issue with the APW method was the energy dependency of the set of basic functions. This dependency could be eliminated in the LAPW+LO method but at the cost of a larger base size, where both APW and LAPW+LO methods acquire an important limitation.

Sjösted, Nordström and Singh **[38]** have improved on this by developing a basis that combines the advantages of the APW method with those of the LAPW+LO method. This method is called "APW+lo", it corresponds to an energy independent basis (as was in the LAPW+LO method), In addition, it requires only one plane wave cut-off energy, where this cut-off energy is very slightly higher than that required in the APW method.

It consists in using a standard APW basis but considering $\boldsymbol{U_l(R)}$ for a fixed energy $\boldsymbol{E_l}$ in order to keep the advantage brought by the linearization of the problem at eigenvalues. Since an energy base is fixed, this method does not provide a satisfactory description of the eigenfunctions, local orbitals are also added to provide variational flexibility in the radial basis functions.

An "APW+lo" base is defined by the combination of the following two types of wave functions wave functions:

- APW plane waves with a set of fixed $\boldsymbol{E_l}$ energies **[39]**:

$$\boldsymbol{\varphi}(\mathbf{r}) = \begin{cases} \frac{1}{\Omega^{1/2}} \sum_G \boldsymbol{C_G} e^{i(\mathbf{R}+\mathbf{G})\cdot\mathbf{r}} & r\rangle \boldsymbol{R_\alpha} \\ \sum_{lm} \boldsymbol{A_{lm}} \boldsymbol{U_l^\alpha}(\boldsymbol{r}, \boldsymbol{E_l}) \boldsymbol{Y_{lm}}(\boldsymbol{r}) & r\langle \boldsymbol{R_\alpha} \end{cases} \quad \textbf{(I.36)}$$

- Local orbitals different from those of the LAPW+LO method, are defined by **[39]** :

$$\boldsymbol{\varphi}(\mathbf{r}) = \begin{cases} 0 & r\rangle \boldsymbol{R_\alpha} \\ [\boldsymbol{A_{lm}} \boldsymbol{U_l}(\boldsymbol{r}, \boldsymbol{E_l}) + \boldsymbol{B_{lm}} \dot{\boldsymbol{U}}_l(\boldsymbol{r}, \boldsymbol{E_l})] \boldsymbol{Y_{lm}}(\boldsymbol{r}) & r\langle \boldsymbol{R_\alpha} \end{cases} \quad \textbf{(I.37)}$$

In a calculation, a mixed LAPW and APW+lo basis can be used for different atoms and even for different values of the and even for different values of the *l*. In general, orbitals that converge more slowly with the plane wave number (such as the 3d states of the transition elements), or atoms with a small sphere size are described by the APW+lo basis and the rest by the LAPW basis **[39]**.

I.3.The WIEN2k code

The FP-LAPW method was implemented in the WIEN2k code, a set of programs developed by Blaha, Schwarz and their colleagues **[41]**. This code has successfully dealt with high temperature superconducting systems **[42]**, minerals, transition metal surfaces **[43]**, non-ferromagnetic oxides **[44]**, molecules as well as the electric field gradient. The calculation procedure involves three steps:

The initialization

It consists of constructing the spatial configuration (geometry), the starting densities, the number of special points required for integration in the Brillouin irreducible zone, etc. All these operations are performed by a series of auxiliary programs that generate:

NN: It is a program that gives the distances between the nearest neighbours, and helps to determine the atomic radius of the sphere.

LSTART: A program that generates the atomic densities and determines the different orbital's are processed in the band structure calculation.

SYMMETRY: it generates the symmetry operations of the space group and determines the point group of individual atomic sites.

KGEN: it generates a number of k points in the Brillouin zone.

DSTART: it generates a starting density for the self-consistent cycle (the SCF cycle) by the superposition of the atomic densities generated in LSTART.

Self-Consistent Calculation

In this step, the energies and electron density of the ground state are calculated according to a convergence criterion (energy, charge density, strength). The sub-programs used are:

LAPW0: Generates the potential from the density.

LAPW1: Calculation of valence bands, eigen values and eigenvectors.

LAPW2: it calculates the valence densities for the eigenvectors.

LCORE: it calculates states and core densities.

MIXER: it mixes the input and output densities

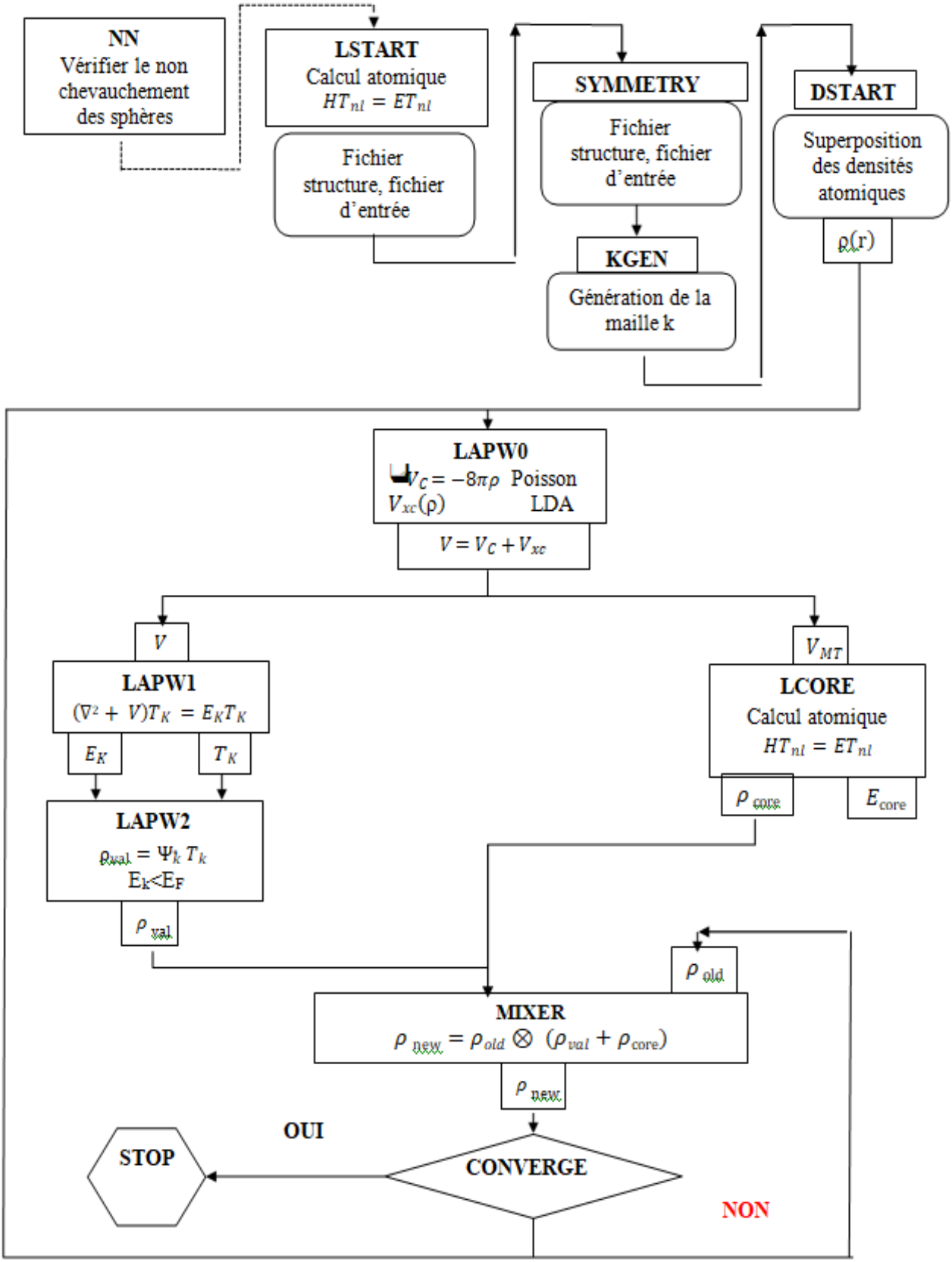

***Figure I.2*:** The structure of the WIEN2k program.

I.4.Conclusion

In this chapter, the different approximations used for various electronic states in a solid have been discussed. Density Functional Theory (DFT) provides an alternative quantum mechanical methodology to the Hartree-Fock method. The main interest of this formalism lies in the fact that it allows the modelling of large relative systems with excellent accuracy compared to other methods which require a considerable numerical effort to take into account electronic correlations. The density functional theory has the advantage of taking into account electronic correlation within its formalism.
This type of method has become very efficient since the 1980s thanks to the substantial improvement of algorithms for solving the Khon-Sham equation in a self-consistent way by taking the waves as the basis of composition. But the only term it leaves undetermined is: the correlation exchange term. This term is then treated by several approximations such as the local density approximation LDA, the generalized gradient approximation GGA and TB-mBJ. As it is impossible to solve the Kohn-Sham equations, numerical methods and approaches will be used, including the Linearly Augmented Plane Wave (LAPW) method, which is essentially a modification of the Slater APW method.
The basic function (LPAW) consists of plane waves in the interstitial region and augmented in the spheres.it aims to obtain precise band energies in the vicinity of the linearization energies $E_{l.}$
The LAPW method has been improved, including the LAPW+LO method, which offers a better treatment of the problem compared to a solution based on the LAPW method as well as the APW+lo method which is a further improvement.

Bibliography

[1] E. Schrödinger, Phys. Rev. 28, 1049 (1926).

[2]. Parr, R.G., Yang, W.: Density Functional Theory of Atoms and Molecules, Oxford University Press, Oxford, pp 5-15 vol3 (1989).

[3] P. Hohenberg, W. Kohn, Phys. Rev. 136 864-871 (1964).

[4] W. Kohn, L. J. Sham, Phys. Rev. 140 1133(1965).

[5] T. Seddik, these de Doctorat, Université de Sidi Belabess (2013).

[6] E. Schrödinger, Quantisierung, Ann. D. Phys. 79 361(1926).

[7] E. Schrödinger, Ann.phys,79, 489, (1926); E.Schrondinger, Ann.Phys.,79 361(1926).

[8] W. Kohn, Rev. Mod. Phys, 71, pp. 1253-1266 (1999).

[9] M. Born, J.R. Oppenheimer, Ann. Phys. 389 (1927) 457-484.

[10] R.G.Parr and W.Yang, "Density-Functional Theory of Atoms and Molecules ", ed. Oxford Sciences Publications, Oxford, pp. 1-325 (1989).

[11] V. Fock, Z. Phys. 61 (1930) 126 ; ibid 62 795(1930).

[12] D.R. Hartree, Proc. Combridge Philos. Soc. 24 89 (1928).

[13] X. Blase, "DFT- les fondements ", Ecole Semat (2000).

[14] S.Cottenier, "Density Functional Theory and the Family of (L) APW-methods: a step-by-step introduction", ed. Ghent University Technologiepark, Belgium (1st ed), pp. 1-77 (2002).

[15] U. von Barth and L. Hedin, J. Phys. C 5 1629 (1972).

[16] O. Gunnarsson, B.I. Lundqvist, Phys. Rev. B 13 4274 (1976).

[17] S. Lundqvist, N. H. March. Plenum Press, New York, vol 38 pp135-221.(l983).

[18] S. H. Vosko, L. Wilk, M. Nussair, *Can. J. Phys.*58 1200 (1980).

[19] J. P. Perdew, Y. Wang. *Phys. Rev. B 45 (*1992) 13244 P. Hohenberg and W. Kohn. Phys Rev. B, 136,31 864-870 (1994)

[20] L.J.Sham, W.Kohn, Phys.Rev 145 (1966).

[21] P. Hohenberg and W. Kohn. Phys. Rev. B, 136, 31 (1994).

[22] J. P. Perdew and K. Burke, Int. J. Quant. Chem. 57 (1996).

[23] A. D. Becke, Phys. Rev. A 38 (1988).

[24] J. P. Perdew and Y. Wang, Phys. Rev. B 45 (1992).

[25] J. P. Perdew, K. Burke, and M. Ernzerhof, Phys. Rev. Lett. 77 (1996) 3865-3868.

[26] A. D. Becke, E. R. Johnson, J. Chem. Phys. 124 (2006).

[27] F. Tran, P. Blaha, Phys. Rev. Lett. 102 (2009).

[28] F. Tran, P. Blaha, K. Schwarz, *J. Phys.: Cond. Mat.* 19 (2007).

[29] T.M. Henderson, J. Paier, G.E. Scuseria, Phys. Stat. Sol. (b) 248 (2011).

[30] V. Faleev, M.V. Schilfgaarde, T. Kotani. Phys. Rev. Lett. 93 (2004).

[31] WG. Aulbur, L. Jonsson, JW. Wilkins, Sol. Stat. Phys. 54 (2000).

[32] A D. Becke, M R. Roussel, Phys. Rev. A 39 (1989).

[33] *M*. Shishkin, M. Marsman, G. Kresse. *Phys*. *Rev*. *Lett*. 99 (*2007)*.

[34] P. Blaha, K. Schwarz, G. K. H. Madsen, D. Kvasnicka, J. Luitz, Vienna University of Technology, Austria, vol2, n°2. (2001).

[35] H.L. Skriver, *the LMTO method*, Springer, Berlin (1984)

[36] J.C.Slater , Phys. Rev. 81 (1951).

[37] A.Ouahab ., thèse de magister, université d'Ouargla (2008)

[38] E. Sjöstedt, L. Nordström, D.J. Singh, Sol. Sta. Com. 114 (2000).

[39] P. Blaha, K. Schwarz, G. K. H. Madsen, D. Kvasnicka, J. Luitz, Vienna University of Technology, Austria, (2001).

[40] J.D.Singh . Phys. Rev. A 3100 (1994).

[41] P.Blaha, K.Schwarz and R.Augustyn, Computer Code WIEN93, Technical University,Vienna (1993) .

[42] K.Schwarz, C.Ambrosch-Draxl and P. Blaha, Phys. Rev, B42, pp. 2051-2061 (1990).

[43] B.Kohler, P.Ruggerone, S.Wilke and M.Scheffler, Phys. Rev. Lett, 74, pp. 1387-1390 (1995).

[44] X.G.Wang, W.Weiss, Sh. K.Shaikhutdinov, M.Ritter, M.Petersen, F.Wagner, R. Schlögl and M.Scheffler, Phys. Rev. Lett, 81, pp. 1038-1840 (1998).

Chapter

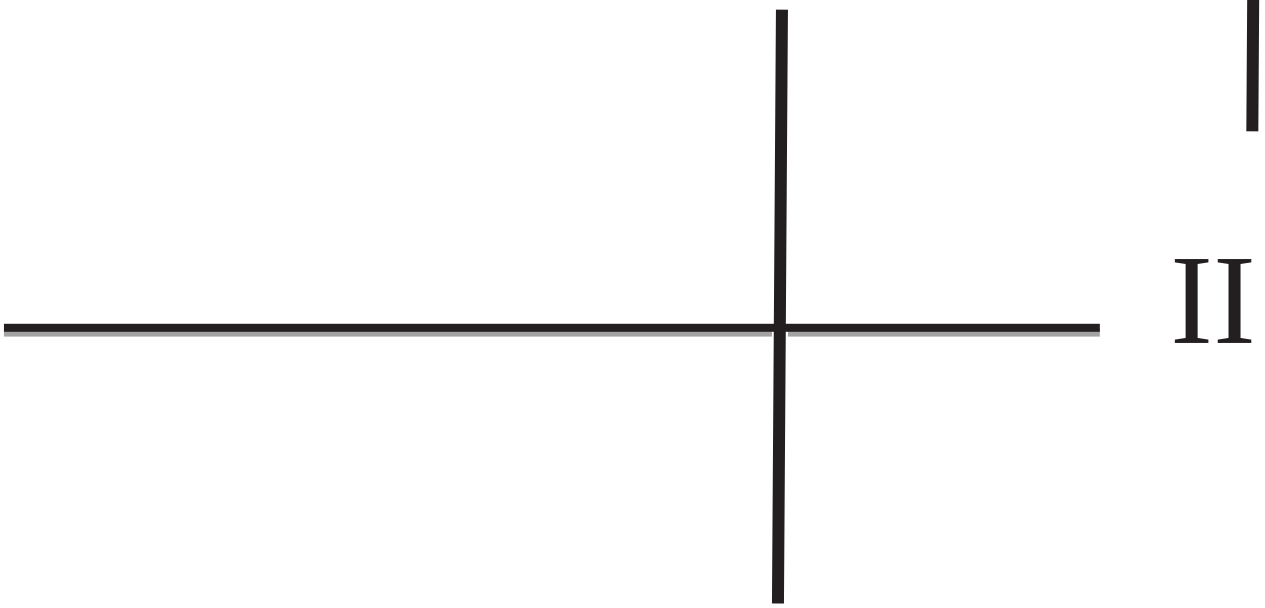

II

Overview on chalcopyrite family

Chapter II

Overview on chalcopyrite family

II.1.Introduction

A high cost of a material will automatically reduce the need for it and make its use unnecessary. Currently, the affordability of PV systems is one of the main barriers to the large-scale production and application of these systems. The efficiency of such a device is a very crucial factor for researchers, and for this aim they are constantly carrying out experiments and research to find the best materials to improve it and obtain better results.

In recent years, several investigations have been directed towards the use of ternary materials of the I-III-VI2 group (I, III, and VI represent elements in the corresponding columns of the periodic table) which crystallize in the chalcopyrite structure due to their broad technological applications such as solar energy converters **[2]**, optical non linear device (NLO) **[1]**, frequency conversion in the field of lasers **[4],** light emitting diodes (LED) **[3]**…

Thin film solar cells based on the use of chalcopyrite materials with the general formula $A^{I}B^{III}C_2^{VI}$ (A = Li, Na, Cu, Ag; B = Al, Ga, In; C = S, Se, Te) are currently considered as the next generation of photovoltaic cells **[5]** due to their unique electronic and optical properties, direct band gap **[1]**, a wide range of transparency of the visible and infrared spectra, a high absorption coefficient and a lifetime in outer space longer compared to that of Si.

the silver (Ag-III–VI_2) based chalcopyrites receive much attention due to their suitability for non-linear optical and photonic applications **[6]**.

The $AgGaS_2$ and $AgGaSe_2$ which is the subject of this study are known as part of the chalcopyrite family with a direct band gap. Those compounds are used as commercial material for NLO applications due to its large NLO coefficient d_{36} = 39 pm/V for $AgGaS_2$ and d_{36} = 28.9 pm/V and excellent transparency in the mid-IR range (1–18 μm).Besides **[7]**, the $AgGaS_2$ compound was proposed as a promising candidate for X-ray dosimetry**[8].**

II.2.Background and history

The crystal structure of chalcopyrite has been the topic of numerous analyses since it was first described by Burdick & Ellis in 1917. The currently recognized atomic structures of chalcopyrite are those first identified by Pauling & Brockway (1932) and by Donnay, Corliss, Elliott and Hastings (1958), respectively. This study sought to provide more accurate structural parameters than those presently available and thus allow a meaningful comparison with those

of other chalcopyrite-like minerals chalcopyrite, talnakhite $Cu_9Fe_8S_{16}$ (Hall & Gabe, 1972), mooihoekite $Cu_9Fe_9S_{16}$ and haycockite $Cu_{10}Fe_8S_{16}$ (Cabri & Hall, 1972) **[9].**

II.3.Name source

First described by Johann Friedrich Henckel in 1725 **[10]**, the term "Chalcopyrite" (or copper pyrite) stems from the two words from the Greek χαλκός "chalkos" which means "copper; Cu" and the word πυρίτες which refers to the yellow colour of the mineral "pyrites; FeS_2" **[25]** that signifies to light a fire (or only a fire) .

II.4.Définition

The chalcopyrite structure is named after a mineral species composed of double sulphide (34.63%), copper (30.43%) and iron (34.94%), of the formula $CuFeS_2$ **[11]** .With traces of Ag; Au; In; Tl; Se and Te. It has also adopted a number of compounds, it an equivalent (ternary compound) of diamond structure, where each atom is bonded to four first neighbours in a tetrahedral structure **[2]**.

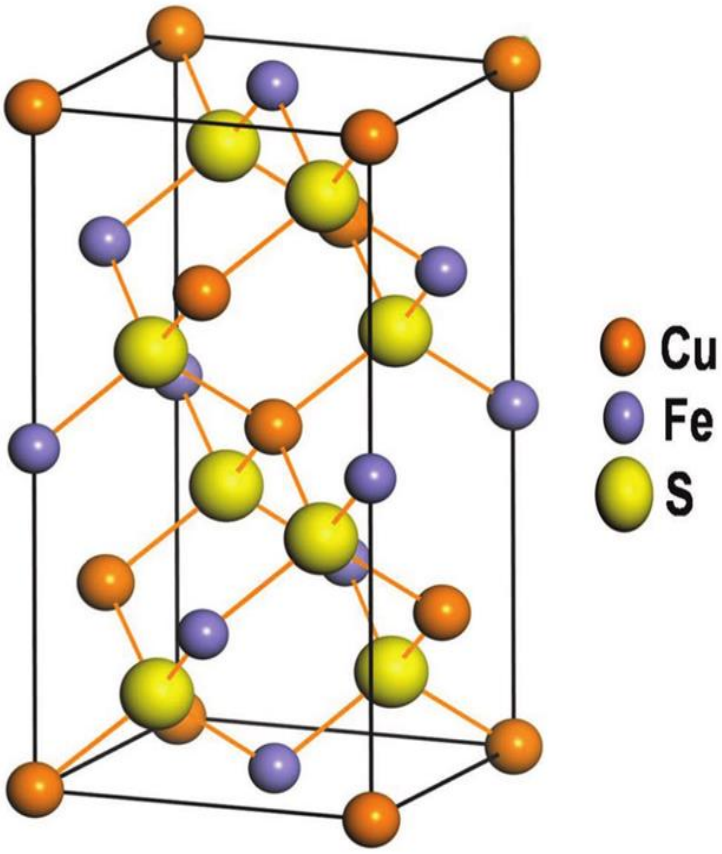

Fig.II.1: the crystal structure of $CuFeS_2$

The chalcopyrite semiconductors have two families: one composed of a first column B element, a third column A element and a sixth column A element: I-III-VI_2, and the other composed of a second column B element, a fourth column A element and a fifth column A element: II-IV-V_2. column A and an element from column A: II-IV-V2 **[26,27].**

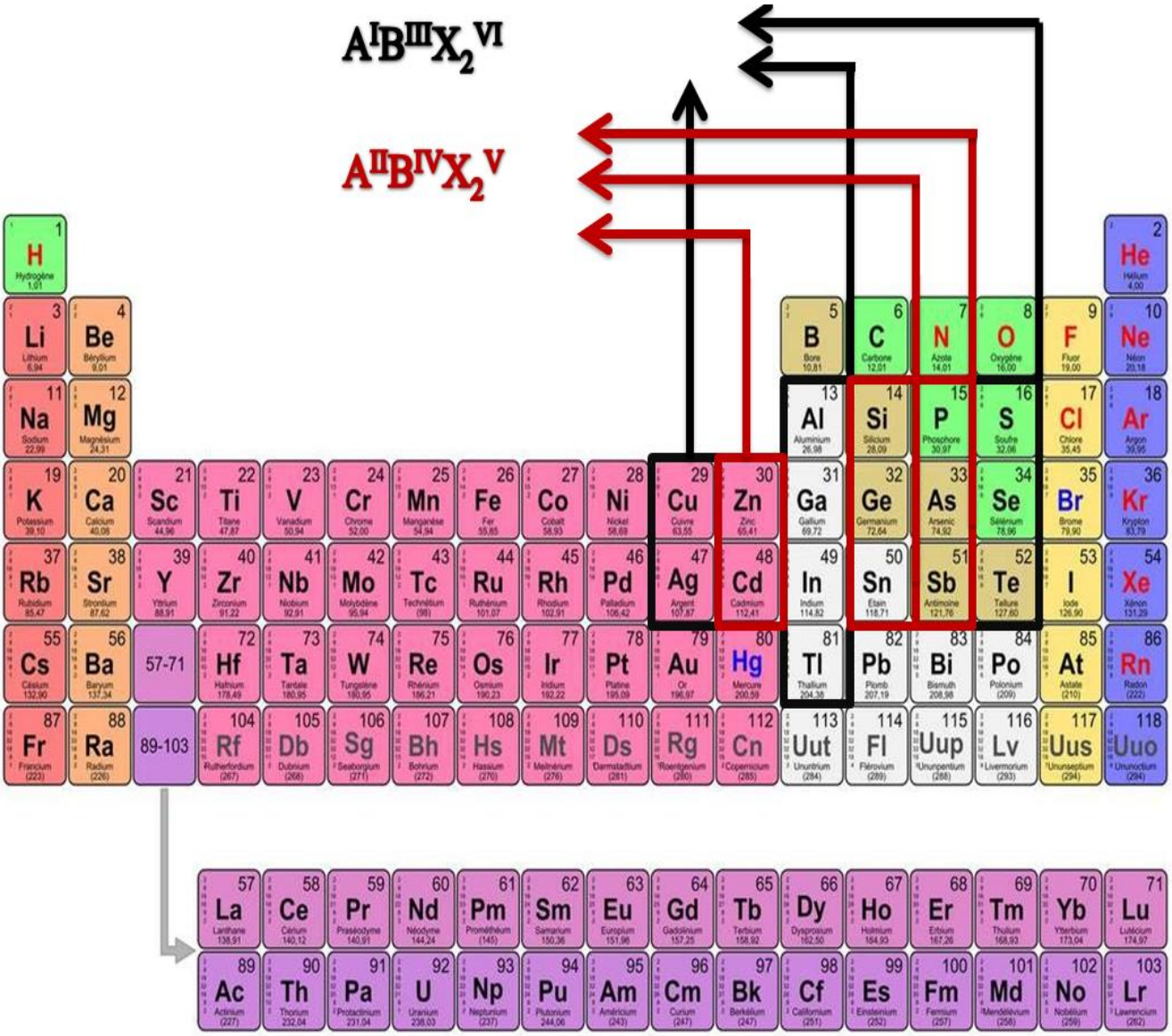

Fig.II.2: Portion of a periodic table showing the two families of chalcopyrite phase semiconductors

II.5.Type III-III-V_2 and III_2-V-V chalcopyrites:

In addition to these two families (I-III-VI_2) and (II-IV-V_2) **[10]**, there are other families that have been recently studied by several researchers, such as the ordered ternary II-IV alloys known as chalcopyrites of type (III-III-V_2), theoretically and experimentally analyzed by

Zunger and his co-authors **[22,33]**. As well as the ternary ordered III-V alloys called chalcopyrites of type (III2-V-V) and (VI2-II-II) also studied by Zunger **[22]** and Teng et al **[34],[11]**.

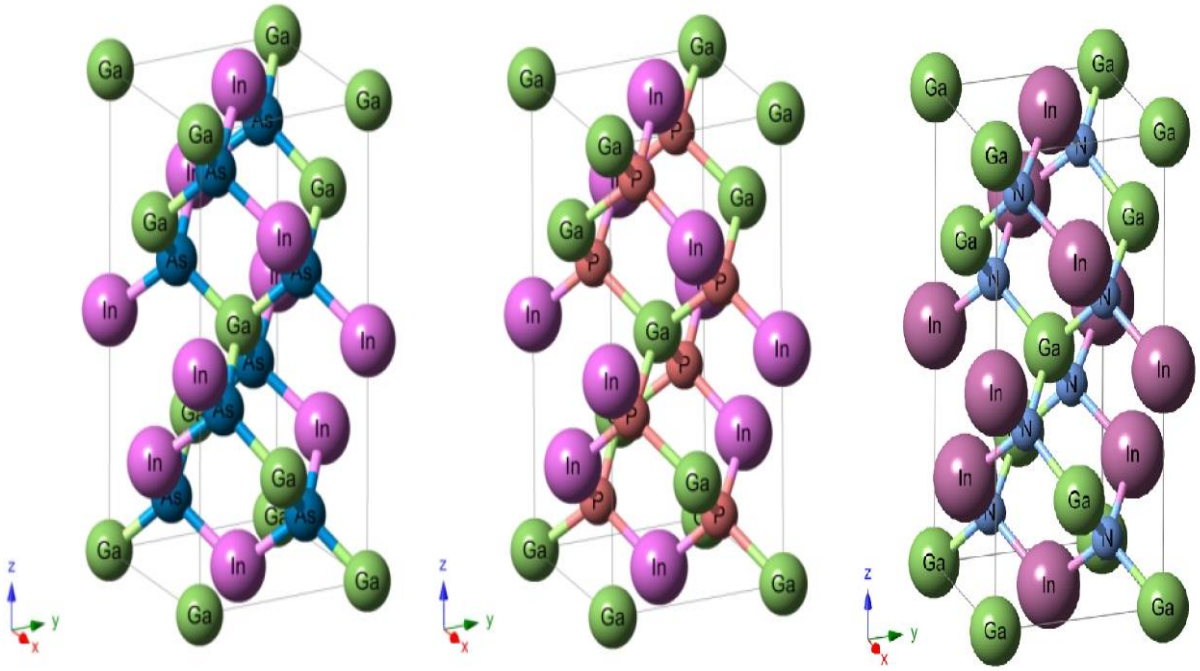

Fig.II.3: Schematic representation of chalcopyrite structures of type (III2-V-V) and (VI_2-II-II) GaInAs2,GaInP2, GaInN2.

Table.II.1: Mesh parameter **a** for some type III-III-V2 or III2-V-V ternary chalcopyrites **[11, 35].**

ABC_2	***a* (Å)**	**ABC_2**	***a* (Å)**
$AlGaAs_2$	5.656	$AlGaP_2$	5.459
$InGaSb_2$	6.298	$InAlAs_2$	5.870
$InGaAs_2$	5.866	$InGaP_2$	5.672
$InAlP_2$	5.674	$AsPGa_2$	5.552
$SbAsGa_2$	5.884	$SbPGa_2$	5.787

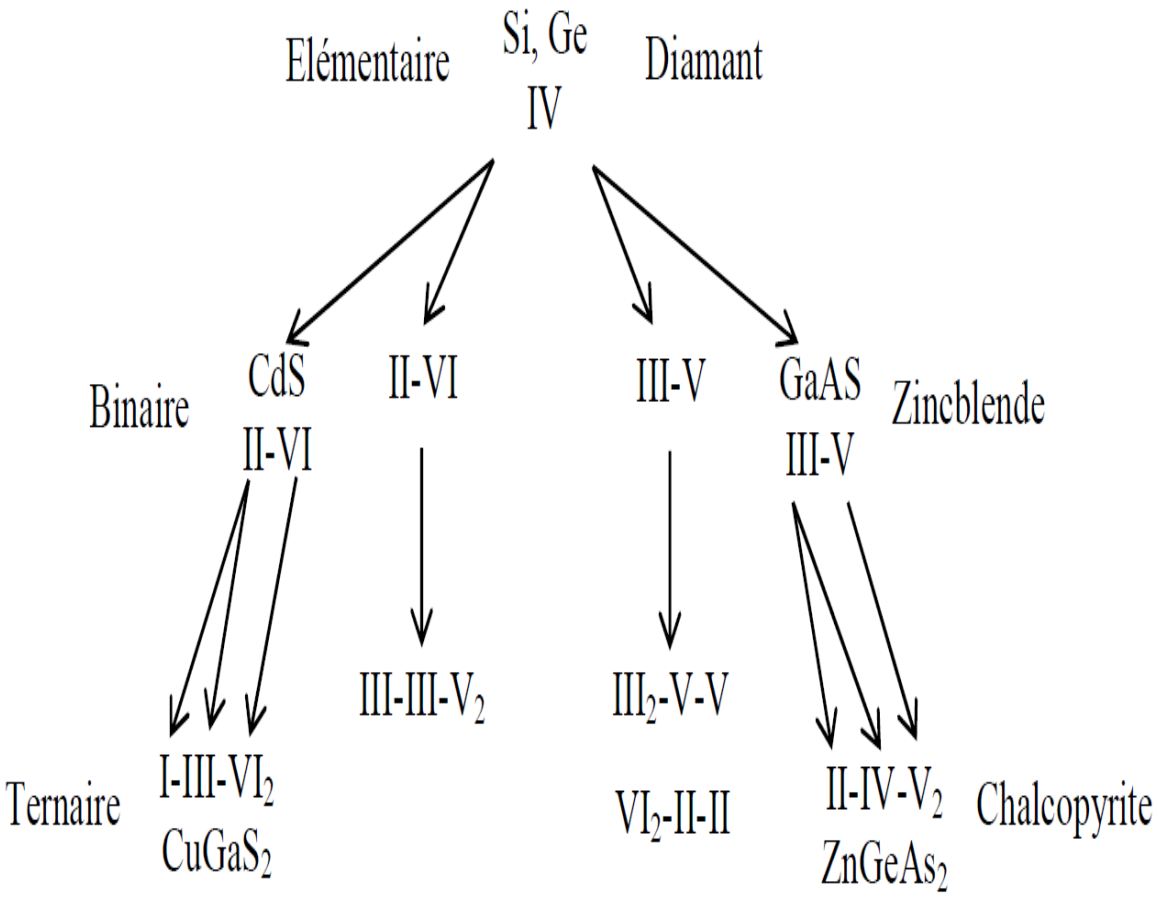

Fig.II.4: Cation substitution diagram with corresponding structures **[28, 29]**

II.6.Crystal structure of chalcopyrite

Semiconductors often crystallize in one of the following structures: diamond structure, Zinc blende structure (Cubic), Wurtzite structure (Hexagonal) and the NaCl (Cubic) structure. A variety of semi-conductors such as Si, Ge, GaP and GaAs crystallize in a diamond structure (composed of the same types of atoms: Si), or a zinc blende structure (composed of two different types of atoms: GaAs). Both structures have covalent bonds (diamond structure) and ionic (zinc blende structure) tetrahedral bonds where each atom is surrounded by four neighboring atoms located on the corners of a regular tetrahedron.

II.7.Structures overview:

II.7.1.Diamond structure:

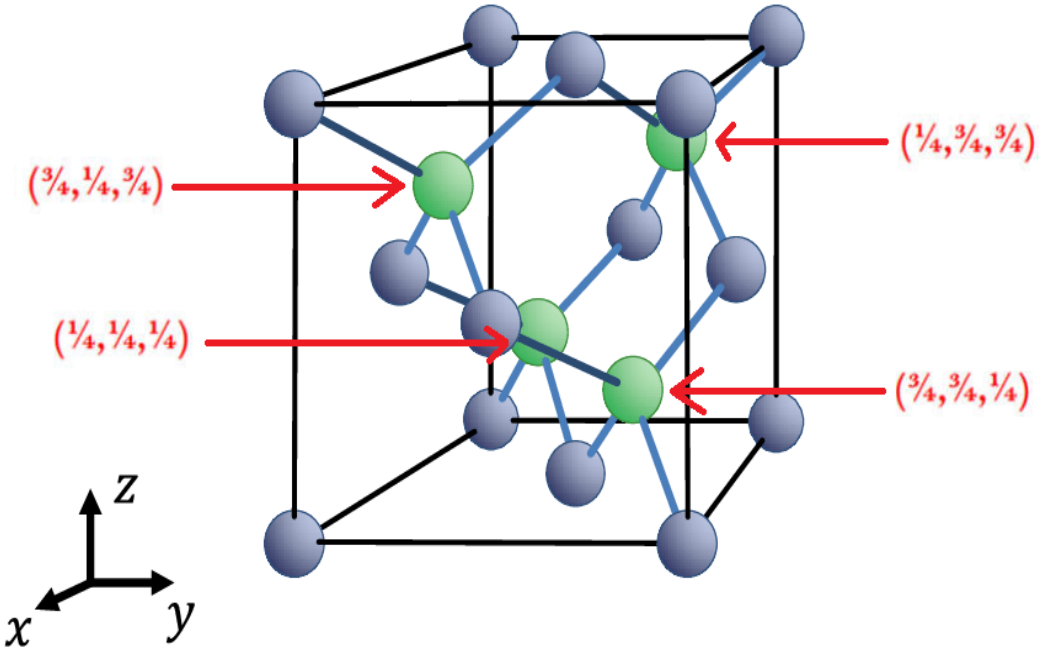

Fig.II.5: diamond structure

In the diamond structure shown below, there are 14 (grey) carbon atoms C placed at the corners of the CFC lattice and a further 4 carbon atoms (green) placed at (¼, ¼, ¼), (¾, ¼, ¾), (¼, ¾, ¾) and (¾, ¾, ¼)

- Each carbon atom is surrounded by four other C atoms (the nearest neighbours), so the coordination of the carbon atoms with each other is therefore four.
- The number of atoms per cell is 8 and the cell parameter a = 3.5668 Å **[12]**.
- The diamond structure can also be viewed as two face-centred cubic structures offset from each other by (1/4, 1/4, 1/4), from this structure and by substitution, the binary compounds (II-VI) and (III-V) are derived which have the structure zinc blende.

II.7.2.Zinc Blende Structure

In the zinc blende structure, the four carbon atoms inside the diamond structure are substituted by four atoms of another element. In the case of ZnS, the four S atoms (in yellow) occupy the coordinate sites (¼, ¼, ¼), (¾, ¼, ¾), (¼, ¾, ¾) and (¾, ¾, ¼).the zinc atoms occupy the network nodes CFC (in grey). one can also say that the zinc blend structure can be considered as two face-centred cubic structures of (1/4, 1/4, 1/4) (as the diamond structure but the two cfc's do not contain the same atom).

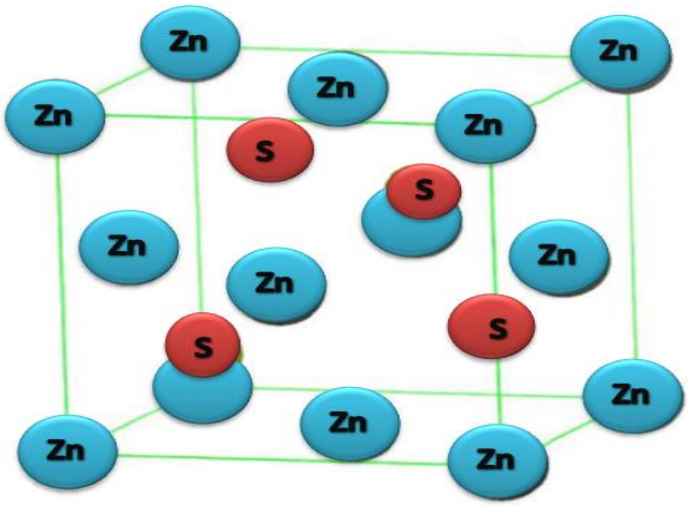

Fig.II.6: Zinc-Blend structure (ZnS)

- The mesh contains 4 cations Zn^{2+} and 4 anions S^{2-}.
- Each anion of sulphur S^{2-} is surrounded by 4 cations Zn^{2+}.The S atom is then located at the centre of the regular tetrahedron formed by the 4 cations Zn^{2+}.
- The mesh parameters of ZnS are: a = b = c =5.404 A **[13]**

II.7.3.Chalcopyrite structure:

The ternary **I-III-VI$_2$** and **II-IV-V$_2$** (ABC_2) (semiconductor) compounds can be considered as the ternary analogues of the binary compounds **II-VI** and **III-V**, respectively, belonging to space group I42d of the tetragonal system with four groupings forms per cell Z = 4. The known phases with this structure are presented in tables I.2 and I.3. The Bravais lattice of chalcopyrite is quadratic centred.

The atomic distribution is as follows [1]:

1. Equivalent position (0,0,0; $\frac{1}{2}, \frac{1}{2}, \frac{1}{2}$)
2. Coordinates of the eight atoms in the elemental lattice of chalcopyrite :

4A in (a) positions (0, 0, 0;0, $\frac{1}{2}, \frac{1}{4}$)

4B in (b) positions (0,0, $\frac{1}{2}$; 0, $\frac{1}{2}, \frac{3}{4}$)

8C in (d) positions (u, $\frac{1}{4}, \frac{1}{8}$; ū, $\frac{3}{4}, \frac{1}{8}$; $\frac{3}{4}$,u, $\frac{7}{8}$; ; $\frac{1}{3}$, ū, $\frac{7}{8}$)

If we add the coordinates of the equivalent positions to the coordinates of the sites a, b and d we obtain the coordinates of all the atoms.

Generally, a ternary compound ABC_2, composed of a mixture between two Zinc- Blende structures, introduces a symmetry group change from F43m to I42-d thus characterising a quadratic chalcopyrite structure for these types of crystals, the transition from the structure to the chalcopyrite structure causes a decrease in symmetry and a change in volume, due to two types of cations, leads to an elemental lattice of eight atoms in the chalcopyrite structure compared to a two-atom unit cell in the zinc blende structure.

The chalcopyrite structure is a superlattice of the zinc-blende structure, it can be obtained by doubling the zinc-blende structure along the z-axis. Then the mesh parameter c should be twice the a parameter, chalcopyrites have, due to the alternation of the cations. Consequently, each A and B cation is tetrahedrally linked by four C anions, while each C anion is tetrahedrally bonded by two A and two B cations . The tetrahedral coordination implies that the bonding is mainly covalent, although there are some ionic characters present because the atoms are different.

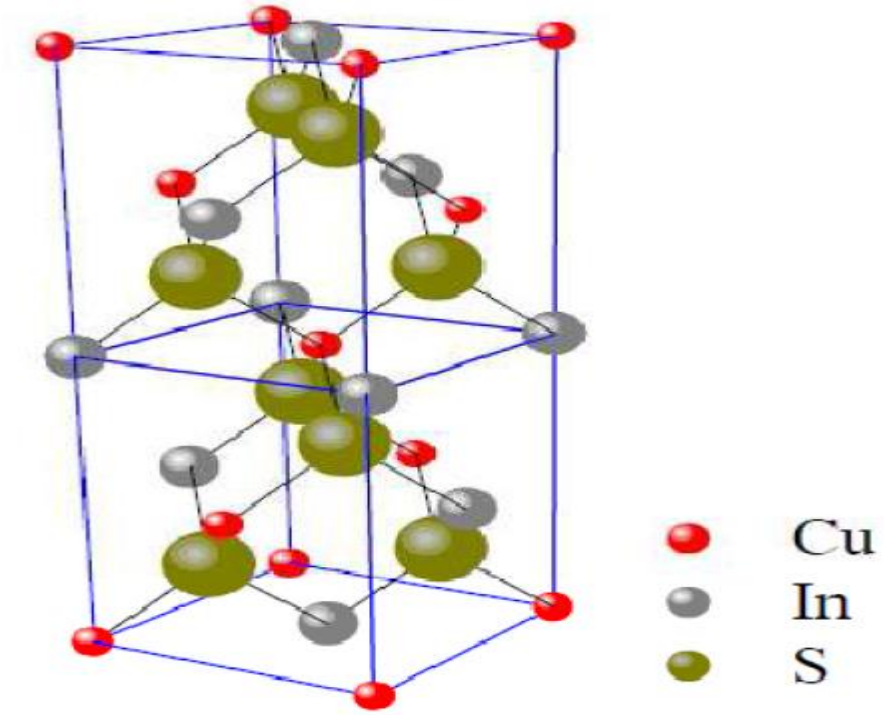

Fig.II.7: Structure of $CuInS_2$ (two Zinc- Blende structures)

II.8.Different types of chalcopyrite:

There are three basic types of the chalcopyrite structure:

Pure chalcopyrites

Chalcopyrites defects

Doped chalcopyrites.

II.8.1.Pure chalcopyrites

Semiconductors with formula I-III-VI_2 that crystallise in the chalcopyrite structure are pure chalcopyrites.

II.8.2.Chalcopyrite defects:

If we take the structure chalcopyrite $A^{I}B^{III}C_2^{VI}$ and replace four atoms A^{I} by two A^{II} (a non-isovalent substitution), we obtain the mesh $A^{II}B_2^{II}C_4^{VI}$ (these compounds are called defect chalcopyrites). In this way, it differs from that of pure chalcopyrite by the presence of two vacant metal sites **[17]**. According to Hahn **[18]**, the thologallate structure, with metal atoms in tetrahedral coordination, appears only when there is an anion with a strong polarising effect on these atoms. The order of the cations and vacancies induces a c/a ratio superior to 1, up to c/a = 2 for $CdAl_2Se_4$.The vacancies in the tetrahedra, which are relatively small, are distorted for the selenides. The existence of I4 (D_{11}^{2d}) (compared to (I-42m) with order, is explained by a more regular distribution of electrons between different lattice planes, giving a character closer to that of Zincblende. This structure is characterised by these three internal free positions x, y and z. As shown in **fig.II**

Table.II.2: Positions of defect chalcopyrite structure according to Wyckoff **[11]**.

	x	y	z
_	0	0	0
	0	0	1/2a
(I4(S_2^4))	0	1/2a	1/4a
	1/2a	1/2a	0
	xa	ya	za

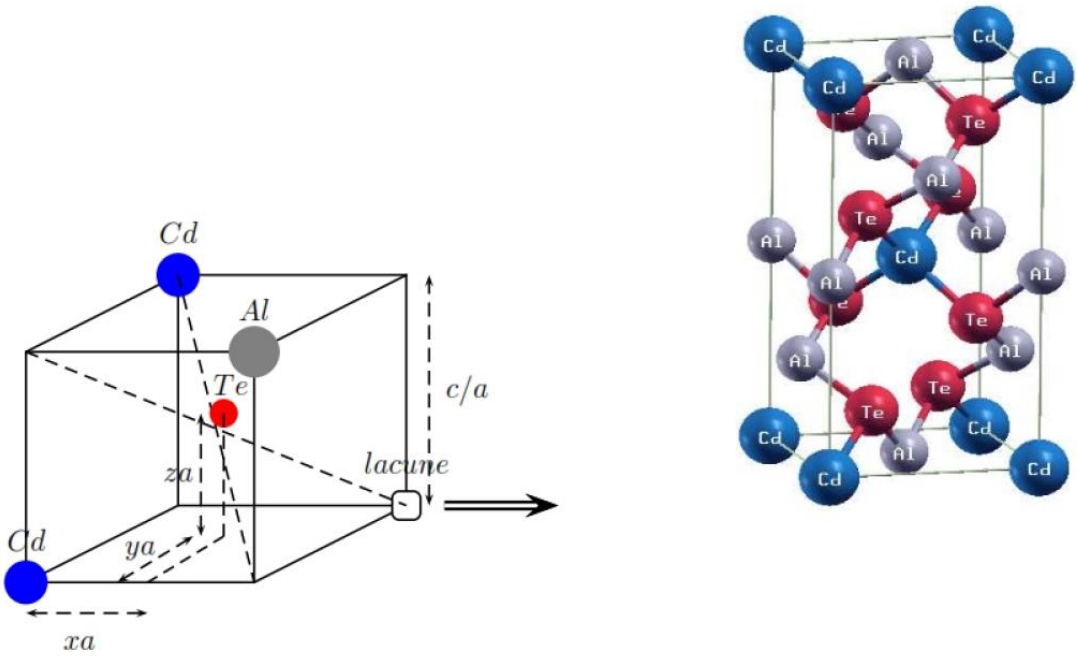

Figure.II.8: Graphical representation of the effective chalcopyrite structure as well as the distortion c/a and the internal x, y and z positions along the x, y, z axes **[11].**

Table.II.3: Some known defects ternary chalcopyrites **[33].**

Phase N°	The ternary phase	
1	$A^{I}B^{II}C^{VII}$ (Ag_2HgI_4)	$2A^{I}C^{VII}+B^{II}C^{VII}$ (2AgI + HgI_2)
2	$A^{II}B^{III}C^{VI}$ ($ZnGa_2S_4$)	$A^{II}C^{VI}+B^{III}C^{VI}$ (ZnS + Ga_2S_3)
3	$A^{II}B^{IV}C^{VI}$ (Zn_2GeS_4)	$2A^{II}C^{VI}+B^{IV}C^{VI}$ (2ZnS + GeS_2)
4	$A^{II}B^{IV}C^{VI}$ ($ZnGeS_3$)	$A^{II}C^{VI}+B^{IV}C^{VI}$ (ZnS + GeS_2)
5	$A^{III}B^{V}C^{VI}$ (Ga_3PSe_3)	$A^{III}B^{V}+A^{III}C^{VI}$ (GaP + Ga_2Se_3)
6	$A^{III}B^{V}C^{VI}$	$A^{III}C^{VI}+B^{V}C^{VI}$

II.8.3.Doped chalcopyrite:

Ternary chalcopyrite compounds can be derived from its analogues It is possible to additionally replace an additional metal M in a ternary system compound $A^{I}B^{III}X_2^{VI}$ without violating the four electrons per site of the network. In general, in the case of isovalent substitution, for example $A^{I}B^{III}_{1-x}M^{III}_{x}\ X_2^{VI}$ (substitutes M for B), the new quaternary compound will always be a chalcopyrite, while a non-isovalent substitution will be accommodated in crystal lattices by the formation of associated vacancies, for example $A^{I}_{1-2x}\ B^{III}M^{II}_{x}\ X_2^{VI}$. These compounds are called chalcopyrites defects. If we dope an atom in the vacant space of the defect chalcopyrite it is then called doped chalcopyrite.

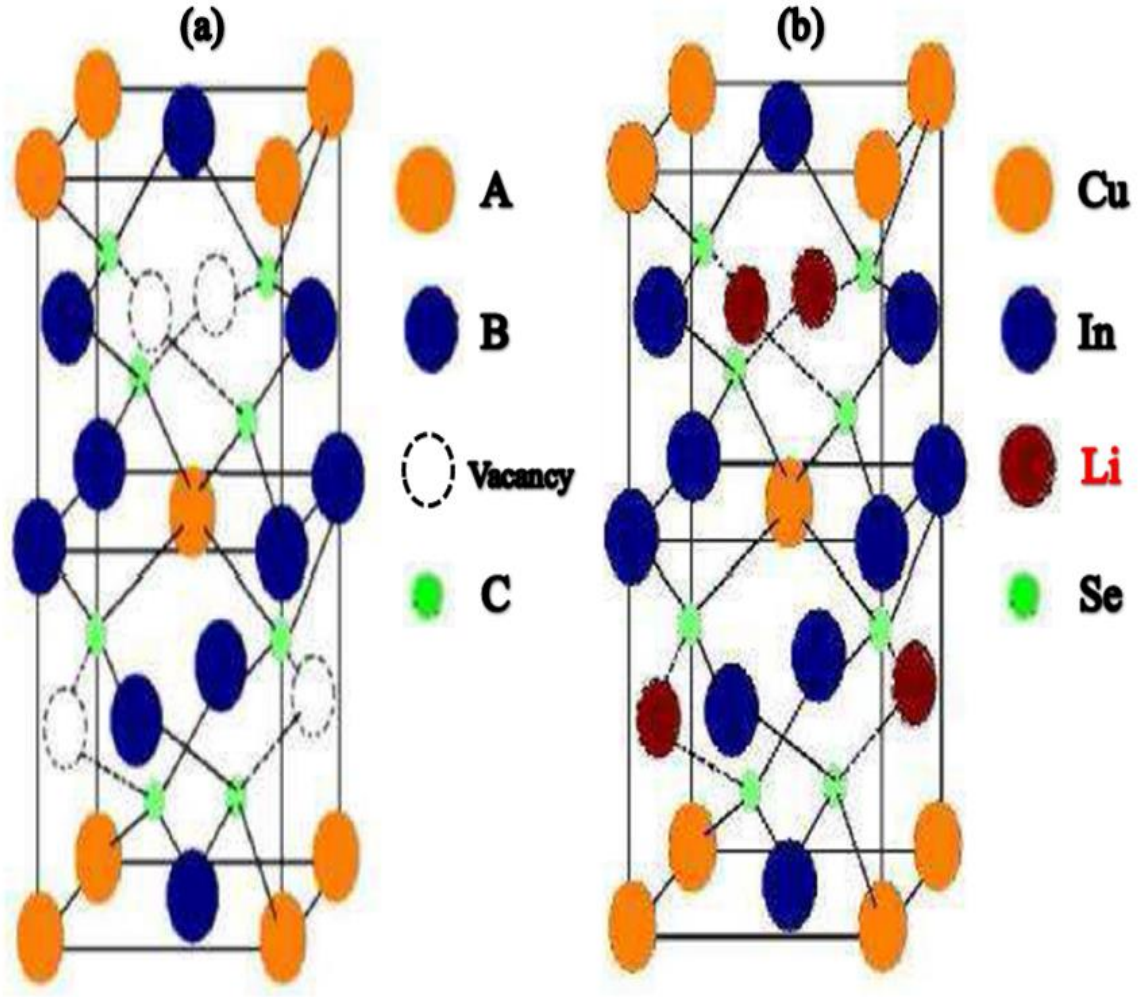

Fig.II.9: a) defect chalcopyrite, b) doped chalcopyrite

II.9.physico-chemical characteristics of chalcopyrite [9]:

Colour: brassy yellow, iridescent, especially warm brassy yellow, more yellow than chalcopyrite, chalcopyrite often has red, blue, purple or green tones, which can be confused with bornite

Mineral shine: Matte metallic

Transparency: opaque

Fracture: brittle and fragile

Hardness: from 3.50 to 4.00 (Mohs scale)

Crystal clear habits: The predominant disphenoid is like two opposing wedges and looks like a tetrahedron. Crystals sometimes twinned

Associated minerals: Quartz, fluorite, baryte, dolomite, calcite, pentlandite, pyrite and other sulphides.

Better indicators: Crystal habit, soft and delicate.

Electricity: conductor

II.10.Varieties and mixtures:

Gold-bearing chalcopyrite: Gold-bearing chalcopyrite seems to be fairly widespread in the United States (USA); in Europe, it is only recorded in Colle Panestra, Molazzana, Alpi Apuane,Lucca, Tuscany, Italy **[13].**

Chalcopyrite stannifère : variété stannifère de chalcopyrite trouvée à Toyoha, Sapporo, île d'Hokkaido, Japon **[15].**

Blister Copper: botroidal variety known in the USA and especially in Cornwall: Cook's Kitchen Mine, Carn Brea and Tincroft United Mine, Carn Brea area, Camborne - Redruth - St Day District **[14].**

II.11.Known phases with the chalcopyrite structure

Table.II.4: Some known ternary chalcopyrites type I-III-VI_2

The compound	a (A°)	c (A°)	c/a	μ	Fusion point (K)	E(eV)	Ref
$LiBO_2$	4.196	6.511	1.55	-	-	-	[31]
$CuBSe_2$	5.539	10.734	-	-	-	-	[31]
$CuAlTe_2$	5.976	11.80	1.97	-	1160	2.06	[31]
$CuGaS_2$	5.359	10.49	1.96	-	1513	2.43	[20]
$CuGaSe_2$	5.596	11.004	1.96	-	1310	1.71	[21]
$CuInS_2$	5.528	11.08	2	-	1300	1.54	[22]
$CuInSe_2$	5.782	11.62	2.01	-	1259	0.95	[23]
$CuInTe_2$	6.161	12.360	2	-	970	0.96	[24]
$CuTIS_2$	5.591	11.19	2	-	-	-	[31]
$CuTISe_2$	5.844	11.65	1.99	-	680	1.07	[32]
$CuLaS_2$	5.25	10.86	1.93	-	-	-	[31]
$AgAlS_2$	5.706	10.28	1.80	-	1323	3.13	[31]
$AgAlSe_2$	5.968	10.77	1.80	-	1220	1.66	[31]
$AgAlTe_2$	6.309	11.85	1.88	-	1000	0.56	[31]
$AgGaS_2$	5.755	10.28	1.78	-	-	2.55	[31]
$AgGaSe_2$	5.985	10.90	1.82	-	1120	1.8	[31]
$AgGaTe_2$	6.301	11.96	1.90	-	990	1.1	[31]

Table.II.5: Some known ternary chalcopyrites type II-IV-V_2

The compound	a (A°)	c (A°)	c/a	μ	Fusion point (K)	Eg (eV)	Ref
$ZnSiP_2$	5.407	10.451	1.93	-	-	2.3	[33]
	5.399	10.435	1.932	0.269	-	2.96	[32]
$ZnSiAs_2$	5.606	10.890	1.940	-	1357	2.12	[23,33]
	5.666	11.051	1.951	0.264	-	-	[31]
$ZnGeP_2$	5.466	10.722	1.961	-	1295	2.34	[32,30]
$ZnGeAs_2$	5.672	11.153	1.970	-	1150	0.85	[33]
$ZnSnP_2$	5.651	11.303	2.000	0.239	-	1.66	[31]
$ZnSnAs_2$	5.852	11.703	2.000	-	910	0.65	[31]
$ZnSnSb_2$	6.28	12.56	2.000	-	-	-	[32]
$ZnSiSb_2$	6.077	-	1.922	0.270	-	0.9	[32]
$ZnGeSb_2$	6.111	-	1.95	0.263	-	0.5	[32]
$CdSiP_2$	5.671	10.423	1.838	-	1470	2.20	[32]
$CdSiAs_2$	5.884	10.882	1.85	-	-	1.55	[30]
$CdGeP_2$	5.741	10.775	1.880	-	1060	1.80	[30]
	5.811	10.976	1.889	0.283	-	1.49	[31]

II.12.The crystal structure of the compounds $AgGa(S,Se)_2$

The materials subject of my study are called silver gallium Sélénium/Sulfur of formula $AgGaS_2$ and $AgGaSe_2$, they are important members of the ternary semiconductor family III-VI_2 (ABC_2) (where A: Cu, Ag; B: Al, Ga, In, Tl and C: S, Se and Te) which are isoelectronic analogues of the analogues of the binary II - VI semiconductors. They adopt the typical structure of chalcopyrite, with a space group I-42d and a tetragonal system. Its lattice is described by a mesh having a shape of a rectangular parallelepiped with sides a, a and c. The

mesh consists of two interpenetrating face-centred cubic networks. One lattice is composed of selenium/Sulfur and the other is an ordered row of silver and other cations (Ga), it therefore follows that each S/Se atom in the $AgGa(S,Se)_2$ compounds is surrounded by two atoms of the other species.The quadratic elemental lattice of the chalcopyrite structure can be also considered as two blende meshes one above the other along the z-axis but with alternately two different cationic planes (Ag and Ga) in this direction as well as in the (110) direction.The fact that replacing the single cation in the blende structure with two different cations (involving different bond strengths of Ag-S/Ag-Se and Ga-S/Ga-Se) creates two major distortions in the "parent" structure. One is the displacement of the anion sites from their equilibrium position (a/4; a/4; a/4) in blende. because the angles between the bonds in the tetrahedron are different from each other (Ag-S/Se-Ga ~ 106.581°, Ag-S/Se-Ag ~ 100.020° and Ga-S/Se-Ga ~ 111.0°) **[14]**, This difference is due to the electronegativity effect of Sulfur/selenium **[15]**. The other is the compression of the elementary mesh along the direction (001) forming the quadratic structure which is characterised by the ratio c/a =1.888; the distortion parameter (n= c/2a = 0.944) **[16]**. These two distortions give the chalcopyrite structure an anisotropy that was not present in the blende structure.

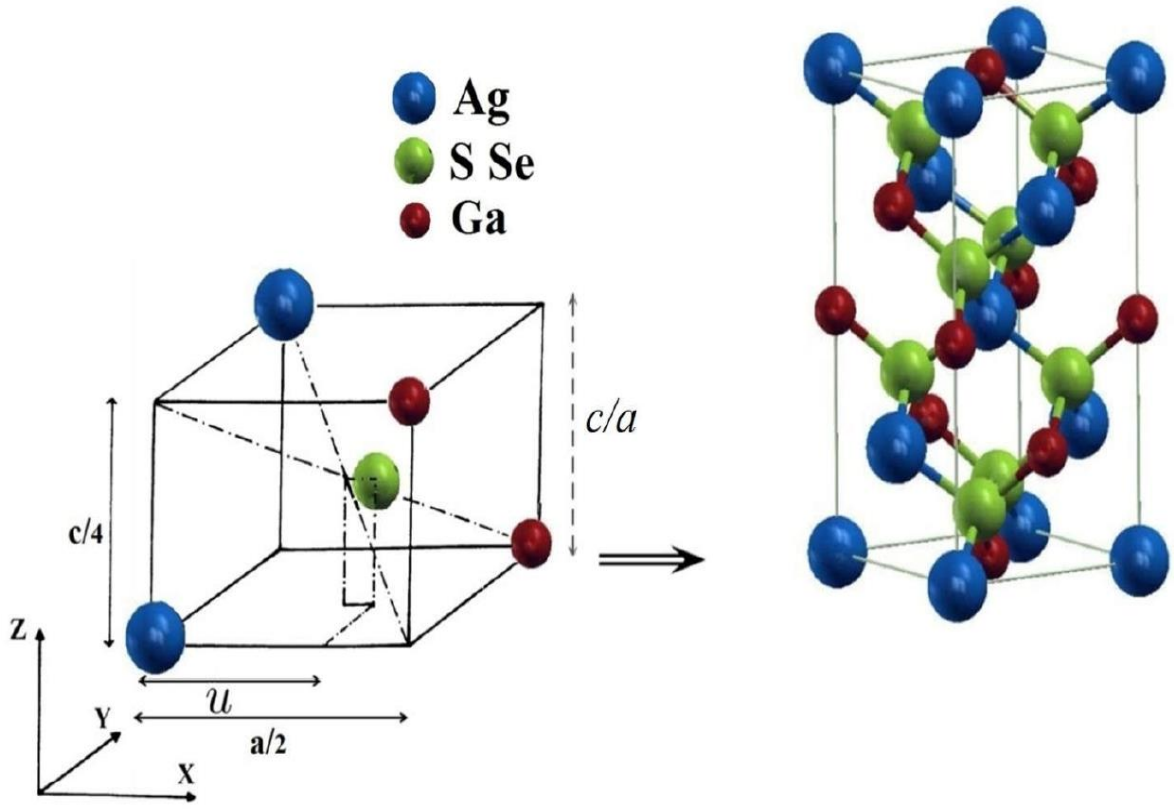

Fig.II.10: Graphical representation of the chalcopyrite structure $AgGaSe_2$, as well as the distortion and the internal position u in the z direction **[26]**.

This type of chalcopyrite occupies the Wyckoff positions given in the table [26].

Table.II.6: Wyckoff positions of $AgGa(S,Se)_2$

(I42-d)	x	y	z
Ag	0	0	0
Ga	0	0	(1/2)c
(S,Se)	u	(1/4)a	(1/8)c

II.13.Chalcopyrite applications

Semiconductors with the formula I-III-VI_2 which crystallize in the chalcopyrite structure have recently attracted attention for their applications in non-linear optical devices, and solar cell detectors.

They can have potential optoelectronic applications such as solar energy converters, non-linear optical devices (NLOs), light emitting diodes (LEDs), and detectors.

CuInSe2 chalcopyrite compounds and CuInS2 -CuGaS2 system alloys have been used as absorber layers for thin film solar cells.

They reduce nucleation and improve crystal morphology.

They are useful for non-linear optical frequency conversion applications.

The $CuGaS_2$ alloy system has attracted considerable attention, because this material has a wide direct band gap, which is within the desirable range for applications in solid state lighting and high efficiency tandem solar cells a solar cell [19].

II.14.Prominence of chalcopyrite compounds

The advantages of chalcopyrites include:

1/ They are manufactured as thin films, either p-type or n-type, which allows the production of a variety of low-cost homo- and heterojunction components.
2/ They are direct-gap semiconductors, a factor that minimises the diffusion length of minority charge carriers.
3/ They have gap energy in the optimal range for the conversion of solar energy into electrical energy at the earth's surface.

4/ Their lattice parameters and electron affinity are in good coordination with those of CdS, which is a large direct gap semiconductor which has already proven its effectiveness in solar cells. It can be said that the importance of these materials applications, especially in the visible and infrared range through solar cells, light emitting diodes, and infrared detectors.

II.15.Conclusion

Chalcopyrite materials are promising in many fields of electronics, optics and photonics because of their excellent properties. In this chapter we have reviewed the knowledge about the chalcopyrite family such as the crystal structure, the different types, etc. We have also presented the materials that are the subject of our study.

Bibliography

[1] L. L. Kazmerski, Nuovo Cimento, 20, 1983(2013).

[2] J. L. Shay and J. H. Wernic Ternary chalcopyrite semiconductors growth, in: Electronic Properties and application, Pergamum Press, Newyork (1975).

[3] F. K. Hopkius, Laser Focus World 31, 87 (1995)

[4] S. K. Deab and A. Zunger Ternary Multinary Compounds. Mater. Res. Soc. Conf. Proc, 37,(1987).

[5] D. E. KERROUM, « *Etude des propriétés structurales, électroniques, élastiques et optiques des chalcopyrites CuInX2 (X=S, Se ,Te)* », Université d'USTO , Oran, Mémoire (2013).

[6] P.C. Ricci, A. Anedda, R. Corpino, C.M. Carbonaro, M. Marceddu, I.M. Tiginyanu, V.V. Ursaki, Temperature dependence of the photoluminescence spectra in AgGaS2, J. Phys. Chem. Solid. 66 1950–1953 (2015).

[7] J.J. Zondy, D. Touahri, O. Acef, Absolute value of the d36 nonlinear coefficient of AgGaS2: prospect for a low-threshold doubly resonant oscillator-based 3:1 frequency divider, J. Opt. Soc. Am. B 14 (10) 2481–2497 (1997).

[8] M.M. Asadov, S.N. Mustafaeva, Xray dosimetry of an AgGaS2 single crystal, Bull. Russ. Acad. Sci. Phys. 79 (9) 1113-1117 (2015).

[9] Canadian Mineralogist, volume 018, pp. 157(1980)

[10] Henckel, J.F. Pyritologia, oder Kieß Historie. Verlegts Johann Christian Martini (Leipzig), pages 114-115 (1725).

[11] Biagioni, C. Minerali della Provincia di Lucca. Associazione Micro-Mineralogica Italiana, Crémone, 352 pp. (2009).

[12] Canadian Mineralogist, volume 018, pp. 157(1980)

[13] TAN Jia-Jin, JI Guang-Fu, CHEN Xiang-Rong and GOU Qing-Quan, Commun. Theor. Phys. (Beijing, China) 53, pp. 1160–1166 (2010).

[14] O. BRISSON, « *Elaboration et caractérisation de monocristaux de AgGaX2 (X=S, Se) pour l'optique non-linéaire dans l'infrarouge* », Université de Bordeaux 1, Thèse (1995).

[15] A. Chahed, O. Benhelal, S. Laksari, B. Abbar, B. Bouhafs, N. Amrane, Physica B 367, 142 (2005).

[16] E. I. Rogacheva, Cryst. Res. Technol, 31, S, 1-10 (1996)

[17] I Berger and D. Prochuchan, *Ternary diamon like semiconductors* édité par Soviet Physics Semiconductors, Consultants Bureau -New York- London p 80 (1969).

[18] V. H. Hahn and W. Klinlgler, *Z. Anorg. Chem.* 263 177 (1950).

[19] J.E.Jaffe,A.Zunger,Phys.Rev.B 29 1882 (1984).

[20] B.Tell, J. L. Shay, and H. M. Kasper, phys. Rev. B4, 246 (19781).

[21] V. V. Kindyak, A. S. Kindyak, V. F/Gremenok, I. A. Vicrorov, Thin. Solid. Films 293, 75 (1989).

[22] B.M. Basol,V. K. Kapur, A. Halani and C. Leidsholm. Solar Ener. Mater. Solar Cells 29, 163 (1993).

[23] C. Guillén and J. Herrero, Solar. Energy. Materials and Solar, Cells 23, 31 (1991).

[24] M. J. Thwaites, R. D. Tomlinson, and M. J. Hampshire, in Ternary Compounds1977, edited by G, D, Holah (Institute of Physics London, 237 (1977).

[25] David L. Jones, '' The Leaching of Chalcopyrite'', Thèse de doctorat, University of British Colombia, Vancouver 8, Canada, (1974).

[26] Ouahrani Tarik, '' Calcul des properties structurales, thermiques et optiques des composes chalcopyrites par la méthode FP-(L)APW '', Thèse de doctorat en physique, Université de Tlemcen, (2011).

[27] Chahed Abbes, "Etude Ab-initio des propriétés structurales, électroniques et optiques des semi- conducteurs chalcopyrites $AgXY_2$ (X=Al, Ga, In et Y=S, Se, Te), thèse de doctorat d'état en physique, université de Sidi Bel Abbes, (2006).

[28] Wernicke et al, ''Ternary Chalcopyrite Semiconductors: Growth, Electronic Properties, and Applications'', (livre), Pergamon press, (1975).

[29] Siebentritt. S, Rau. U, ''Wide-Gap chalcopyrite'', (Livre), Springer-Verlag Berlin Heidelberg (2006).

[30] J. E. Jaffe and Alex Zunger, Physical Review B, Vol 28, N° 10, p5822-5847,(1983).

[31] Brian R. Pamplin et al, Prog. Crystal Growth Charact. Vol. 1, pp. 331-387 (1979).

[32] J. E. Jaffe and Alex Zunger, Physical Review B, Vol 29, N° 4, p1882-1906, (1984).

[33] V. L. Shaposhnikov et al, Physical Review B 85, 205201 (2012).

[34] T.Ouahrani, '' Calcul des properties structurales, thermiques et optiques des composes chalcopyrites par la méthode FP-(L)APW, Thèse de doctorat en physique, Université de Tlemcen, (2011).

[35] A. Miller, A. Mackinnon and D. Weair, Solid State Physics, Vol. 36, No. C, p. 119-175 (1982).

Chapter

III

Study of the structural and optoelectronic properties of the material $AgGa_{x-1}Tl_xS_2$

Chapter III

Study of the structural and optoelectronic properties of the material $AgGa_{x-1}Tl_xS_2$

III.1.Introduction

The materials of the chalcopyrite family are very promising candidates for solar cell applications due to their ideal optical properties as well as relatively low-cost preparation methods **[1–3]**. Those physical properties give rise to numerous applications in everyday life such as light-emitting diodes (LEDs), nonlinear optics (NLO) and other optoelectronic components **[4–9]**. Our main focus in this section was to analyse the impact of Ga substitution by Tl on the structural, electronic and optical properties of the compound $AgGaS_2$. For all of the calculations, we used the FP-APW+Io method implemented in the wien2k code within the framework of the density functional theory DFT. Indeed, we have opted for numerical simulation which plays an important role in the determination of the properties of our materials to reduce the costs of expensive experiments and to model phenomena that are difficult or impossible to carry out experimentally and to minimize the risks of dangerous experiments or even inaccessible in the laboratory. The material $AgGaS_2$, which is a material of the chalcopyrite family, was chosen for study because of its characteristics such as unique electronic and optical properties, direct band gap, transparent behavior against visible and infrared radiation, a high absorption coefficient and a lifetime in outer space longer compared to that of Si and III-V compounds **[10].** The high yield of 5.85% has been reported using $AgGaS_2$ chalcopyrite as the absorber layer **[11].** Hence, the main aim is to improve the optical and electronic properties of $AgGaS_2$ using band convergence strategy by substitution of thallium (Tl) in the gallium (Ga) site in the compound $AgGaS_2$ for the formation of an $AgGa_{1-x}Tl_xS_2$ alloy.

III.2.Calcul details

All calculations are done using the FP-APW+lo method **[12,13]**, implemented in the WIEN2k code **[14]**. In this technique, the system space is divided into two regions the interstitial one and the muffin-tin spheres with muffin-tin radius (RMT) are chosen in a manner that the MT spheres do not overlap. The RMT values are adjusted to be 2.5, 2.3, 2.41, and 1.88 a.u for Ag, Ga, Tl, and S, respectively, with the following electronic configuration Ag: [Kr] $4d^{10}5s^1$, Ga: [Ar] $4s^23d^{10}4p^1$, S: [Ne] $3s^23p^4$, Tl: [Xe] $4f^{14}5d^{10}6s^26p^1$. The electronic wave functions are expanded up to l_{max} equal to 4 and 10 outside and inside the MT sphere, respectively. Besides, the expansion of the wave functions and charge density were cut off by the $R_{MT}K_{max}$ = 7.5 and Gmax = 12 parameters. The exchange-correlation potential is treated by the generalized

gradient approximation performed by Wu and Cohen (GGA-WC) **[15]**. However, since the GGA approximation yields an underestimated band gap value, the Tran-Blaha modified Becke-Johnson (mBJ) exchange potential is employed **[16,17]**. Besides, the $AgGa_{1-x}Tl_xS_2$ alloys are modeled using 1x1x2 periodic supercells with 16 atoms in the primitive cell. The gallium atoms are substituted by thallium atoms to adopt all the possible configurations with Ga and Tl mixed atoms to generate $AgGa_{1-x}Tl_xS_2$ alloys with x = 0.25, 0.50, and 0.75. (See **Fig. III.1**).

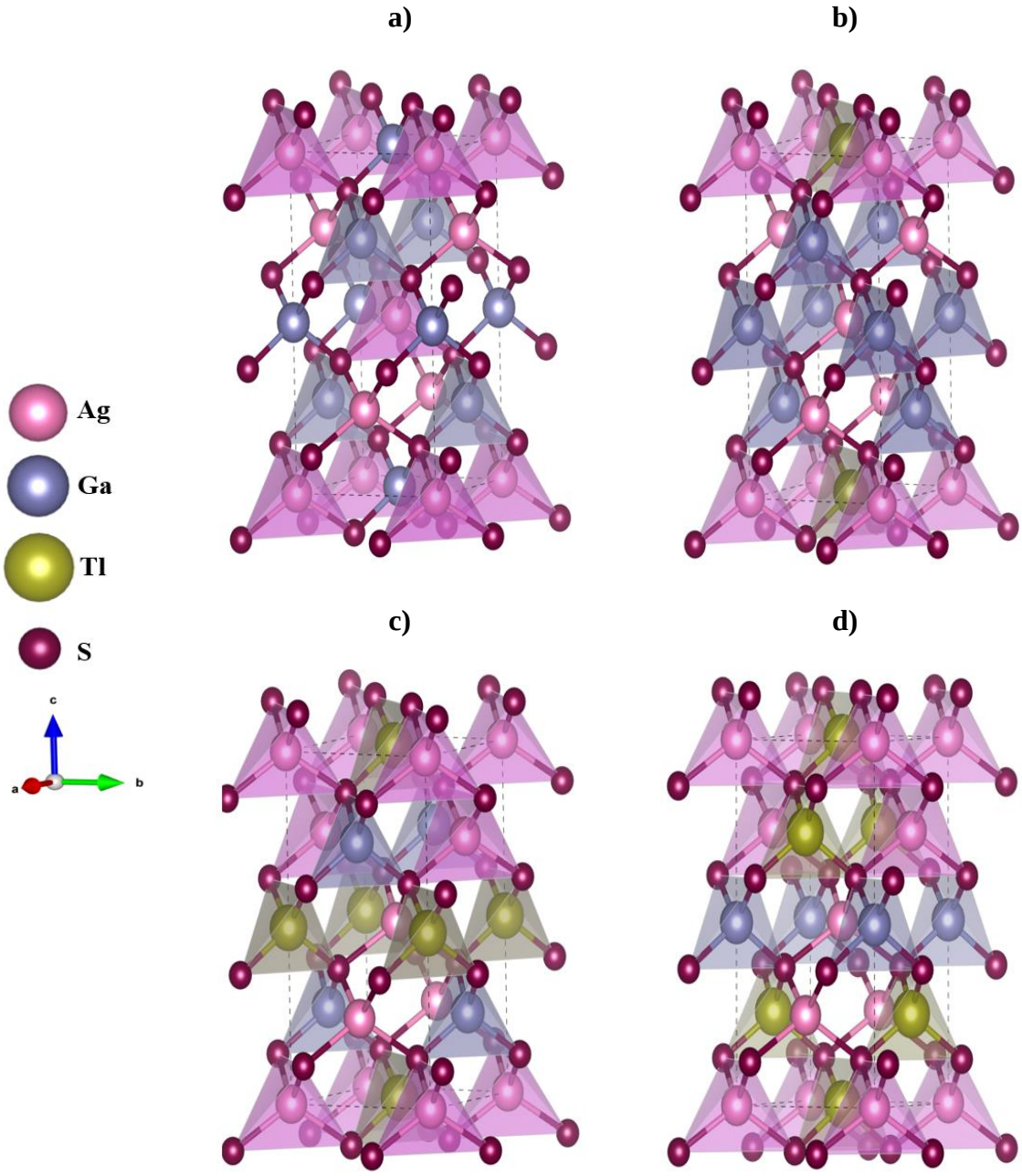

Fig. III.1: Visualization of crystal structure of $AgGaS_2$ **(a)**, and $AgGa_{0.75}Tl_{0.25}S_2$ **(b)**, $AgGa_{0.5}Tl_{0.5}S_2$ **(c)**, $AgGa_{\mathbf{0.25}}Tl_{\mathbf{0.75}}S_2$ alloy **(d)** obtained using VESTA software **[18]**.

III.2.1.Optimization of calculation parameters

It consists in achieving a compromise between good accuracy and minimum computation time. The optimisation is done using an SCF cycle based on the convergence of basic quantities related to the properties to be calculated **[16]**. In the case of structural, electronic and optical properties, the basic quantity is the total energy. This operation is often referred to as "convergence testing" because it aims to ensure the convergence of the quantity according to a criterion which will be chosen according to the desired precision of calculation. The convergence criterion we have chosen is: ec = 0.0001 Ry which is the default value.

The optimised parameters are as follows:

- The number of points k in the Brillouin zone,
- The product $Rmt \times Kmax$,
- The parameter $Gmax$.

The optimization results are shown in the following figure:

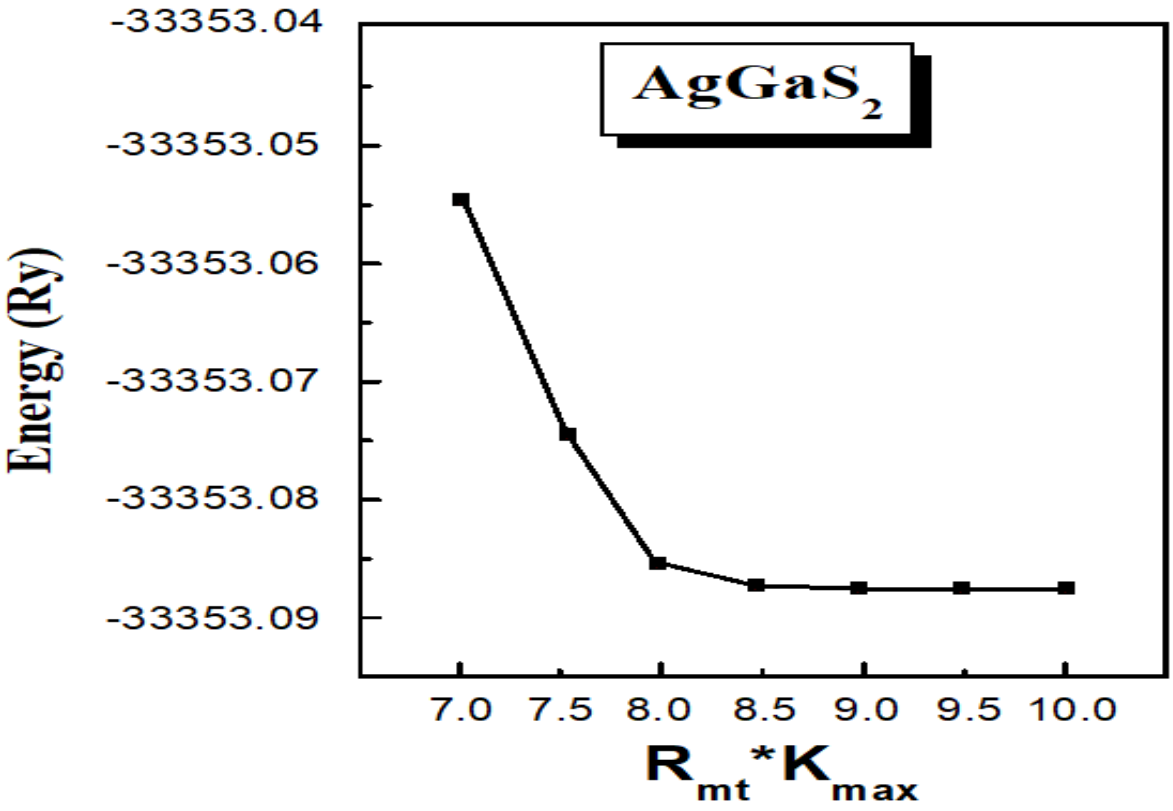

Fig.III.2: Curve of E_{Tot}(Ry) as a function of $Rmt \times Kmax$

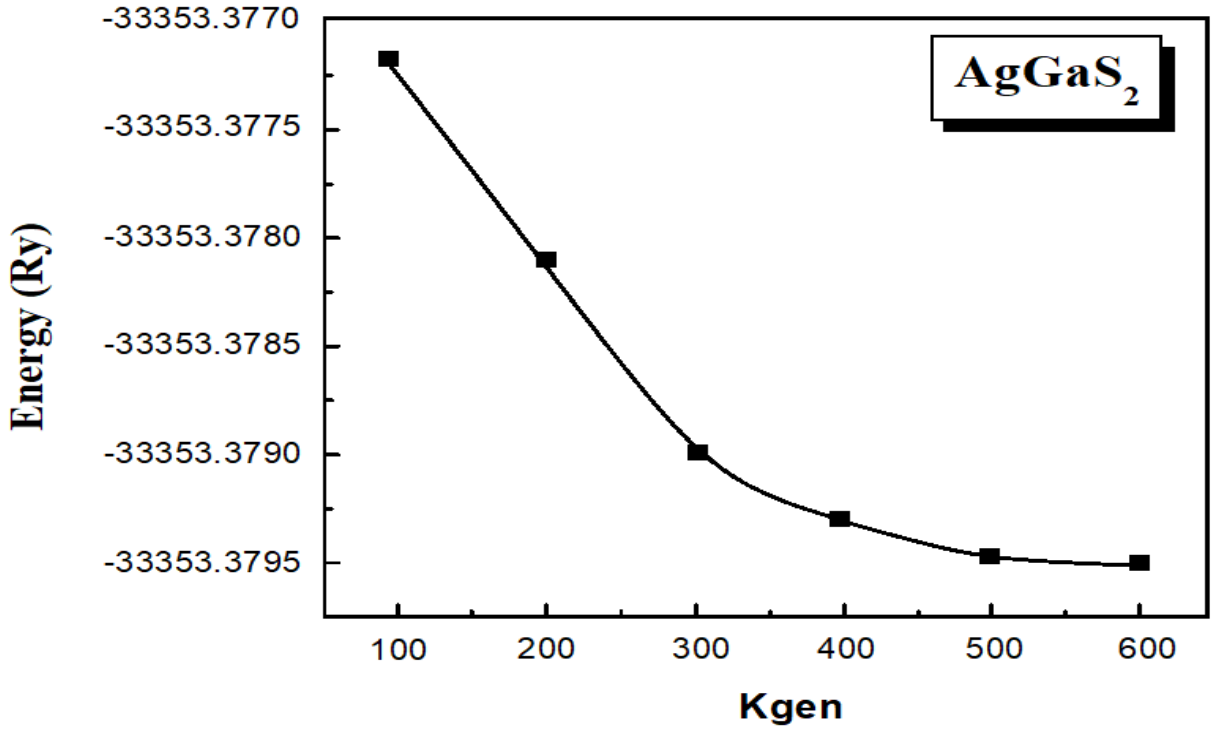

Fig.III.3: Curve of E_{Tot}(Ry) as a function of the number of points k

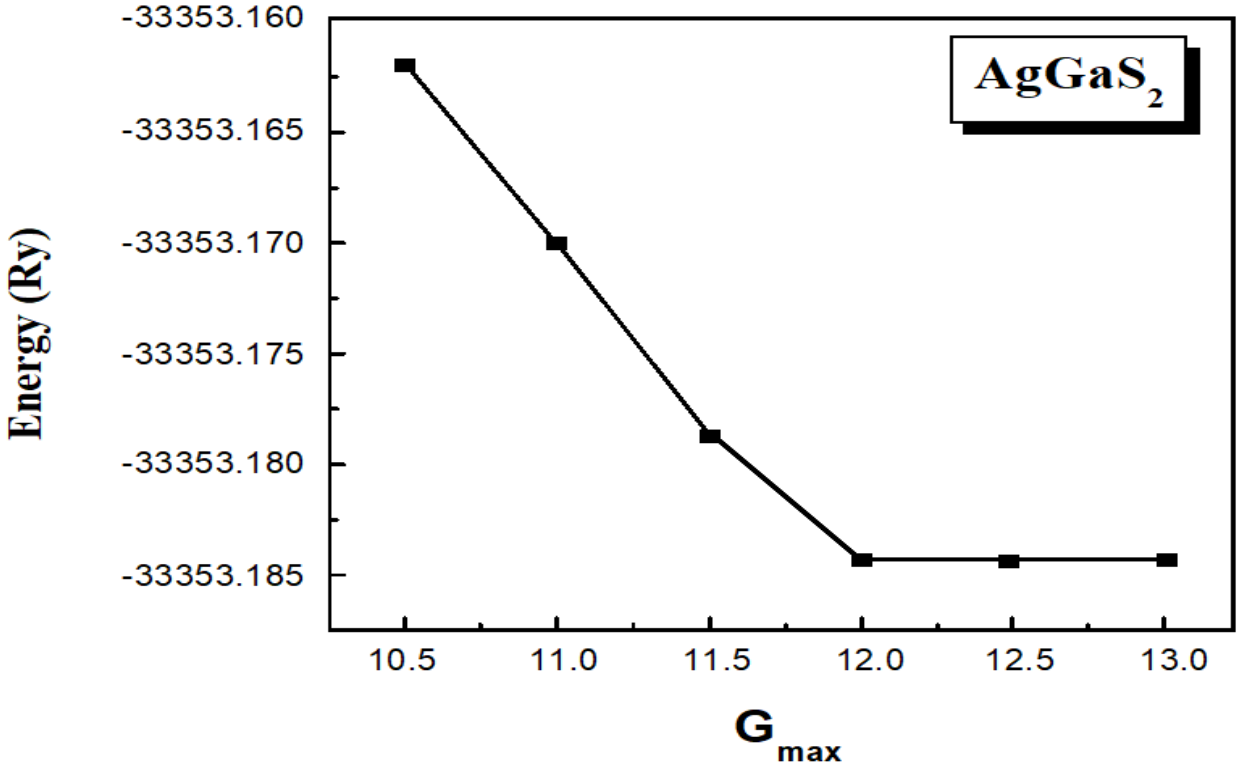

Fig.III.4: Curve of E_{tot} (Ry) as a function of G_{max}.

III.3.Structural properties

At ambient conditions, the $AgGaS_2$ material is reported to crystallize in chalcopyrite type-structure (space group l-42d) **[19]** (**see fig. III.1).** In this structure, the Ag atoms are situated at 4a (0, 0, 0), the Ga atoms at (0, 0, 1/2) and the S atoms at (0.28, 1/4, 1/8). Regarding this structure, we first optimized the anion displacement parameter u_S with $1x10^4$ Ry/a.u. force convergence criteria, and then calculated the total energy as a function of volume and c/a ratio for $AgGaS_2$ (**see fig.III.5 & fig.III.6)** and then for each alloy. After that, the ground-state properties such as lattice parameters (a and c), bulk modulus B and its first pressure derivative B_0 are determined through the Murnaghan equation **[20]** fitting of the energy vs. volume optimization curves. The results of the estimated structural properties (a, c, B and B') of $AgGa_{1-x}Tl_xS_2$ alloys are reported in **Table III.1** along with experimental **[21,22,23]** and theoretical results **[24–28]**. The resulting values are in reasonable agreement when compared to the experimental values. The difference in values between the calculated unit cell parameters and the experimental values is less than 0.2%. From **Table III.1**, one can observe that both a and c increase when Tl atoms are gradually substituted into Ga atoms in the $AgGaS_2$ unit cell. Conversely, the bulk modulus was found to decrease with increase in Tl concentration owing to increase in the interatomic distance in the $AgGa_{1-x}Tl_xS_2$ alloys from x=0 to x = 1 (see **Table III.2**).

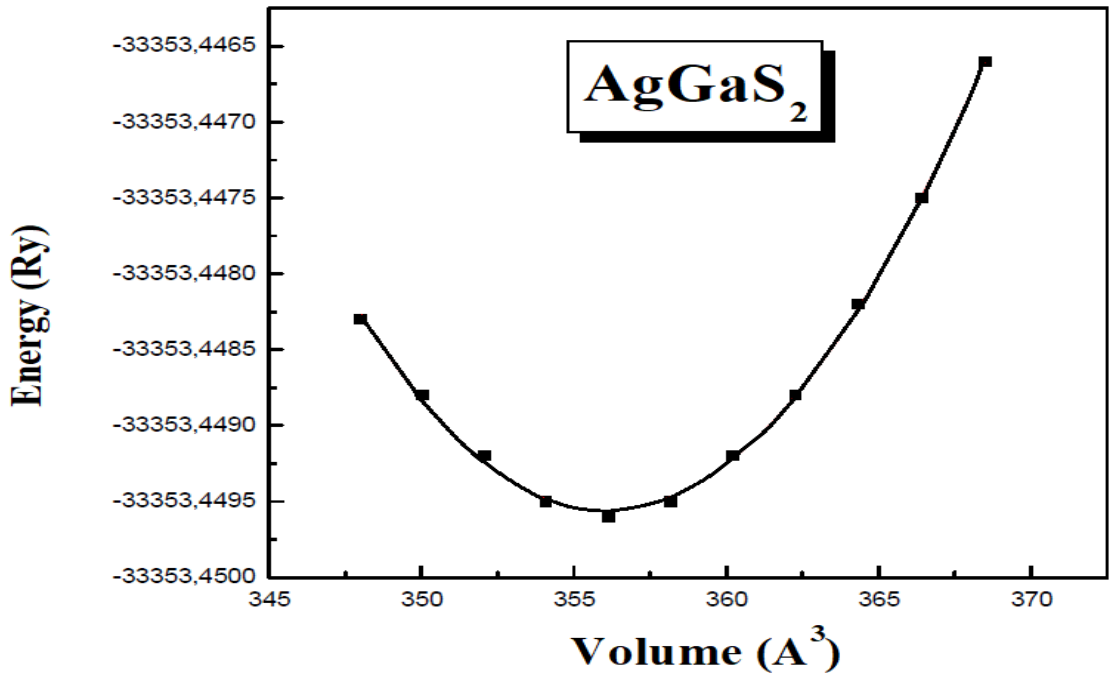

Fig.III.5: variation of the total energy as a function of the volume of the $AgGaS_2$

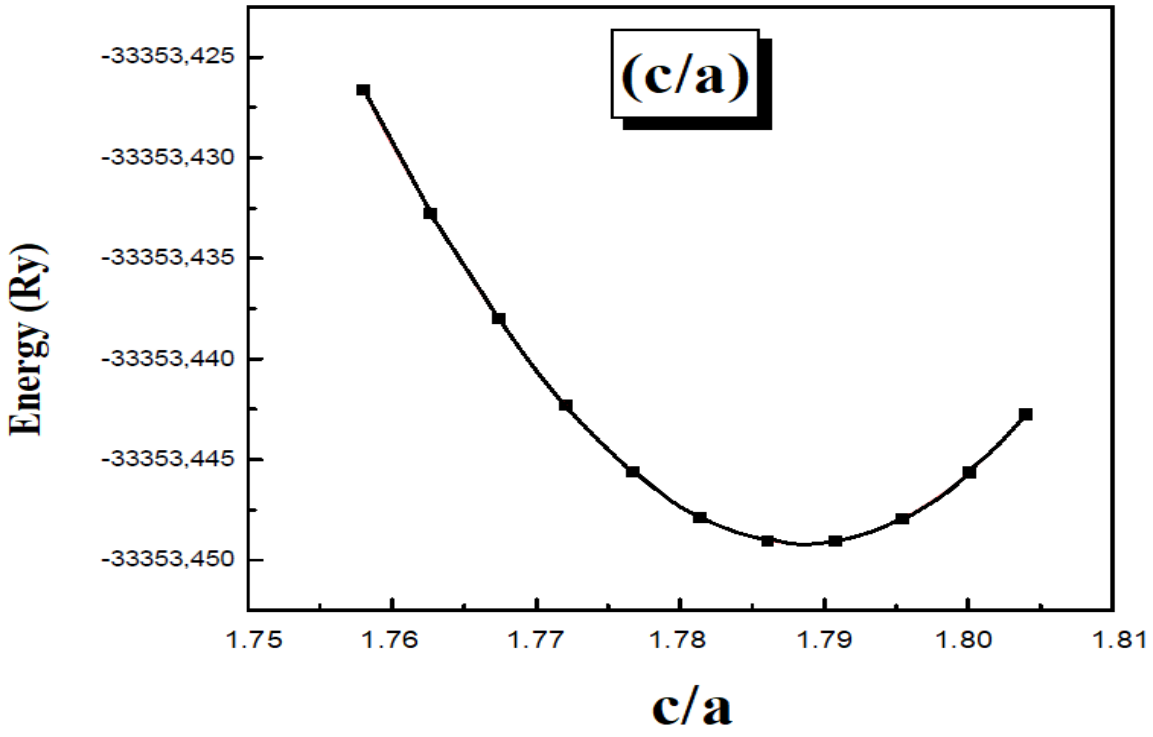

Fig.III.6: variation of the total energy as a function of the c/a of the $AgGaS_2$ compound

Table III.1: The calculated lattice constant (*a* and *c*) (Å), the anion displacement parameter *u*, bulk modulus (GPa) and its pressure derivative, and formation energy (KJ/mol) for $AgGa_{1-x}T_xS_2$ Alloys.

$AgGa_{1-x}Tl_xS_2$		*a*	*c*	*u*	*B*	*B'*	E_f
x = 0	This work	5.746	10.266	0.287	75.08	4.88	-328.05
	Expt.	5.755[32]	10.278[32]	0.282[32]	77.6[32]	4[30]	
	Other calc.	5.587[31]	10.408[31]	0.288[24]	67.15[25]	4.744[25]	-386.5[29]
		5.742[26]	10.26[26]	0.2844[27]	72.62[26]	4.7[27]	-359.4[29]
		5.75[28]	10.299[28]	0.281[28]	76.2[28]	5[28]	
x = 0.25	This work	5.868	10.493	0.268	68.82	4.56	-275.948
x = 0.5	This work	5.98	10.67	0.257	61.45	4.63	-300.069
x = 0.75	This work	6.09	10.86	0.244	56.95	4.73	-262.44
x = 1	This work	6.22	11.12	0.239	59.95	4.77	-246.92
	Other calc.	5.882[28]	10.92[28]	0.257[28]			

Table III.2: Interatomic distance for $AgGa_{1-x}Tl_xS_2$ alloys.

$AgGa_{1-x}Tl_xS_2$		Ag—S	Ga--S	Tl—S
x = 0	This work	2.524	2.293	-
	Expt. [32]	2.556 ± 1	2.276 ± 1	-
x = 0.25	This work	2.577	2.342	2.342
x = 0.5	This work	2.625	2.385	2.385
x = 0.75	This work	2.673	2.429	2.429
x = 1	This work	2.565	-	2.644

In the aim of analyzing the stability and formation of $AgGa_{1-x}Tl_xS_2$ alloys, the formation energy Ef is predicted as below:

$$E_f(AgGa_{1-x}Tl_xS_2) = 1/N\left(E_T(AgGa_{1-x}Tl_xS_2) - \left[E_{Ag} + (1-x)E_{Ga} + xE_{Tl} + 2E_S\right]\right) \quad \textbf{(III.1)}$$

Where, E_T ($AgGa_{1-x}Tl_xS_2$) is the total energy and E_{Ag}, E_{Ga}, E_{Tl} and E_S are the energies of Ag, Ga, Tl and S atoms, respectively (see **Table III.3**). From **Table III.1** it is remarked that the estimated E_f is negative suggesting thermodynamic stability of all $AgGa_{1-x}Tl_xS_2$ alloys. It is also noticed that the current calculated E_f of pure $AgGaS_2$ is in good agreement with that estimated by Kumar et al. **[29].**

Table III.3: The total energy E_T of $AgGa_{1-x}Tl_xS_2$ alloys and the energies of Ag, Ga, Tl and S atoms in (eV).

E_T ($AgGaS_2$)	E_T ($AgGa_{0.75}Tl_{0.25}S_2$)	E_T ($AgGa_{0.5}Tl_{0.5}S_2$)	E_T ($AgGa_{0.5}Tl_{0.75}S_2$)	E_T ($AgTlS_2$)
-4.385 517 $x10^5$	-1.376 255 $x10^9$	-1.875 427 $x10^6$	-2.374 59 $x10^6$	-1.056085 x 10^5
E_{Ag}	E_{Ga}	E_S	E_{Tl}	
-5.288 679 x 10^4	-1.446 705 x 10^5	-1.085 236 x 10^4	-5.520 529 x 10^5	

III.4.Electronic properties

III.4.1.Band structures

The energy bands give the possible energies of an electron as a function of the wave vector. For simplicity, only the directions of highest symmetries in the first Brillouin zone are treated. The access to the band structure is the essential parameter for the realisation of optoelectronic devices. The critical point of the band structure corresponds to the value of the energy separating the valence band maximum from the conduction band minimum (gap).We have calculated the band structure of $AgGaS_2$ and $AgGa_{1-x}Tl_xS_2$ alloys along the high symmetry lines in the first Brillouin zone. **Fig. III.7** demonstrates clearly that both the top of the valence band (VB) and bottom of the conduction band (CB) are located at the same high symmetry point (Γ), without overlapping between them. Thus, $AgGaS_2$ is a semiconductor material with a direct band gap of about 0.96 eV with GGA-WC. This band gap value is significantly lower than the experimental measurement (see **Table III.4**) which is due to the well-known shortcoming of the GGA approximation. Hence, the band structure is also estimated employing the WC-GGA þ TB-mBJ where the band gap value found is equal to 2.59 eV, which agrees well with the experimental values **[32–35]**. Moreover, using WC-GGA+TB-mBJ, the band structure of $AgGa1_{-x}Tl_xS_2$ alloys is calculated **Fig.III.7**. We remarked that when the Ga atom is substituted by the Tl atom the nature of the band gap and the semiconducting character is retained, however the minimum of the CB is shifted towards the Fermi level resulting in a reduction of the band gap value to be 2.17 eV, 1.84 eV, 1.53 eV, 0.65 eV for $AgGa_{0.75}Tl_{0.25}S_2$, $AgGa_{0.5}Tl_{0.5}S_2$, $AgGa_{0.25}Tl_{0.75}S_2$, and $AgTlS_2$, respectively. This behavior is mainly coming from the increase of the atomic size from Ga to Tl atom. In addition, due to the presence of the heavy atom (Tl) the spin-orbit coupling (SOC) is included **Fig.III.7**. It is well observed that SOC influences the band structures causing reduction of the energy band gap to be 1.91 eV, 1.61 eV, 1.28 eV, and 0.61 eV for $AgGa_{0.75}Tl_{0.25}S_2$, $AgGa_{0.5}Tl_{0.5}S_2$, $AgGa_{0.25}Tl_{0.75}S_2$, and $AgTlS_2$, respectively. This spin-orbit coupling also increases the degeneracy of the bands near VBM in Γ-point. We note here that the band gap values of $AgGa_{0.75}Tl_{0.25}S_2$, $AgGa_{0.5}Tl_{0.5}S_2$, and $AgGa_{0.25}Tl_{0.75}S_2$are quite similar to the established absorbent materials such as Cu_2ZnSnS_4 **[36]**, GaAs **[37]**, CdTe **[38]**, and $CH_3NH_3PbI_3$ **[39]**, which proving their promising candidates for photovoltaic (PV) applications.

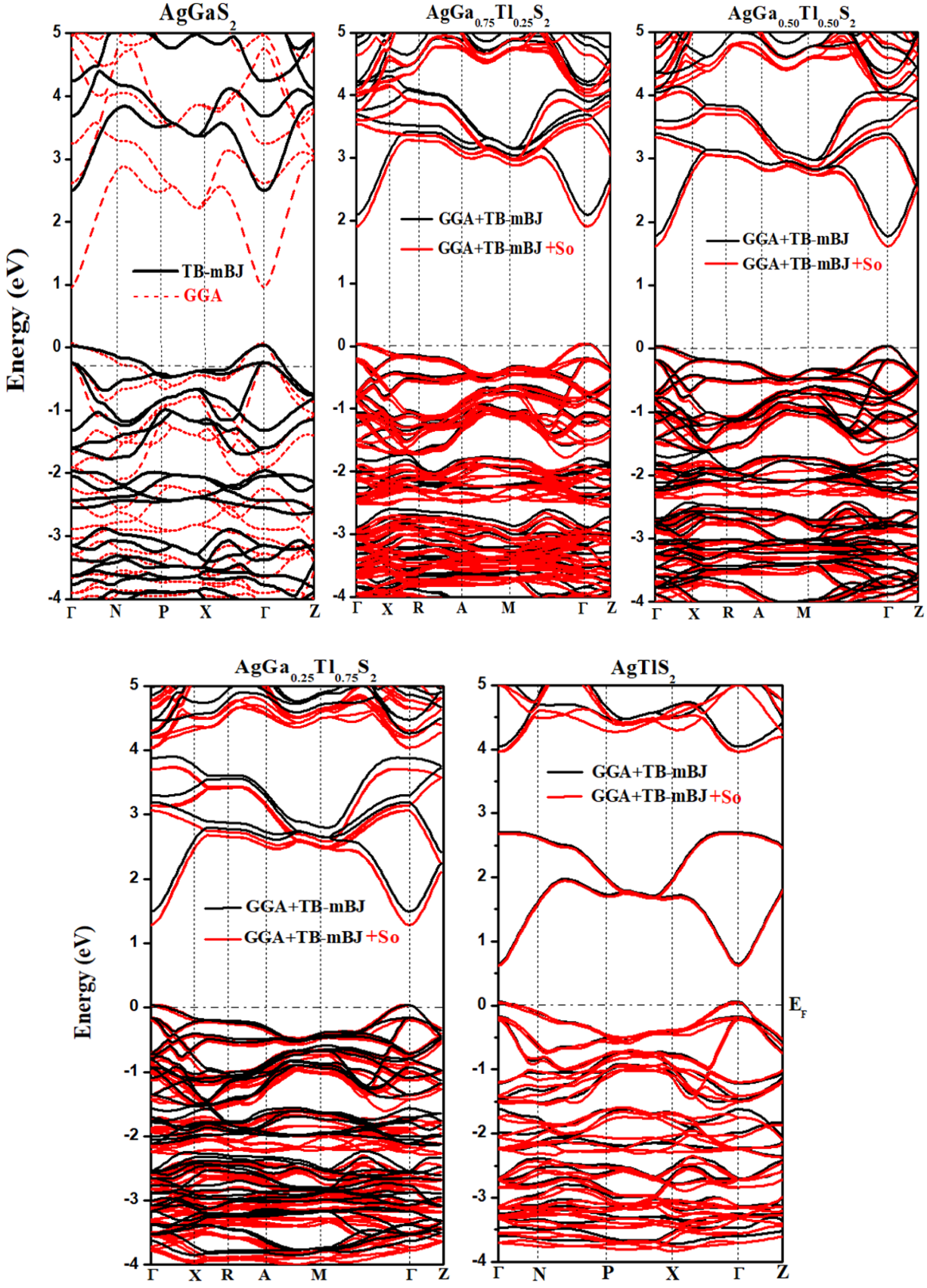

Fig.III.7: The calculated band structure of $AgGa_{1-x}Tl_xS_2$ alloys.

III.4.2.Density of states

The density of electronic states (DOS) N(E) is defined as the quantification of the number of electronic states with a given energy in a material. It can also be defined by N(E)dE which is the number of electronic states of energy between E and E + dE per unit volume of the solid or, more frequently, per unit cell of the crystal studied. The density of states is equal to the integral of the spectral function over the first Brillouin zone and is given by the following relation:

$$\boldsymbol{N(E) = \sum_n \int \frac{d^2K}{4\pi^2} \delta(E - \varepsilon)} \qquad \textbf{(III.2)}$$

In order to accurately identify the states forming each band we have plotted the total (TDOS) and partial (PDOS) densities of states for $AgGa_{1-x}Tl_xS_2$ alloys at different concentrations x, through the WC-GGA+TB-mBJ approximation for (x =0) and including the SOC for (x = 0.25, 0.5, 0.75, and 1). From **Fig.III.8** one can remark that the valence band of $AgGaS_2$ is divided into two sub-bands. The first one is starting from the top (zero energy) to -5 eV labeled as VB_1 and the second one from -5 eV to -8 eV labeled as VB_2. The VB_1 is mostly originated from the cation Ag '4d' states hybridized with S '3p' states suggesting covalent character for Ag–S bond. While in VB_2 the bands are derived from a combination of Ga '4s' states and anion S '3p' states. Whereas, the conduction band of $AgGaS_2$ mainly comes from Ga '4s, 4p' states hybridized with the anion S '3p' states, the bottom of the conduction band has a dominant contribution from Ga '4s' states. However, when Gallium is replaced by thallium, the valence band structure of $AgGa_{1-x}Tl_xS_2$ (x = 0.25, 0.5, 0.75, and 1) alloys remains unchanged except near the Fermi level where a small contribution of Tl 'd' state is observed. However, with increasing Tl content the S'3p'-Ag'4d' hybridization state is pushed up towards higher energy to become between -3.8 eV and EF level in the case of $AgTlS_2$ compound. Inversely the substitution of Tl atoms into Ga sites highly affects the conduction band. This Tl substitution leads to the formation of new states in the CB minimum, which mainly comes from the Tl '6s' states. These Tl '6s' states are hybridized with Ga '4s' states for $AgGa_{1-x}Tl_xS_2$ (x = 0.25, 0.5, and 0.75) alloys and lowered the CBM and thus the band gap value is diminished. In contrast, for $AgTlS_2$ the CB minimum is derived from a combination of Tl '6s' states and anion S '3p' states. It is previously reported that the anion displacement affected the band gap value of the $AgGaX_2$ chalcopyrite **[46]**. Hence the band gap reduction can be explained by the increase of the atomic size from Ga to Tl and the decrease in the internal parameter u (see **Table III.1)** as the Tl concentration increase.

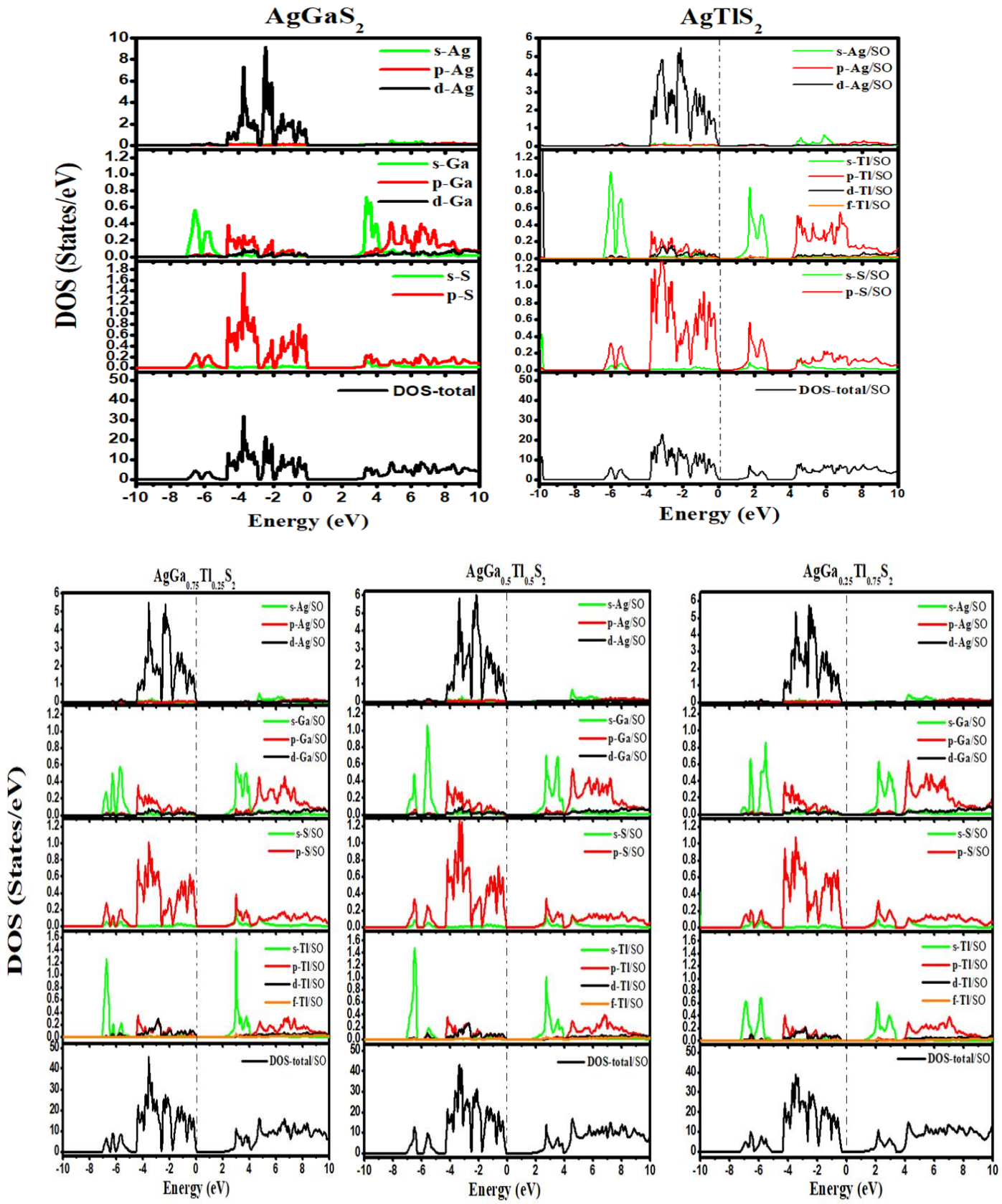

Fig.III.8: Total and partial density of states (DOS) of $AgGa_{1-x}Tl_xS_2$ alloys.

III.5.Carrier effective mass and mobility

Using the calculated band structure we have calculated the effective mass of holes (m_h*) from the maximum VB and the electrons effective mass (m_e*) from the minimum CB for $AgGa_{1-x}Tl_xS_2$ alloys using the following Equation:

$$\boldsymbol{m^*} = \hbar^2 \left(\frac{\partial^2 E}{\partial^2 k}\right)^{-1} \quad \textbf{(III.3)}$$

The results are summarized in **Table III.3**. It is remarked that the electron effective mass is lower than the hole effective mass for pure $AgGaS_2$, which agrees reasonably with the previous finding **[40,41]**. Besides, as this mass is linked to the band gap and this later is tuning after Tl substitution, it is also expected that this mass will be affected. Therefore, we have also calculated both hole and electron effective mass of $AgGa_{1-x}Tl_xS_2$ alloys (**Table III.4**). One can see that both hole and electron effective masses decrease when Ga is substituted by the Tl atom. Relying on the deformation potential theory **[42]**, the carrier mobility for this compound is determined using the following relation:

$$\boldsymbol{\mu} = \frac{(8\pi)^{1/2}\hbar^4 e C_{ii}}{3(m^*)^{5/2}(k_B T)^{3/2} E_\alpha^2} \quad \textbf{(III.4)}$$

where ħ, C_{ii}, e, m*, k_B, T, E_α are respectively, the reduced Planck constant, elastic modulus, the element charge, effective mass (of a hole (m_h*) or electron (m_e*)), Boltzmann constant, temperature, and deformation potential constant of the CB minimum for electron or VB maximum for the hole **[43]**. The calculated electron and hole carrier mobility are listed in **Table III.4**. We noticed that the electron carrier mobility of the pure $AgGaS_2$ is much larger than hole carrier mobility. After Ga substitution by Tl, both hole and electron carrier mobility increases with the increase of Tl concentration, where the increase is about 70% for electron and 66% for hole after 75% Tl substitution. This carrier mobility augmentation is principally owing to increased elastic constant and reduced carrier effective masses after doping. Besides, when Ga is replaced by Tl the carrier mobility is slightly reduced compared to the other concentration especially in the case of hole carrier mobility. It is noteworthy to say that the high mobility value is one of the most wanted properties for a superior photovoltaic response since it will help to separate efficiently the photo-generated carriers without giving way to recombination.

Table III.4: The calculated band gap values and the effective mass of electron and hole, m_e^*, m_h^* , elastic constant C_{ii} (Kbar), deformation potential constants E_{CBM} (eV) and E_{VBM} (eV), and carrier mobility μ ($\times 10^3$ cm^2 V^{-1} s^{-1}) of $AgGa_{1-x}Tl_xS_2$ alloys.

$AgGa_{1-x}Tl_xS_2$		E_g	m_e^*/m_0	m_h^*/m_0	C_{ii}	E_{CBM}	E_{VBM}	μ_e	μ_h
x = 0	This work	2.59	0.196	0.388	322.8	-3.5	-6.11	0.946	0.119
	Exp.	2.63[32], 2.7[30, 33] 2.48[31], 2.75[31]	0.230	0.72	-	-	-	-	-
	Other calc.	2.4[28]	0.137[58]	0.383[58]	-	3.59[58]	6.09[58]	0.307[58]	0.044[58]
x = 0.25	This work	1.91	0.115	0.331	681.59	-3.98	-5.88	2.06	0.181
x = 0.5	This work	1.61	0.110	0.296	721.3	-4.11	-5.72	2.45	0.264
x = 0.75	This work	1.28	0.107	0.283	831.3	-4.29	-5.57	2.93	0.379
x = 1	This work	0.61	0.151	0.328	364.49	-4.48	-5.09	1.48	0.127

III.6.Band alignment

In the designing of a solar cell it is very important to consider the band edge position between the p-type absorber materials and the n-type window layer (p-n junction), because the electron charge carrier transport can be affected by the band misalignments from incompatible cell architecture design. Here we discuss the band alignments of $AgGa_{1-x}Tl_xS_2$/CdS heterojunction taking the CdS compounds as n-type window layer (**Fig.III.9**). The positions of the conduction and valence bands (E_{CBM} and E_{VBM}) with respect to the vacuum level of $AgGa_{1-x}Tl_xS_2$ alloys are calculated using the method described in **Ref [44],** however, those of CdS compound are taken from the literature **[45]**. From **Fig.III.9** it is observed that the $AgGaS_2$/CdS heterojunction forms a type-II band alignment, with the conduction band edge of $AgGaS_2$ positioning 0.78 higher than that of CdS compound. This conduction band offset (CBO) could be one of the reasons which reduce their PCE. Recently, using $AgGaS_2$ as p-type absorber materials and CdS as n-type window layer the $AgGaS_2$/CdS solar cell shows an open circuit voltage V_{OC} = 0.60 V, short circuit courant J_{SC}=7.5 mA cm^2, and a PCE of about 5.85%**[27]**. On the other hand, the valence band offset (VBO) is about 0.61 eV. When Tl is substituted into Ga site of $AgGaS_2$ the CBO is decreased to be 0.3 eV, and 0.17 eV, for $AgGa_{0.75}Tl_{0.25}S_2$, and $AgGa_{0.5}Tl_{0.5}S_2$, respectively **Fig.III.9**. Conversely, for x= 0.75 and 1, the $AgGa_{1-x}Tl_xS_2$/CdS

heterojunction forms a type-I band alignment, with the conduction band edge of $AgGa_{0.25}Tl_{0.75}S_2$ and $AgTlS_2$ positioning 0.01 and 0.2 lower than that of CdS compound, respectively. This decrease in CBO is resulting from the downshift of the conduction band edge which also leads to a reduction of the band gap value and then to the VBO enlargement. Consequently, one can conclude that the band gap and the band alignment of the $AgGa_{1-x}Tl_xS_2$/CdS heterojunction can be tuned by controlling Tl content.

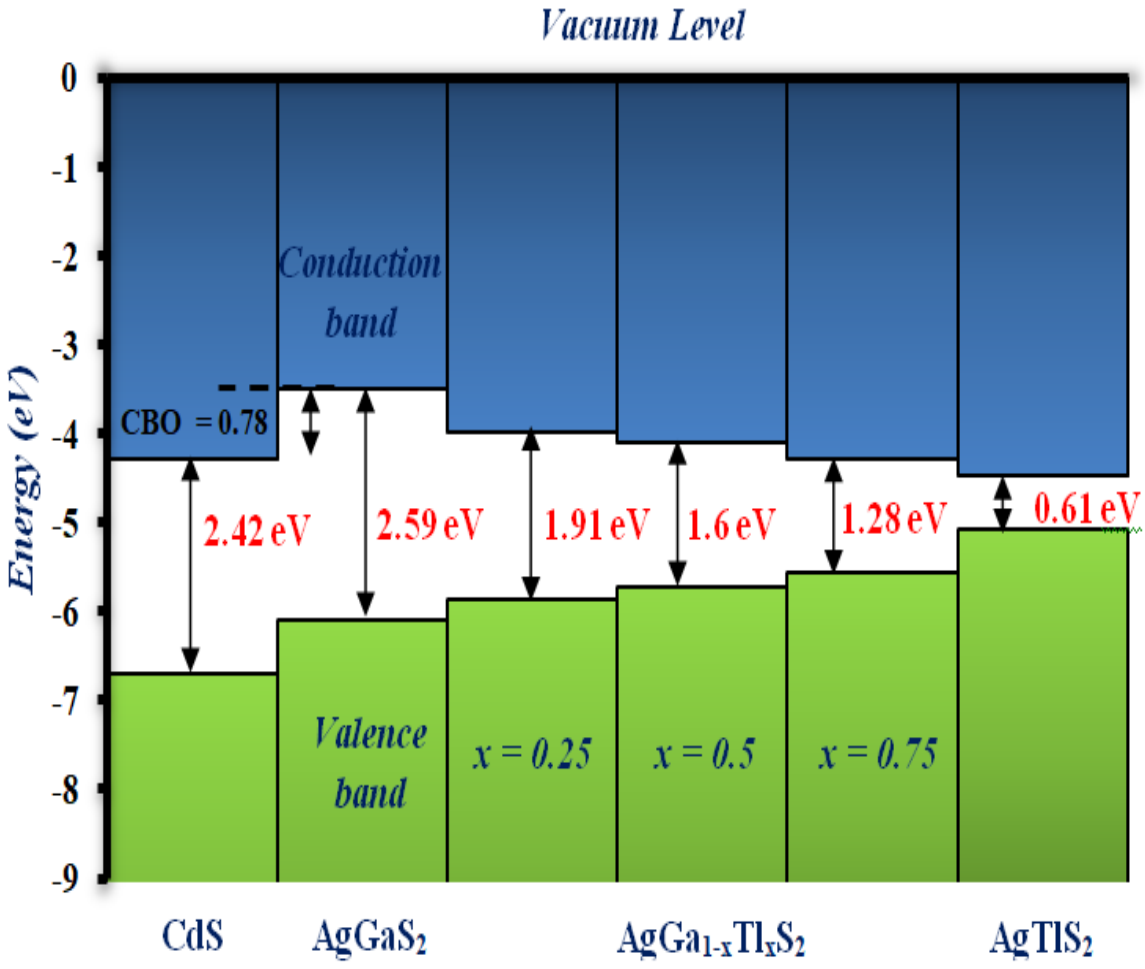

Fig.III.9: Vacuum-aligned band diagram for $AgGa_{1-x}Tl_xS2$ alloys compared with n type window layer material CdS.

III.7.Optical properties

The optical properties of solids are a major theme in both fundamental research and industrial applications. According to research, light interacts with matter with discrete energy, which is now called photons. More recently, it has been shown that in solids, and under the influence of

photons, the distribution of their electrons among their quantified energy states is transitorily modified. Understanding these effects has important consequences from both a technological and fundamental point of view. Indeed, the optical properties of chalcopyrite can be exploited as materials for the production of optoelectronic components, which are used in the manufacture of light detectors, light-emitting diodes, lasers and solar cells. For this purpose we have calculated the different optical quantities for the $AgGa_{1-x}Tl_xS_2$ alloys such as complex dielectric function, refractive index, reflectivity, and absorption coefficient

III.7.1.Dielectric function

Several optical properties are related to the band structure of the crystal. Most of these properties can be derived from the dielectric function which defines the linear behavior of the material when exposed to an external electromagnetic field, and therefore governs the propagation behavior of radiation in a medium, the frequency-dependent dielectric function is a real quantity, but in the case of a dynamic field, the dielectric function $\varepsilon(\omega)$ is a complex function known as [55]:

$$\boldsymbol{\varepsilon(\omega) = \varepsilon_1(\omega) + i\varepsilon_2(\omega)} \qquad \textbf{(III.5)}$$

Where ε_1 represents the real component, related to the polarisation of the environment, and ε_2 is the imaginary component of the dielectric function which characterises the absorption of the material.

The imaginary part of the dielectric function can be calculated from the matrix elements of the moment between the occupied and unoccupied electronic states in the first Brillouin zone. The imaginary part ε_2 of the dielectric function can be calculated via the following relation [57]

$$\boldsymbol{\varepsilon_2(\omega) = \frac{e^2\hbar}{\pi m^2\omega^2}\sum_{v,c}\int_{BZ}|M_{ev}(k)|^2\delta[\omega_{ev}(k)-\omega]d^3k} \qquad \textbf{(III.6)}$$

Where M is the dipole matrix, v and c are the initial and final states respectively. $M_{ev}(k)$ represents the momentum dipole of the elements, e is the potential vector defined by the electric field, which represents the elements of the matrix for the direct transitions between the valence band states $u_{vk}(r)$ and the conduction band states u_{ck} (r). The real part $\varepsilon_1(\omega)$ is deduced from the imaginary part of the dielectric function through the Kramers-Kronig relation [74,76]:

$$\boldsymbol{\varepsilon_1(\omega) = 1 + \frac{2}{\pi}P\int_0^\infty \frac{\omega'\varepsilon_2(\omega')}{\omega'^2-\omega^2}d\omega'} \qquad \textbf{(III.7)}$$

Where ω is the frequency and P is the principal part of the Cauchy integral. The rest of the optical functions, such as the index of refraction, n(ω), the reflectivity R(ω), and the absorption coefficient, α, can be derived easily from the dielectric function.

With the knowledge of the calculated electronic structure of $AgGa_{1-x}Tl_xS_2$ alloys and using the GGA TB-mBJ approximation for (x=0) and including the SOC for (x = 0.25, 0.5, 0.75, and 1) we calculated the real and imaginary part of the dielectric function for an incident photon of energy $\hbar\omega$ in the range 0 eV to 14eV.

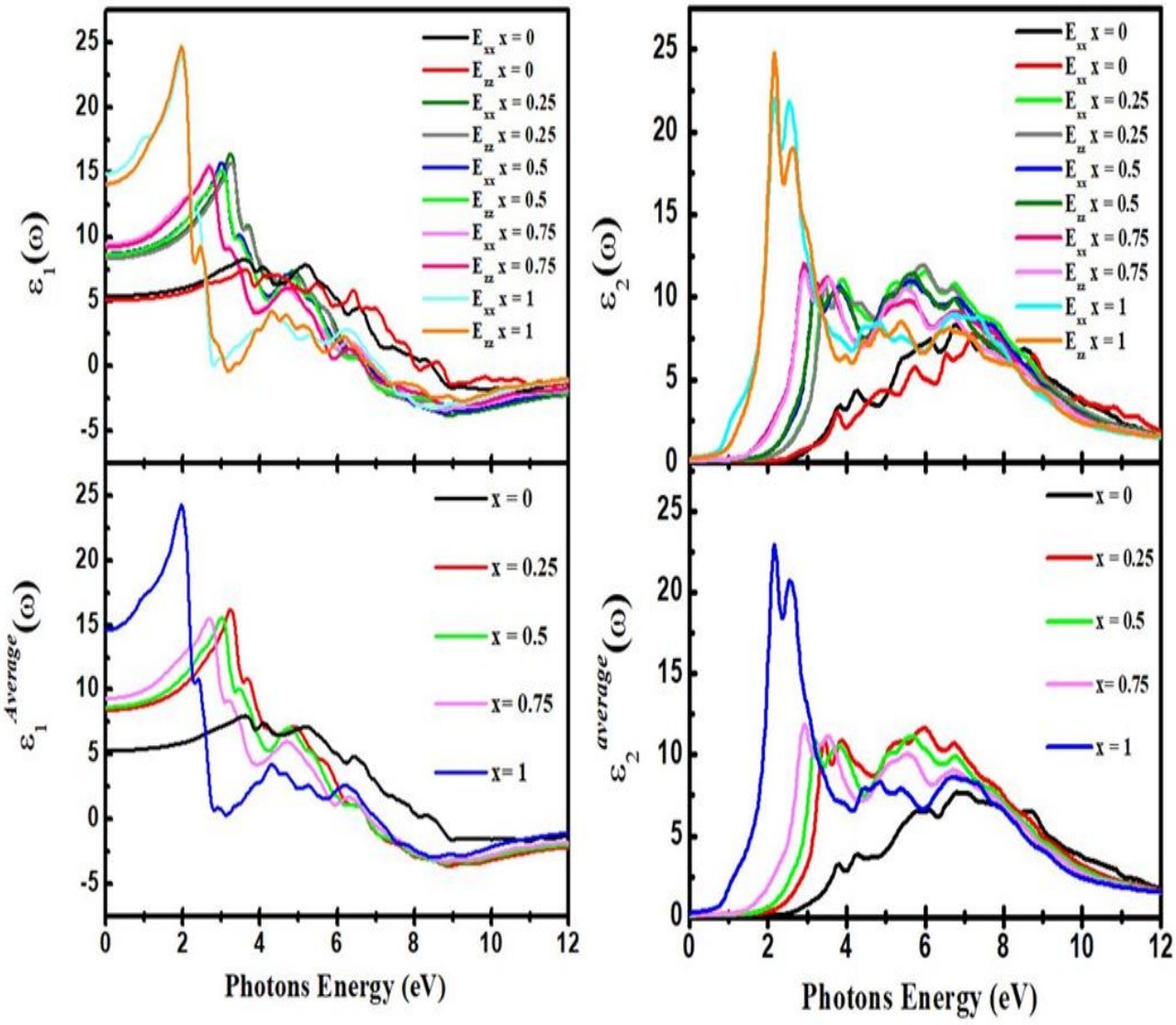

Fig.III.10: The imaginary ε_1 (ω) (left panel) and real ε_2 (ω) (right panel) part spectra of complex dielectric function for $AgGa_{1-x}Tl_xS_2$ materials.

Fig.III.10 shows the calculated real ($\varepsilon_{1xx}(\omega)$, $\varepsilon_{1zz}(\omega)$) and imaginary ($\varepsilon_{2xx}(\omega)$, $\varepsilon 2_{zz}(\omega)$) parts of the complex dielectric function of $AgGa_{1-x}Tl_xS_2$ alloys as a function of the photon energy hν. We also present in these figures the average values that may be representative for polycrystalline structures:

An imaginary average part: $\boldsymbol{\varepsilon_2^{average}(\omega) = (\varepsilon_{2xx}(\omega) + 2\varepsilon_{2zz}(\omega))/3}$

An average real part: $\boldsymbol{\varepsilon_1^{average}(\omega) = (\varepsilon_{1xx}(\omega) + 2\varepsilon_{1zz}(\omega))/3}$

As shown in **Fig.III.10** the $\varepsilon_1(\omega)$ spectra of pure $AgGaS_2$ reveal the main peak around 3.6 eV which is shifted towards lower energy in the other four alloys due to the Tl atom substitution. Besides, the average static dielectric value $\varepsilon_1^{average}(\omega)$ for $AgGa_{1-x}Tl_xS_2$ alloys which corresponds to the value of the real part taken at zero energy is listed in the **table III.5**

Table III.5: The values of the static dielectric constant $\varepsilon_1^{average}(0)$for $AgGa_{1-x}Tl_xS_2$ alloys.

$AgGa_{1-x}Tl_xS_2$	x=0	x=0.25	x=0.5	x=0.75	x=1
$\varepsilon_1^{average}(0)$	5.14	8.43	8.72	9.34	14.62

This value is increased from 5.14 for $AgGaS_2$ pure to 9.34 for $AgGa_{0.25}Tl_{0.75}S_2$ alloy, and 14.62 for $AgTlS_2$ which is consistent with the decrease of the band gap value. This static dielectric constant can be expressed by the following relationship:

$$\boldsymbol{\varepsilon(\omega) = 1 + \left(\frac{h\omega_p}{Eg}\right)} \qquad \textbf{(III.8)}$$

Where ω_p is the plasma frequency.

On the other hand, as can be seen in the $\varepsilon_2(\omega)$ spectra from **Fig.III.10,** doping $AgGaS_2$ by 25% Tl leads to appearing of new peaks in the visible region. These new peaks are resulting from the photon absorption provoked by the direct interband transition from the occupied VB to the Tl 's' states in the MCB. Interestingly, these novel peaks are red-shifted along with the increased Tl concentrations from 3.42 eV for $AgGa_{0.75}Tl_{0.25}S_2$ to 2.12 eV for $AgTlS_2$ compound.

The determination of the two parts of the dielectric function allows us to evaluate other optical properties such as absorption α(ω), reflectivityR(ω), loss energyL(ω)and refractive index n(ω).

III.7.2.Refractive index

The refractive index of a material is usually encountered in its real form.However, it can be found in its complex form:

$$N(\omega) = n(\omega) + ik(\omega) \quad \textbf{(III.9)}$$

With *N* the complex refractive index, *n* the real refractive index, *k* the extinction coefficient.

The refractive index (n) of a material represents the factor by which electromagnetic radiation is slowed down as it crosses the boundary between two media [53].Using the calculated imaginary and real parts of the dielectric function as a function of frequency, the refractive index n(ω) is calculated by the relation:

$$n(\omega) = \left[\frac{\varepsilon_1(\omega)}{2} + \frac{\sqrt{\varepsilon_1^2(\omega)+\varepsilon_2^2(\omega)}}{2}\right]^{\frac{1}{2}} \quad \textbf{(III.10)}$$

For low frequencies (ε ≈ 0) the relation becomes:

$$n(0) = \sqrt{\varepsilon}(0) \quad \textbf{(III.11)}$$

The average value of the static refractive index n(0) of $AgGa_{1-x}Tl_xS_2$ alloys is listed in the **table III.6**

Table III.6: The values of the static refractive index n(0) for $AgGa_{1-x}Tl_xS_2$ alloys.

$AgGa_{1-x}Tl_xS_2$	x=0	x=0.25	x=0.5	x=0.75	x=1
$n(0)$	2.25, 2.40[54]	2.9	2.94	3.05	3.82

The n (ω) spectrum records a maximum value in the visible light region for 25%, 50%, 75% and 100% of Tl concentration whereas this maximum is observed in the UV region for pure $AgGaS_2$. Besides, the value of extinction coefficient k (ω) is zero up to 2.6 eV for $AgGaS_2$ which means it will not attenuate most of the incident visible light. However, a new peak comes in to view when the Ga atom is replaced by the 75% Tl atom improving the optical response of $AgGaS_2$

III.7.3.Optical reflectivity

Reflectivity is defined as a ratio of the intensity of the reflected ray to the intensity of the incident ray at the normal incidence of the electromagnetic wave on the system; it is a function of the refractive index and is given by the following relation:

$$R(\omega) = \left[\frac{\varepsilon(\omega)^{\frac{1}{2}}-1}{\varepsilon(\omega)^{\frac{1}{2}}+1}\right]^2 \qquad \textbf{(III.12)}$$

the average reflection R average at E=0 eV are around 15.5%, 23.8%, 24.2%, 25.6%, and 34.2% for 0, 25%, 50%, 75% and 100% of Tl concentration, respectively. The R (ω) spectra show a maximum in the ultraviolet (UV) region which is enhanced with the increased Tl concentration.

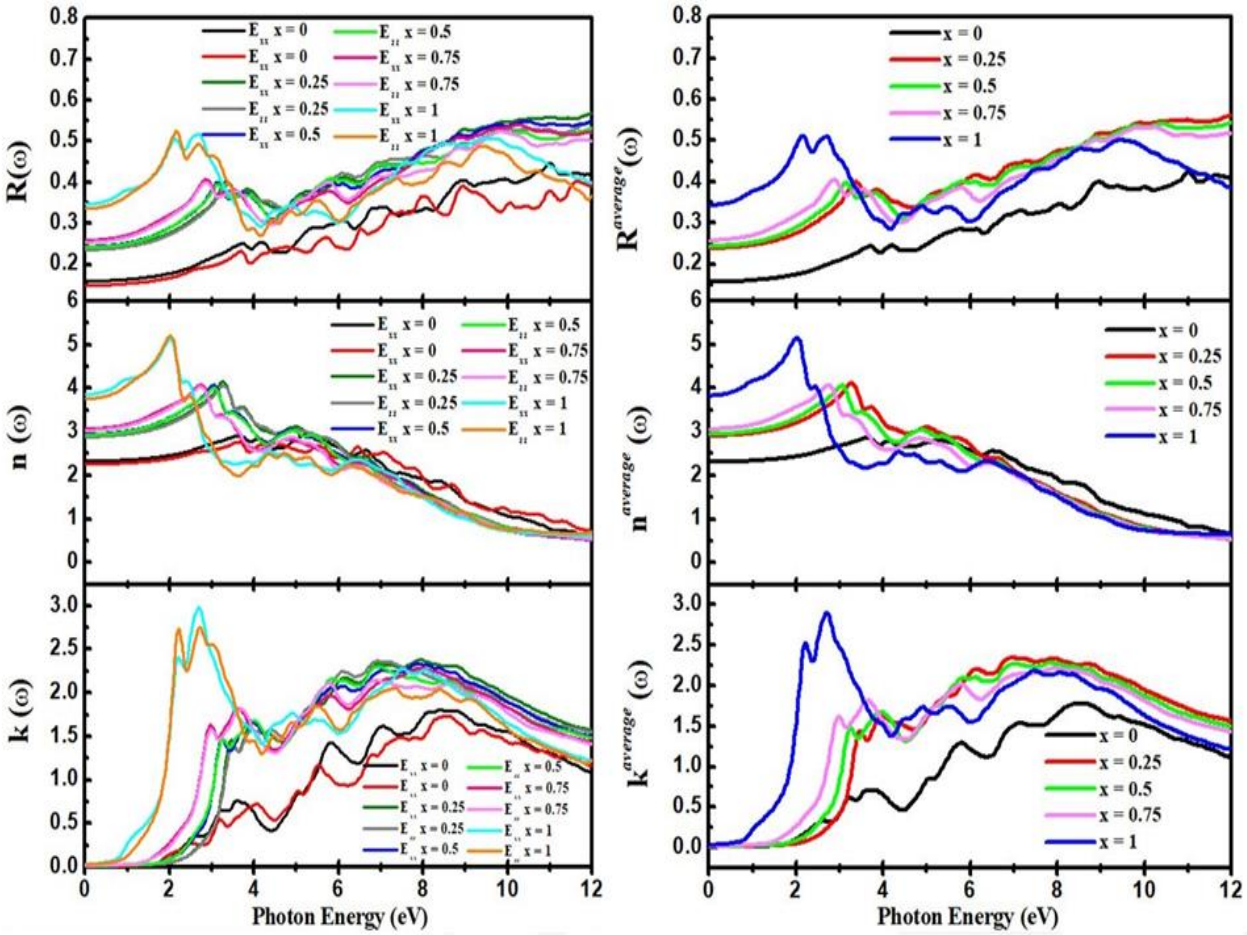

Fig.III.11: The calculated refractive index n (ω), extinction coefficient k (ω), and reflectivity coefficient R (ω) of $AgGa_{1-x}Tl_xS_2$ alloys along xx and zz-direction (left panel), average (right panel).

III.7.4.Absorption

The frequency-dependent absorption coefficient α is defined as the fraction of light absorbed in a unit length of the environment. The variation of the absorption coefficient with photon energy hν is given by the following relation [52]:

$$\alpha = A(h\nu - E_g)^r \qquad \textbf{(III.13)}$$

Where A is a constant, Eg is the "optical" gap energy, and r is an index which can be equal to ½ $\frac{1}{2}$ (for a direct gap) or 2 (for an indirect gap).

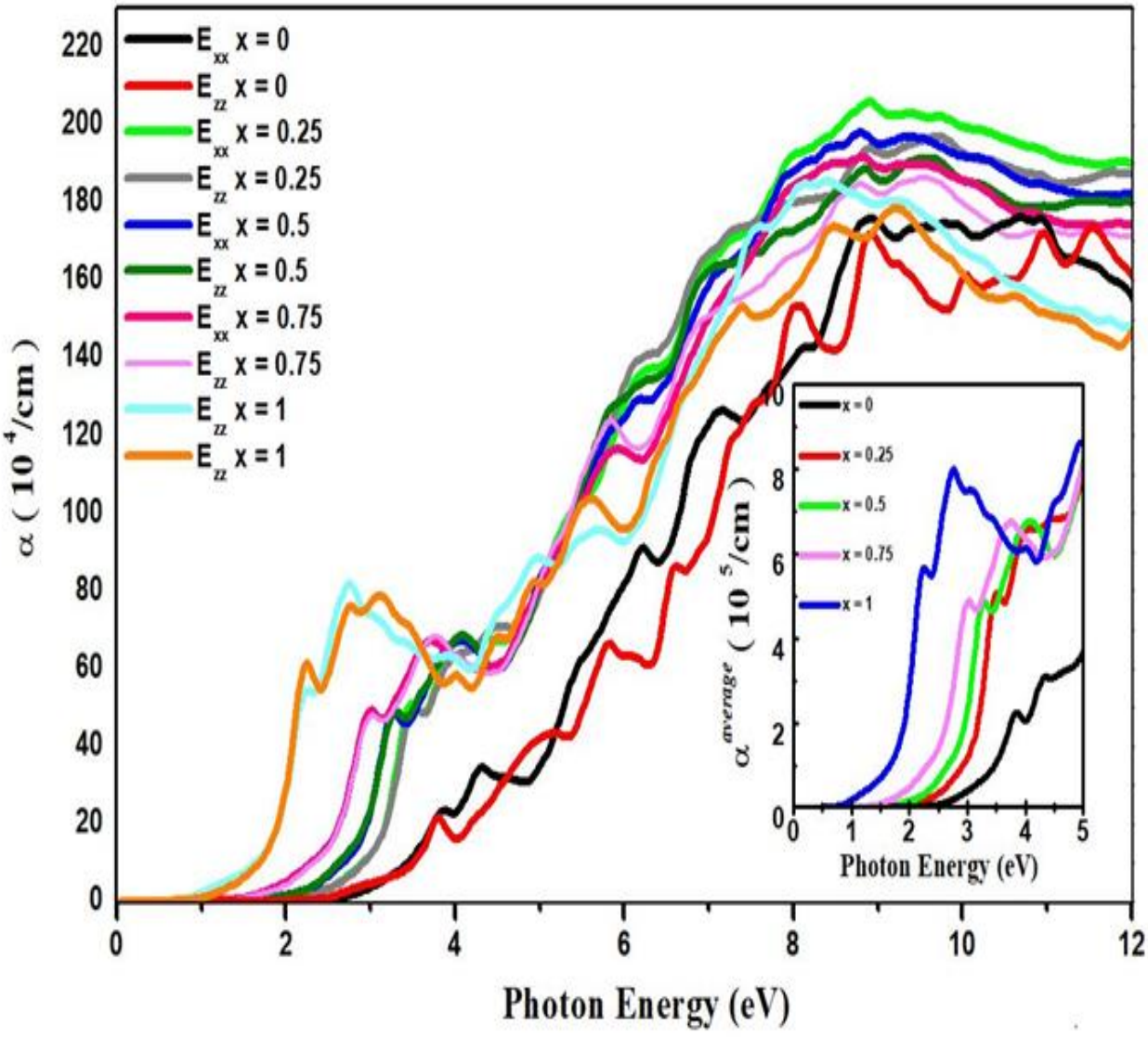

Fig.III.12: The calculated absorption coefficient α (ω) of $AgGa_{1-x}Tl_xS_2$ alloys

Consider **Fig.III.12** which plots the absorption coefficient α (ω) against the photon energy of $AgGa_{1-x}Tl_xS_2$ alloys it is obviously observed that the Tl substitution strongly enhances the absorption coefficient in the visible region. The α (ω) value is about 0.4x 10^5 cm^{-1} for $AgGaS_2$ and is augmented to be 4.8x10^5 cm^{-1} for $AgGa_{0.25}Tl_{0.75}S_2$ Suggesting that this alloy would display high absorption of sunlight in the visible region, and behave as ideal solar absorber. In addition, the square of absorption versus photon energy is plotted (i.e.,$(\alpha h\nu)^2$ versus hν for $AgGa_{1-x}Tl_xS_2$ alloys in **Fig.III.13** Using a linear fitting a direct optical band gap is estimated to be 2.66 eV, 1.98 eV, 1.68 eV, 1.37 eV, and 0.74 eV for $AgGaS_2$, $AgGa_{0.75}Tl_{0.25}S_2$, $AgGa_{0.5}Tl_{0.5}S_2$, $AgGa_{0.25}Tl_{0.75}S_2$, and $AgTlS_2$, respectively. Evaluating the obtained results of α for $AgGa_{1-x}Tl_xS_2$ alloys with other experimental results for established absorber materials such as GICS, CZTS, GaAs, CdTe, and $CH_3NH_3PbI_3$ **Fig.III.14**, we observed that the absorption coefficient of $AgGa_{0.5}Tl_{0.5}S_2$ is comparable to that of CdTe and CZTS, whereas the $AgGa_{0.25}Tl_{0.75}S_2$ shows a good absorption coefficient as GaAs and CIGS compound. Consequently, $AgGa_{1-x}Tl_xS_2$ alloys could be considered as potential materials for photovoltaic and solar cells utilization.

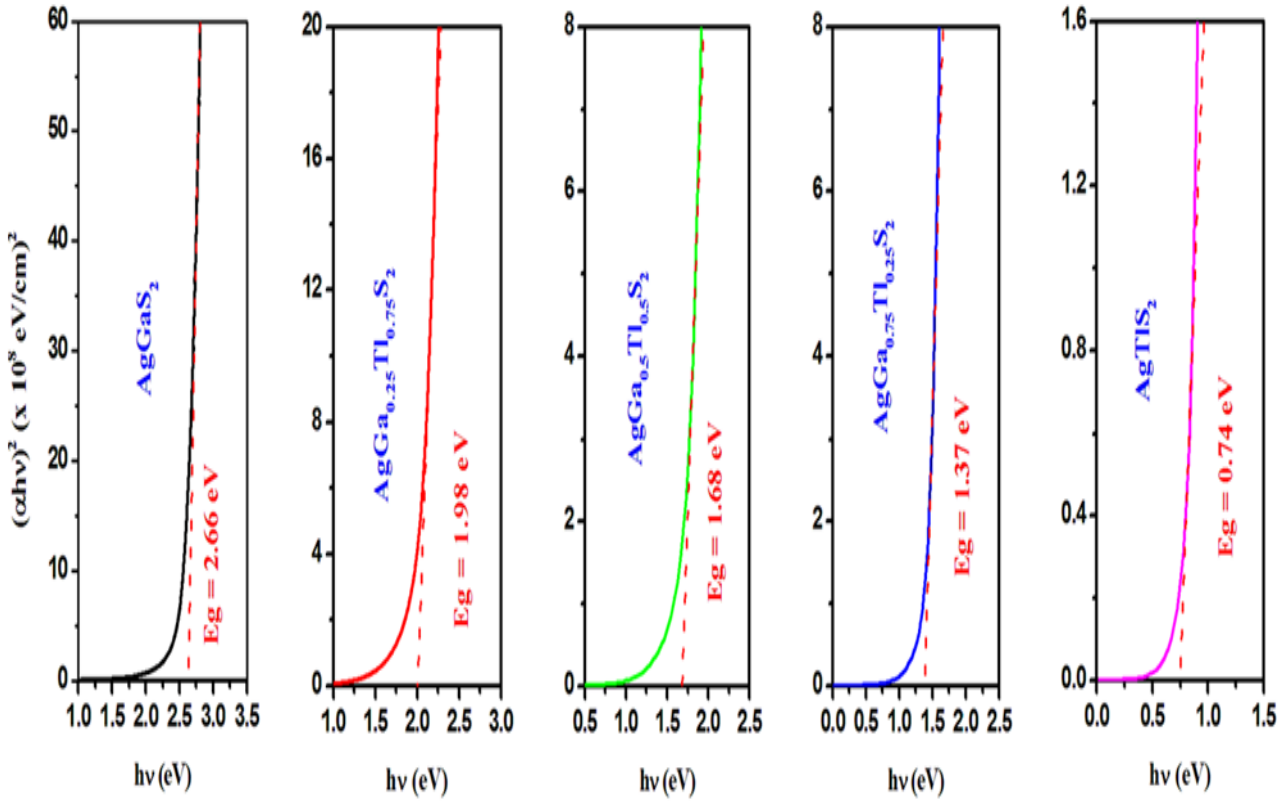

Fig.III.13: Optical band gap of $AgGa_{1-x}Tl_xS_2$ alloys.

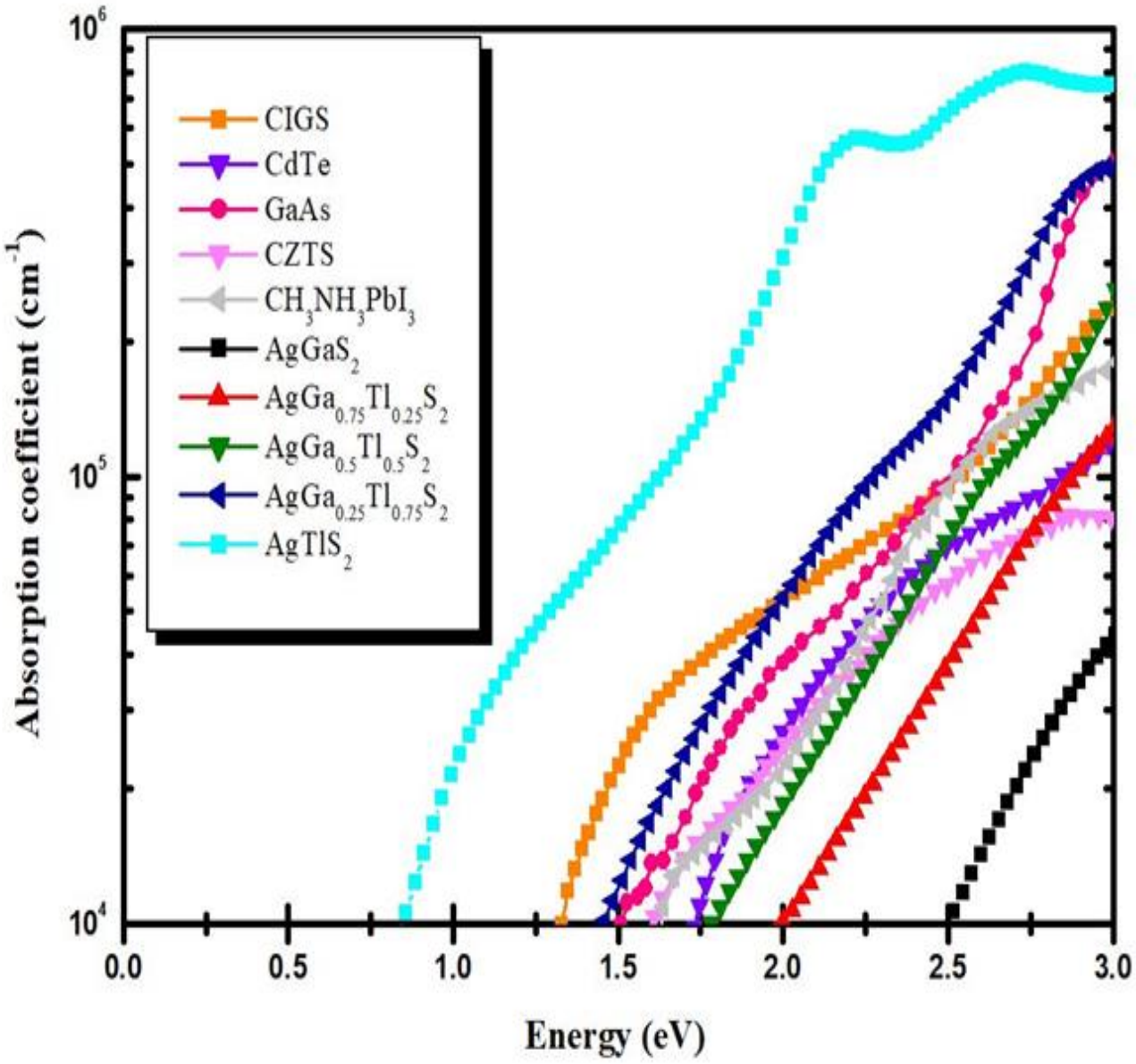

Fig.III.14: The calculated absorption coefficient α (ω) of $AgGa_{1-x}Tl_xS_2$ alloys compared with other materials such as CdTe **[47]**, GaAs **[48]**, CIGS **[49]**, CZTS **[50]**, $CH_3NH_3PbI_3$ **[51]**

III.8.Conclusion

In this section, we performed detailed calculations using the FP-APW+ lo method to determine the effect of Ga substitution by Tl on the structural, electronic and optical properties of the compound $AgGaS_2$. The current DFT calculation reveals that when the gallium is replaced by the thallium, the minimum of the CB is shifted towards the Fermi level, resulting reduction of band gap from 2.59 eV for $AgGaS_2$ pure to 1.91 eV, 1.61 eV, and 1.28 eV for $AgGa_{0.75}Tl_{0.25}S_2$,

$AgGa_{0.5}Tl_{0.5}S_2$, and $AgGa_{0.25}Tl_{0.75}S_2$, respectively. Besides, it is observed that both hole and electron effective masse decrease with the increase of Tl concentration, and thus both hole and electron carrier mobility is increased. Analysis of the band alignments of $AgGa_{1-x}Tl_xS_2$/CdS heterojunction reveals that when Tl is incorporated into $AgGaS_2$, the conduction band offset is decreased, and thus the open-circuit voltage can be improved. From the optical properties calculations, it is established that Tl substitution enhances the optical properties of $AgGaS_2$ by reducing the transparent region and improving the refractive index and the absorption in the visible light region. Consequently, the semiconducting nature with the appropriate direct band gap values and strong absorption ($\alpha > 10^5$ cm^{-1}) of the new $AgGa_xTl_{1-x}S_2$ alloys in the visible light region make them promising candidates for optoelectronic and photovoltaic applications, especially in solar cells.

Bibliography

[1] A.N. Usoltsev, S.A. Adonin, A.S. Novikov, D.G. Samsonenko, M.N. Sokolova, V.P. Fedin, One-dimensional polymeric polybromotellurates (IV): structural and theoretical insights into halogen···halogen contacts, CrystEngComm (2017).

[2] S.A. Adonin, M.A. Bondarenko, P.A. Abramov, A.S. Novikov, P.E. Plyusnin, M.N. Sokolov, V.P. Fedin, Bromo- and polybromoantimonates(V): structural and theoretical studies of hybrid halogen-rich halometalate frameworks, Chem. Eur. J. 24 10165 (2018).

[3] S.A. Adonin, I.D. Gorokh, A.S. Novikov, D.G. Samsonenko, P.E. Plyusnin, M.N. Sokolov, V.P. Fedin, Bromine-rich complexes of bismuth: experimental and theoretical studies, Dalton Trans. 47, 2683–2689 (2018).

[4] S.F. Chichibu, T. Ohmori, N. Shibata, T. Koyama, T. Onuma, Greenish-white electroluminescence from p-type CuGaS2 heterojunction diodes using n-type ZnO as an electron injector, Appl. Phys. Lett. 85, 4403 (2004).

[5] S. Ishizuka, A. Yamada, P.J. Fons, H. Shibata, S. Niki, Structural tuning of wide-gap chalcopyrite CuGaSe2 thin films and highly efficient solar cells: differences from narrow-gap Cu(In,Ga)Se2, Prog. Photovolt. 22, 821–829 (2014).

[6] J.S. Jang, P.H. Borse, J.S. Lee, S.H. Choi, H.G. Kim, Indium induced band gap tailoring in AgGa1_xInxS2 chalcopyrite structure for visible light photocatalysis, Chem. Phys. 128 154717 (2008).

[7] D. Lincota, J.F. Guillemolesa, S. Tauniera, D. Guimarda, J. Sicx-Kurdia, A. Chaumonta, O. Roussela, O. Ramdania, C. Huberta, J.P. Fauvarquea, N. Bodereaua, L. Parissia, P. Panheleuxa, P. Fanouillerea, N. Naghavia, P.P. Granda, M. Benfaraha, P. Mogensenb, O. Kerreca, Chalcopyrite Thin Film Solar Cells by Electro-Deposition Solar Energy, vol. 77, pp. 725–737 2004.

[8] T. Plirdpring, K. Kurosaki, A. Kosuga, T. Day, S. Firdosy, V. Ravi, G.T. Snyder,A. Harnwunggmoung, A. Sugahara, Y. O-hishi, H. Muta, S. Yamanaka, Chalcopyrite CuGaTe2 : a high-Efficiency bulk thermoelectric material, Adv. Mater. 24 (2012).

[9] P.C. Ricci, A. Anedda, R. Corpino, C.M. Carbonaro, M. Marceddu, I.M. Tiginyanu, V.V. Ursaki, Temperature dependence of the photoluminescence spectra in AgGaS2, J. Phys. Chem. Solid. 66, 1950–1953 (2005).

[10] M.V. Yakushev, R.W. Martin, Semiconductor spectroscopy and devices https://ssd.phys.strath.ac.uk/research-areas/chalcopyrites-for-solar-cells/ , 2020.

[11] M. Thirumoorthy, K. Ramesh, Materials Today: Proceedings, Characteristics of pulse electrodeposited AgGaS2 thin films for photovoltaic application (2021) .

[12] G.K.H. Madsen, P. Blaha, K. Schwarz, E. Sjostedt, L. Nordstreom, Efficient linearization of the augmented plane-wave method, Phys. Rev. B 64, 195134 (2001).

[13] K. Schwarz, P. Blaha, G.K.H. Madsen, Electronic structure calculations of solids using the WIEN2k package for material sciences, Comput. Phys.Commun.147, 71 (2002).

[14] P. Blaha, K. Schwarz, F. Tran, R. Laskowski, G.K.H. Madsen, L.D. Marks, WIEN2k: an APWþlo program for calculating the properties of solids, J. Chem. Phys. 152, 074101 (2020).

[15] Z. Wu, R.E. Cohen, More accurate generalized gradient approximation for solids, Phys. Rev. B 73, 235116 (2006) .

[16] D. Koller, F. Tran, F. Blaha, Merits and limits of the modified Becke-Johnson exchange potential, Phys. Rev. B 83, 195134 (2011).

[17] F. Tran, F. Blaha, Accurate band gaps of semiconductors and insulators with a semi local exchange-correlation potential, Phys. Rev. Lett. 102, 226401 (2009).

[18] K. Momma, F. Izumi, VESTA 3 for three-dimensional visualization of crystal, volumetric and morphology data, J. Appl. Crystallogr. 44, 1272–1276 (2011).

[19] T. Sakuntala, A.K. Arora, Pressure-tuned resonance Raman scattering in AgGaSe2, Phys. Rev. B 53, 15667 (1996).

[20] F.D. Murnaghan, The compressibility of media under extreme pressures, Proc. Natl. Acad. Sci. U.S.A. 30, 244 (1944).

[21] J.L. Shay, J.H. Wernick, Ternary Chalcopyrite Semiconductors: Growth, Electronic Properties, and Applications, Pergamon Press, Oxford; New York, 1975.

[22] H. Neumann, Bulk modulus-volume relationship in ternary chalcopyrite compounds, Phys. Status Solidi 96 K121 (1986) .

[23] T. Tinoco, A. Polian, J.P. Itie, E. Moya, J. Gonzales, Equation of state and phase transitions in AgGaS2 and AgGaSe2, J. Phys. Chem. Solid. 56, 481–484 (1995).

[24] J.E. Jaffe, A. Zunger, Theory of the band-gap anomaly in ABC2 chalcopyrite semiconductors, Phys. Rev. B 29 (1882).

[25] R. Asokamani, R.M. Amirthakumari, R. Rita, C. Ravi, Electronic structure calculations and physical properties of ABX2 (A = Cu, Ag; B = Ga, In; X = S, Se, Te) Ternary Chalcopyrite Systems, Phys. Status Solidi B 213 349 (1999).

[26] A.H. Reshak, Linear, nonlinear optical properties and birefringence of AgGaX2 (X=S, Se, Te) compounds, Phys. B Condens. Matter 369, 243–253 (2005).

[27] S. Chen, X.G. Gong, S.H. Wei, Band-structure anomalies of the chalcopyrite semiconductors CuGaX2 versus AgGaX2 (X¼S and Se) and their alloys, Phys. Rev. B 75, 205–209 (2007).

[28] S. Ullah, H. Ud Din, G. Murtaza, T. Ouahrani, R. Khenata, Naeemullah, S. Bin Omran, Structural, electronic and optical properties of AgXY2 (X = Al, Ga, In and Y = S, Se, Te), J. Alloys Compd. 617, 575–583 (2014).

[29] V. Kumar, B.S.R. Sastry, Heat of formation of ternary chalcopyrite semiconductors, J. Phys. Chem. Solid. 66, 99–102 (2005).

[30] T. Tinoco, A. Polian, J.P. Itie, E. Moya, J. Gonzales, Equation of state and phase transitions in AgGaS2 and AgGaSe2, J. Phys. Chem. Solid. 56 , 481–484 (1995).

[31] A. Chahed, O. Benhelal, S. Laksari, B. Abbar, B. Bouhafs, N. Amrane, First-principles calculations of the structural, electronic and optical properties of AgGaS2 and AgGaSe2, Physica B 367 , 142–151 (2005).

[32] J.L. Shay, J.H. Wernick, Ternary Chalcopyrite Semiconductors: Growth, Electronic Properties, and Applications, Pergamon Press, Oxford; New York, 1975.

[33] H.C. Hsu, H. Chen, S.Y. Kuo, C.S. Chang, W.F. Hsieh, Effect of annealing on the structural and optical properties of AgGaS2 thin films prepared by pulsed laser deposition, Thin Solid Films 419, 237–241 (2002).

[34] H. Karaagac, M. Parlak, The investigation of structural, electrical, and optical properties of thermal evaporated AgGaS2 thin films, Thin Solid Films 519, 2055–2061 (2011).

[35] H. Xiao, J. Tahir-Kheli, W.A. Goddard, Accurate band gaps for semiconductors from density functional theory, Phys. Chem. Lett. 212–217 (2011).

[36] S. Ahmed, K.B. Reuter, O. Gunawan, L. Guo, L.T. Romankiw, H. Deligianni, A high efficiency electrodeposited Cu2ZnSnS4 solar cell, Adv. Energy Mater. 2 (2012).

[37] P. Kusch, S. Breuer, M. Ramsteiner, L. Geelhaar, H. Riechert, S. Reich, Band gap of wurtzite GaAs: a resonant Raman study, Phys. Rev. B 86, 075317 (2012),.

[38] S. Lalitha, S.Z. Karazhanov, P. Ravindran, S. Senthilarasu, R. Sathyamoorthy, J. Janabergenov, Electronic structure, structural and optical properties of thermally evaporated CdTe thin films, Physica B 387 227–238 (2007).

[39] B.A. Al-Asbahi, S.M.H. Qaid, M. Hezam, I. Bedja, H.M. Ghaithan, A.S. Aldwayyan, Effect of deposition method on the structural and optical properties of CH3NH3PbI3 perovskite thin films, Opt. Mater. 103, 109836 (2020).

[40] T. Omata, K. Nose, S. Otsuka-Yao-Matsuo, Size dependent optical band gap of ternary I-III-VI2 semiconductor nanocrystals, J. Appl. Phys. 105, 073106 (2009).

[41] C. Rinc_on, J. Gonz_alez, Acoustic deformation potentials in AIBIIICVI 2 chalcopyrite semiconductors, Phys. Rev. B 40, 8552 (1989).

[42] I. Chung, J.H. Song, J. Im, J. Androulakis, C.D. Malliakas, H. Li, A.J. Freeman, J.T. Kenney, M.G. Kanatzidis, CsSnI3: semiconductor or metal? high electrical conductivity and strong near-infrared photoluminescence from a single material. High hole mobility and phase-transitions, J. Am. Chem. Soc. 134 8579 (2012).

[43] S.H. Wei, A. Zunger, Predicted band-gap pressure coefficients of all diamond and zinc-blende semiconductors: chemical trends, Phys. Rev. B 60 5404 (1998).

[44] M. Batouche, T. Seddik, V. Vu Tuan, D. Vo Dat, H.D. Tong, D.M. Hoat, O.Y. Khyzhun, Ternary sulfides BaLa2S4 and CaLa2S4 as promising photocatalytic water splitting and thermoelectric materials: first-principles DFT calculations, Int. J. Hydrogen Energy 45 22600–22612 (2020).

[45] T.J. Whittles, T.D. Veal, C.N. Savory, A.W. Welch, F.W.L. de Souza, J.T. Gibbon, M. Birkett, R.J. Potter, D.O. Scanlon, A. Zakutayev, V.R. Dhanak, Core levels, band alignments, and valence-band states in CuSbS2 for solar cell applications, ACS Appl. Mater. Interfaces 9 (48) 41916–41926 (2017).

[46] C. Gary, Catella, D. Burlage, Crystal growth and optical properties of AgGaS2 and AgGaSe2, MRS Bull. 23 28–36 (1998).

[47] G.B. Dubrovskii, Optical properties of CdTe, Sov. Phys. Solid State 3,1305 (1961).

[48] J.O. Akinlami, A.O. Ashamu, Optical properties of GaAs, J. Semiconduct. 34, 032002 (2013).

[49] S. Minoura, K. Kodera, T. Maekawa, K. Miyazaki, S. Niki, H. Fujiwara, Dielectric function of Cu(In, Ga)Se2-based polycrystalline materials, J. Appl. Phys. 113 (2013).

[50] J.S. Seol, S.Y. Lee, J.C. Lee, H.D. Nam, H.K. Kim, Electrical and optical properties of Cu2ZnSnS4 thin films prepared by rf magnetron sputtering process, Sol. Energy Mater. Sol. Cells 75 155–162 (2003).

[51] X. Ziang, L. Shifeng, Q. Laixiang, P. Shuping, W. Wei, Y. Yu, Y. Li, C. Zhijian, W. Shufeng, D. Honglin, Y. Minghui, G.G. Qin, Refractive index and extinction coefficient of CH3NH3PbI3 studied by spectroscopic ellipsometry, Opt. Mater. Express 5 29–43 (2015).

[52] N. Seddiki, T.Ouahrani, B.Lasri, T.Benouaz, A.H.Reshak, B. Bouhafs ;Materials Science in Semiconductor Processing 16 1454 (2013).

[53] J.M. Li, W.R. Burghardt, B. Yang and B. Khomami. J. Non-Newt 91 189(2000).

[54] H.A. Kramers, Collected Science Papers, North Holland, Amsterdam, 25 333 (1956).

[55] N.V.Smith, Phys.Rev, B3, .pp 1862-1878(1971).

[56] S. Asano, N. Yamashita,Y.Nakao, Phys. Status.Solidi, 89, pp. 663-673 (1978).

[57] H.Ehrenreich ,H.R.Philips,Phys.Rev,128, pp. 1622-1629(1962).

[58] Y-L.Liu ,C-L.Yang,M-S.Wang ,X-G.Ma, Y-G.Yi, Int J Quantum Chem. (2020).

Chapter

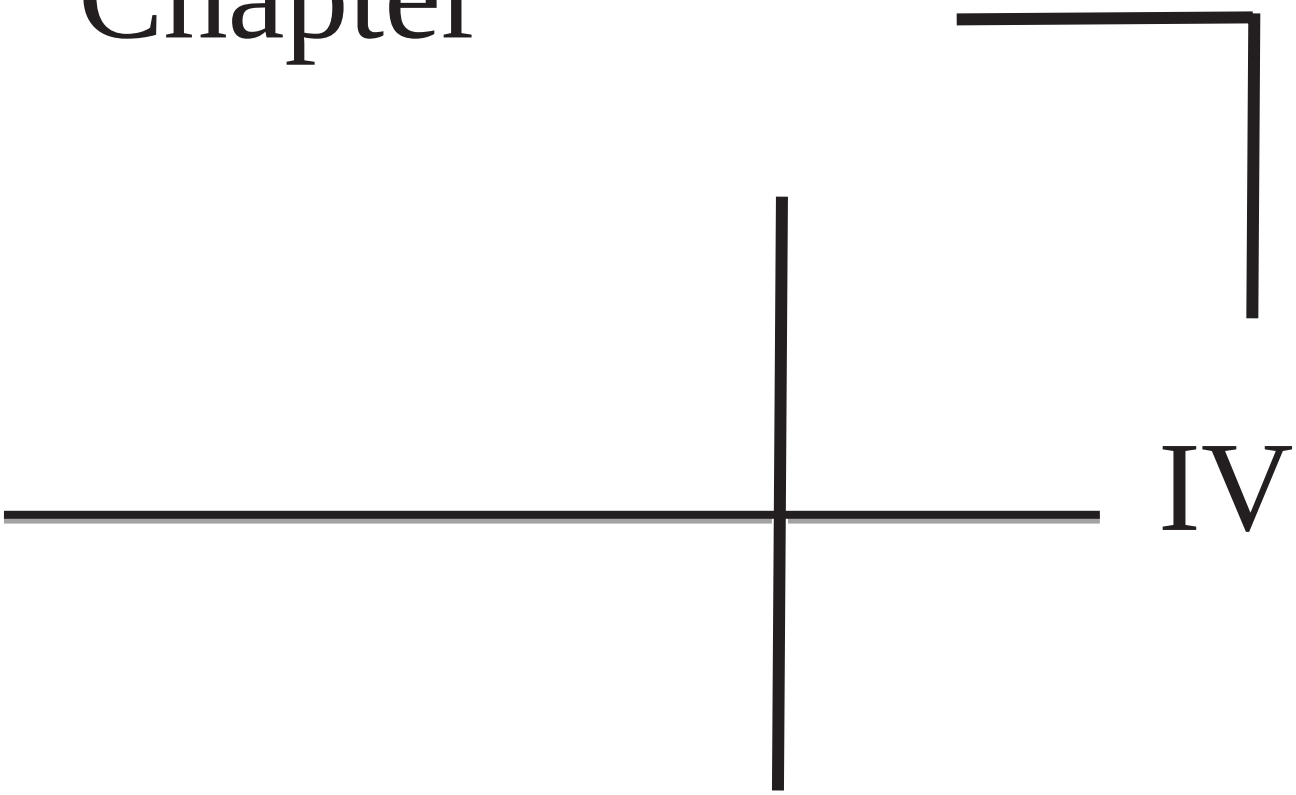

IV

Investigation of the structural and optoelectronic properties of the compound $AgGa_{x-1}Tl_xSe_2$

Chapter IV

Investigation of the structural and optoelectronic properties of the compound $AgGa_{x-1}Tl_xSe_2$

IV.1.Introduction

Due to their ideal optical characteristics and relatively inexpensive processing methods, materials from the chalcopyrite family are well suited to their best known application in solar cells. **[1–3]**. Those physical properties give rise to numerous applications in everyday life such as photodetectors, water splitting, light sensing transistors and other optoelectronic components **[4–9].**The Silver gallium selenide $AgGaSe_2$, which belongs to the group of I-III-VI_2 coumpounds, is nearly opaque in the visible region but highly transparent in the IR from 0.78 to 18 mm, its figure of merit is $M=1.8d^2/n^3$ and it non-linear susceptibility is $\chi(\omega) = 66 \times 10^{12}$ m/V **[16]**. It has also unique intriguing IR optical properties including large non-linear coefficients and birefringence **[17]** which make it suitable for a wide range of three-wave mixing applications **[10]**. It combine strong nonlinear coupling with phase matching across a wide (0.5- 12.5 µm) transmission range **[15]**. These properties provide the basis for CO_2 laser harmonic-generator (HG), visible (VIS), and near-infrared (NIR) pumped optical parametric-oscillator (OPO) and summand difference-frequency-generator (SFG/ DFG) systems for producing tunable laser radiation from approximately 0.65 to 12 µm **[11–14]** . The main aim is to improve the optical and electronic properties of $AgGaSe_2$ using band convergence strategy by substitution of thallium (Tl) into gallium (Ga) site in the compound $AgGaSe_2$ for the formation of $AgGa_{1-x}Tl_xSe_2$ alloys.

IV.2.Calculation detail

The present calculations were accomplished with a self-consistent approach by solving the Kohn-Sham equations using the full potential augmented plane wave and local orbital method (FP-APW+lo) **[18]** Based on density functional theory and embedded in the WIEN2K package **[21,22]**. The exchange correlation energy contribution has been handled via the generalized gradient approximation achieved by Wu and Cohen (GGA-WC) **[19]**. The innovative Tran-Blaha modified Becke-Jonson potential (TB-mBJ) **[20]** is applied to the accurate estimation of the electronic and optical properties, as it is well known that the GGA under-estimates the band gap values. The muffin-tin sphere radius was chosen to be 2.5, 2.39, 2.28, and 2.17 a.u. for Ag, Ga, Tl, and Se, respectively. The valence wave functions inside and outside the muffin-tin sphere were delimited to values of l_{max}^{in} = 10 and l_{max}^{out} = 4, respectively, whereas the charge density is Fourier expanded up to G_{max} = 12 $(a.u.)^{-1}$. Cut-off was done with the condition $R_{MT}^{*}K_{max}$ = 8 (RMT represents the tiniest radius of the atomic sphere and K_{max} is the largest k-

vector in the plane wave expansion). The number of *k*-points which provides the convergence in the Brillouin zone is 600 *k*-points. It is noteworthy that in these calculations energy of −6.0 Ry is used to separate the valence states and the core states. Besides, the $AgGa_{1-x}Tl_xSe_2$ alloys are shaped using 1×1×2 periodic supercells. The gallium atoms are substituted by thallium atoms to adopt all the possible configurations with Ga and Tl mixed atoms to obtain $AgGa_{1-x}Tl_xSe_2$ alloys with x = 0.25, 0.50, and 0.75.

IV.3. Structural properties

At ambient temperature, the ternary $AgGaSe_2$ compound crystallize in the tetragonal chalcopyrite structure (space group I-42d No.122) **[23]** with three separate Wyckoff sites 4a (0, 0, 0), 2c (0, 0, 1/2) and 8c (*u*, 1/4, 1/8) for Ag, Ga, Se respectively. Thus, we have set the internal parameter *u* by relaxing the position of S atom. We then measured the total energy as a function of the unit cell volume at the equilibrium cell volume V_0 using the experimental data for both parameters *a* and *c* from ref **[24]**. We then optimized the *c/a* ratio. Finally, using the two equilibrium parameters *u* and c, we optimized the volume. The ground-state lattice parameters (a and c), bulk modulus *B* and it first pressure derivative *B'* of the $AgGa_{1-x}Tl_xSe_2$ alloys are obtained using the Murnaghan equation of state **[25]:**

$$\mathbf{E(V)} = \boldsymbol{E_0} + \frac{\mathbf{B'}}{\boldsymbol{B'(B'-1)}}\left[\boldsymbol{\gamma}\left(\frac{\boldsymbol{V_0}}{\boldsymbol{V}}\right)^{\boldsymbol{B'}} - \boldsymbol{V_0}\right] + \frac{\boldsymbol{B}}{\boldsymbol{B'}}(\boldsymbol{V}-\boldsymbol{V_0}) \qquad \textbf{(IV.1)}$$

The estimated ground state parameters are summarized in **table IV.2** alongside with experimental and theoretical data. When compared to the experimental data, our calculated values diverges by only 0.34% and 1.1% respectively, which prove the accuracy and relevance of our calculations. From **table IV.2** we remark that the lattice parameters *a* and *c* increase when Ga atoms are incrementally replaced by Tl atoms in the $AgGaSe_2$ unit cell. The bulk modulus decreases too with increasing Tl concentration. The increase of the interatomic distance in the $AgGa_{1-x}Tl_xSe_2$ alloys from x = 0 to x = 0.75 could be the reason of this trend.

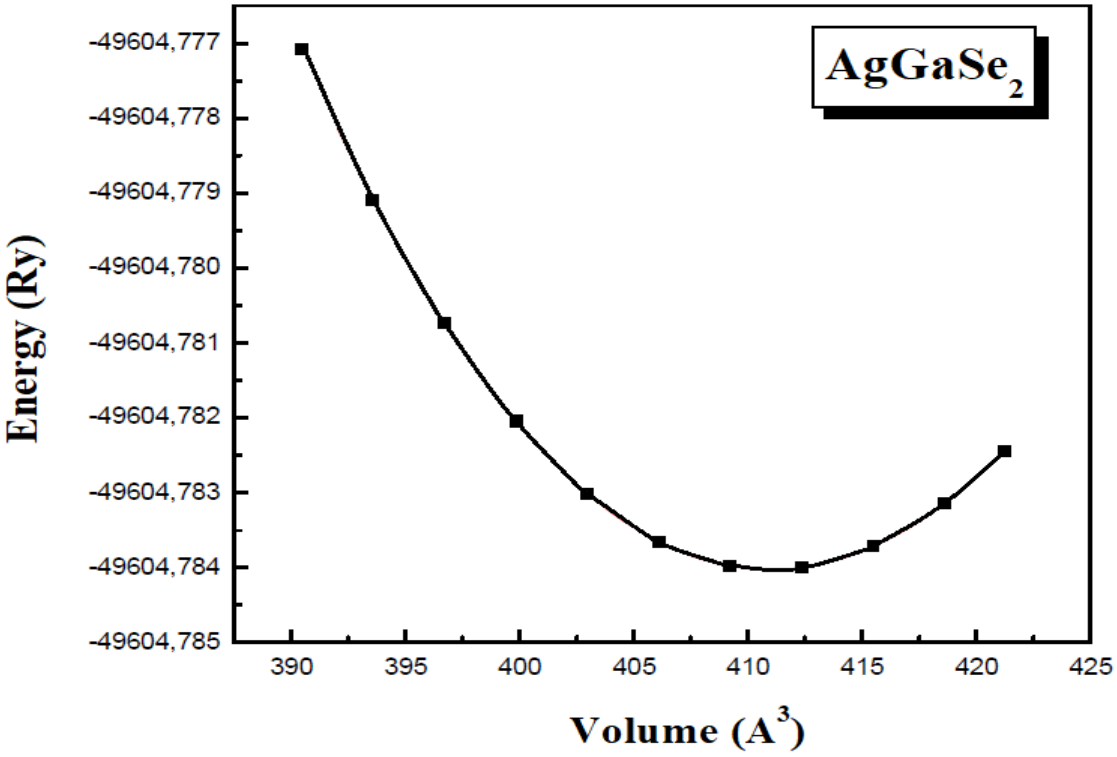

Fig.IV.1: Variation of the total energy as a function of the volume of the $AgGaSe_2$

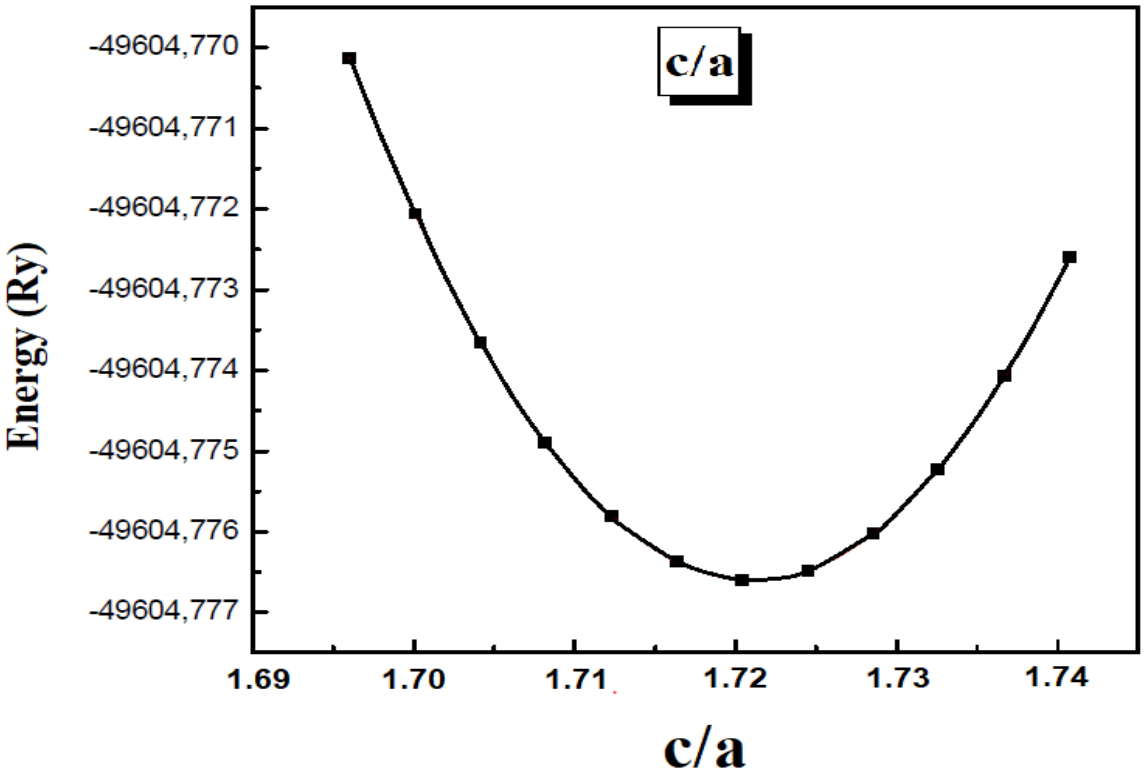

Fig.IV.2: Variation of the total energy as a function of the c/a ratio of the $AgGaSe_2$ compound.

IV.3.1 Formation and cohesive Energy

In order to verify the relative stability of the $AgGa_{1-x}Tl_xSe_2$ (x=0, 0.25, 0.5, and 0.75) alloys we have calculated the formation energy using the following equation:

$$E_f^{AgGa_{1-x}Tl_xSe_2} = \frac{1}{\alpha+\beta+\gamma+\delta}\left(E_{tot}^{AgGa_{1-x}Tl_xSe_2} - \alpha E^{Ag} - \beta E^{Ga} - \gamma E^{Tl} - \delta E^{Se}\right) \quad \textbf{(IV.2)}$$

Where, $E_f^{AgGaSe_2}$ represents the energy of formation, $E_{tot}^{AgGaSe_2}$ indicates the total energy, α + β + γ + δ refer to the number of atoms in the unit cell and E^{Ag}, E^{Ga} and E^{Se} denote the isolated atomic energies of Ag, Ga, and S atoms respectively. The observed E_f values are negative, which is indicative of the thermodynamic stability of all $AgGa_{1-x}Tl_xSe_2$ (see **table IV.2**). Moreover, the resulting E_f for pure $AgGaSe_2$ is in good accordance with results of the previous study.

We can define cohesive energy as the strength of the binding forces between isolated atoms in a solid. It is mathematically given as the total energy of the compound subtracted from the total energy of the constitutive atoms as follow **[41,42]**:

$$E_{coh}^{AgGa_{1-x}Tl_xSe_2} = \frac{(\alpha E^{Ag}+\beta E^{Ga}+\gamma E^{Tl}+\delta E^{Se} - E_{tot}^{AgGa_{1-x}Tl_xSe_2})}{N} \quad \textbf{(With N=α + β + γ + δ)} \quad \textbf{(IV.3)}$$

Where $E_{coh}^{AgGa_{1-x}Tl_xSe_2}$ represent the cohesive energy, $E_{tot}^{AgGa_{1-x}Tl_xSe_2}$ is the total energy of the unit cell, N are the number of Ag, Ga and Se atoms in unit cell, respectively .E^{Ag}, E^{Ga}, E^{Tl} and E^{Se} are the energies of the Ag, Ga, Tl and Se in their unrestricted nature. The calculated cohesive energie for $AgGaSe_2$ is 3.78eV which is in good agreement with the theoretical data available **[42].** The calculated cohesive energies for $AgGa_{1-x}Tl_xSe_2$ alloys are 3.18eV, 3.91eV and 3.08eV for (x=0.25, 0.5, and 0.75) respectively.

Table IV.1: Interatomic distance for $AgGa_{1-x}Tl_xSe_2$ alloys.

$AgGa_{1-x}Tl_xSe_2$		Ag--Se	Ga--Se	Tl--Se
x = 0	This work	2.613	2.429	-
	Other calc.	2.70 [26], 2.56 [27]	2.30 [26] ,2.63 [27]	-
x = 0.25	This work	2.661	2.474	2.474
x = 0.5	This work	2.700	2.514	2.514
x = 0.75	This work	2.747	2.554	2.554

Table IV.2: The calculated lattice constant (*a* and *c*) (Å), the anion displacement parameter *u*, bulk modulus (GPa) and its pressure derivative, and formation energy (KJ/mol) for $AgGa_{1-x}T_xSe_2$ Alloys.

$AgGa_{1-x}Tl_xSe_2$		*a*	*c*	*U*	*B*	*B'*	E_f
x = 0	This work	6.079	10.49	0.275	62.958	4.586	-365.58
	Expt.	5.985[28] 5.992[37]	10.886[37]	0.272[28]	63.8[30] 65[37]	4[37]	446[39]
	Other calc.	5.934[29]	11.21[34]	0.287[32]	59.86[31]	4.46[36]	-288.4[40]
		6.05[34]	11.29[34]	0.295[33]	64.62[37]	4.7[37]	-318.2[39]
		5.83[37]	11.02[37]	0.278[34]	62.53[35]	5.02[38]	
x = 0.25	This work	6.189	10.70	0.251	56.345	4.41	-307.45
x = 0.5	This work	6.289	10.86	0.249	49.856	4.48	-378.11
x = 0.75	This work	6.39	11.05	0.236	43.524	4.53	-297.47

IV.4 Electronic properties

IV.4.1.Band structures

To fully comprehend the physical aspects of the electronic structure of $AgGa_{1-x}Tl_xSe_2$, both band structures and densities of states were calculated for the maximized lattice parameters using the WC-GGA and GGA-TB-mBJ approaches. The valence band maximum is taken at 0 eV as a reference for energy values to match the valence band maximum. Fig.IV.3 shows the calculated band structures of both $AgGaSe_2$ and $AgGa_{1-x}Tl_xSe_2$ alloys, respectively that are considered along selected highly symmetrical directions in the Brillouin zone (BZ). It can be clearly perceived that the valence and conduction bands do not overlap; moreover the valence band maximum and the conduction band minimum are at the same point (Γ). Consequently, the compounds $AgGaSe_2$ and $AgGa_{1-x}Tl_xSe_2$ alloys are direct band gap (Γ_V- Γ_C) semiconductors. The gap value of $AgGaSe_2$ is 0.66 eV using GGA-WC. In fact, the GGA approach does not accurately describe the exchange correlation energy, which leads to a quantitative undervaluation of the band gap compared to the experimental data **[43, 44]**. The TB-mBJ approach is therefore used and the band gap value is found to be 1.83 eV which is consistent with the available theoretical and experimental work. Furthermore, by means of WC-GGA+TB-mBJ, the band structure of $AgGa_{1-x}Tl_xSe_2$ alloys is obtained. We have noticed that once Tl replaces the Ga atom, the shape of the band gap and semiconducting character is kept. However, the CB minimum is pushed down towards low energies, leading to a decrease in the bandgap value to be 1.72 eV, 1.43 eV, 1.29 eV for (x=0.25, 0.5, and 0.75) respectively. Furthermore, the spin-orbit coupling (SOC) is incorporated due to the heavy atom (Tl). It can be seen that the SOC affects the band structures leading to the decrease of the energy band gap to be 1.68 eV, 1.42 eV and 1.27 eV, for $AgGa_{0.75}Tl_{0.25}Se_2$, $AgGa_{0.5}Tl_{0.5}Se_2$ and $AgGa_{0.25}Tl_{0.75}S_2$, respectively.

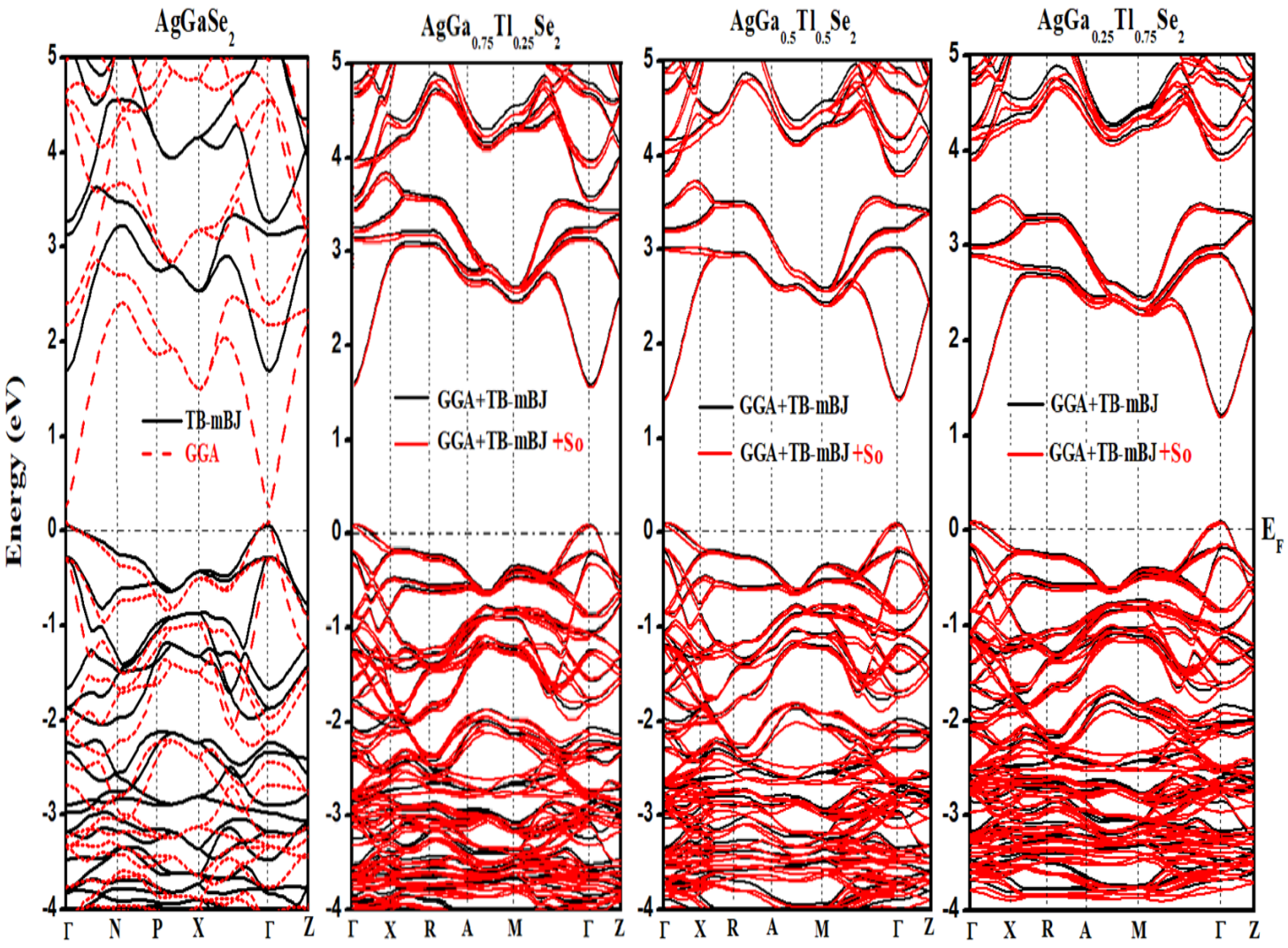

Fig.IV.3: The calculated band structure of $AgGa_{1-x}Tl_xSe_2$ alloys

IV.4.2.Density of states

To provide a further understanding of the electronic structure, we looked at the contribution of each atomic character to a series of bands in the total density decomposition. The total and partial atomic densities of state (TDOS and PDOS) for the pure $AgGaSe_2$ and $AgGa_{1-x}Tl_xS_2$ alloys at various concentrations x have been calculated. The TDOS and PDOS graphs on Fig.III.2 IV.9 have been plotted using the GGA-TB-mBJ+So. As we observe, the low-energy region from -5 eV to -8 eV in the valence band is coming mainly from a mixture of Ga '4s' states and S '3p' anion states. The second region pics from -5 eV to the Fermi level (Ef =0) stems principally from the Ag '4d' cationic states hybridized with the Se '3p' states, hinting at the covalency of the Ag-S bond. One can see the little contribution of Ga '4p' states. Although the $AgGaSe_2$ conduction band is predominantly formed from Ga '4s, 4p' states hybridized with the Se '3p' states of the anion. Going deep in the conduction band we observe a dominant

contribution of Ga '4p' states hybridized with Se '4p' states. Going forward, the replacement of Tl atoms in the Ga sites has a strong impact on the conduction band. This substitution of Tl induces the constitution of new states in the CB minima, which mainly come from the Tl '6s' states. These Tl '6s' states are hybridized with Ga '4s' states and Se '4p' for $AgGa_{1-x}Tl_xS_2$ alloys (x = 0.25, 0.5, and 0.75) and decrease the band gap value. The valence band structure of the $AgGa_{1-x}Tl_xS_2$ alloys (x = 0.25, 0.5, 0.75 and 1) is left invariant, with only a small Tl 6d-state contribution near the Fermi level. Accordingly, the decrease in the band gap can be attributed to the increase in the atomic size from Ga to Tl and the reduction in the internal parameter *u* (see **Table VI.1**) as the Tl concentration grows.

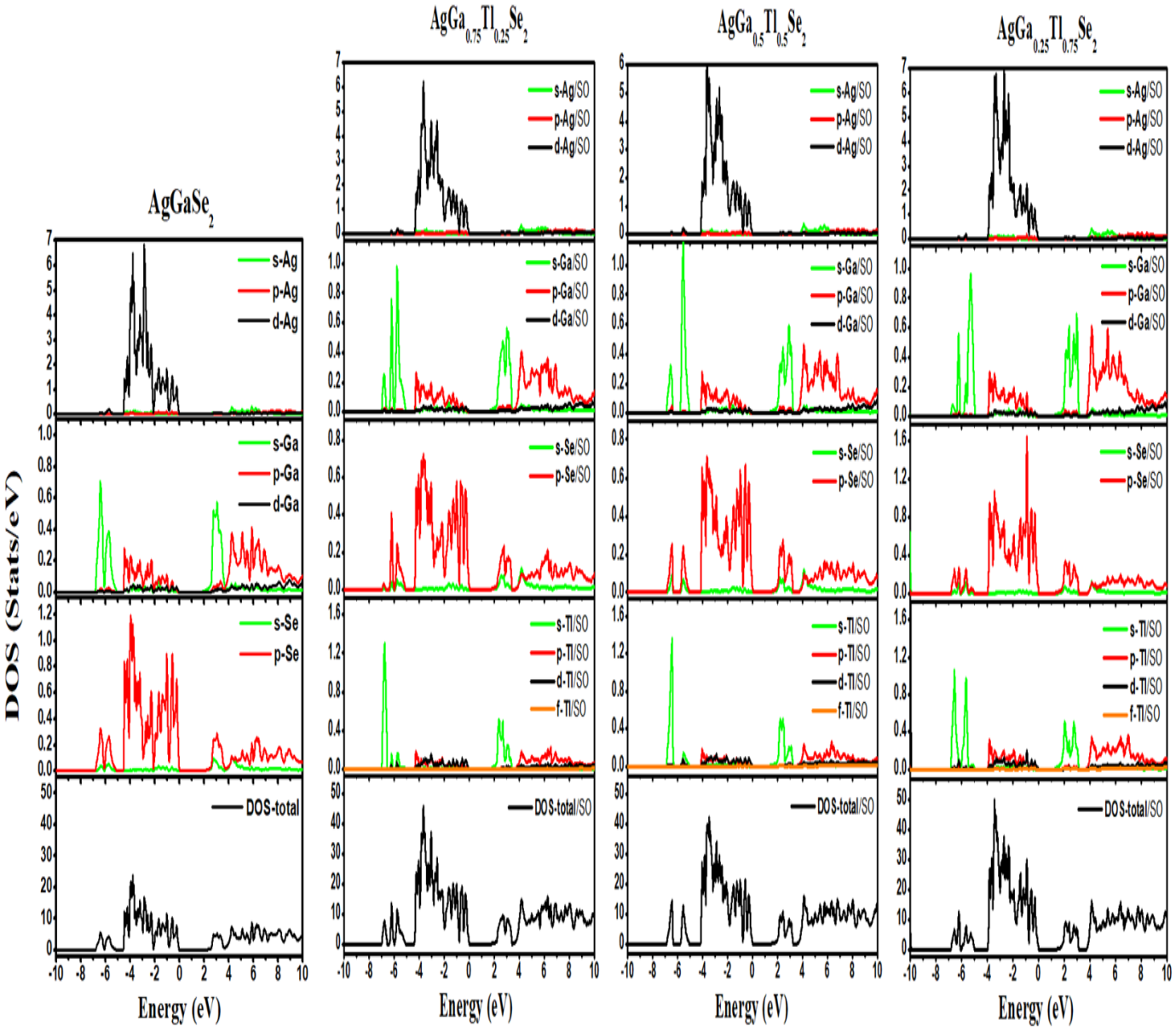

Fig.IV.4: Total and partial density of states (DOS) of $AgGa_{1-x}Tl_xSe_2$ alloys.

IV.5.Carrier effective mass and mobility

Based on the deformation potential theory advocated by Bardeen and Shockley [45], the hole and electron carriers mobility can be determined through the following equation

$$\boldsymbol{\mu = \frac{2\sqrt{2\pi}e\hbar^4 Cii}{3(k_B T)^{\frac{3}{2}}(m^*)^{\frac{5}{2}}E^2}} \quad \textbf{(IV.4)}$$

Where *e*, k_B and *T* denote the electron charge, Boltzmann's constant and the ambient temperature, respectively. C_{ii} is the elastic modulus [46]:

$$\boldsymbol{Cii = V_0(\partial^2 E_{tot}/\partial V^2)} \quad \textbf{(IV.5)}$$

Where E_{tot} and V_0 are the total energies and the equilibrium volume, respectively. The deformation potential constant, *E*, is established by [47]:

$$\boldsymbol{E = (\Delta E_{edge})/(\Delta V/V_0)} \quad \textbf{(IV.6)}$$

This indicates the variation in energy of the CBM or VBM caused by the change in volume. *m** is the effective mass of electrons and holes and is determined using the equation:

$$\boldsymbol{m^* = \hbar^2\left(\frac{\partial^2 E}{\partial^2 k}\right)^{-1}} \quad \textbf{(IV.7)}$$

where *ħ*, *k*, and *E* are the reduced Planck constant, wave vector, and corresponding energy, respectively. Here,we calculated the effective mass of electrons (m_e^*) and holes (m_h^*) along the x, y, and z directions. The results are listed in **Table IV.4.** Here, the band effective mass used in the calculation of the carrier mobility was defined as:

$$\boldsymbol{m_B^* = 3\left(1/m_x^* + 1/m_y^* + 1/m_z^*\right)^{-1}} \quad \textbf{(IV.8)}$$

The elastic modulus C_{ii} and the deformation potential constant *E* were calculated using parabolic and linearly fitting of the corresponding data toward unit strain, respectively. Ultimately, the values of *m**,C_{ii} , *E*, and μ were obtained and summarized in **Table IV.4**

Table IV.3: The calculated effective masses (m*) of electrons and holes for $AgGa_{1-x}Tl_xSe_2$

$AgGa_{1-x}Tl_xSe_2$	Electrons			Holes		
	m_x^*	m_y^*	m_z^*	m_x^*	m_y^*	m_z^*
x=0 (this work)	0.084	0.104	0.87	0.194	0.181	0.203
Other calc. [48]	0.1	0.1	0.8	1.09	1.09	0.096
x=0.25	0.088	0.078	0.091	0.195	0.179	0.187
x=0.50	0.086	0.081	0.69	0.161	0.172	0.184
x=0.75	0.077	0.071	0.069	0.169	0.177	0.162

Table IV.4: The calculated band gap values and the effective mass of electron and hole, m_e^*, m_h^*, elastic modulus C_{ii} (Kbar), deformation potential constants E_{CBM} (eV) and E_{VBM} (eV), and carrier mobility μ ($cm^2\ V^{-1}\ s^{-1}$) of $AgGa_{1-x}Tl_xSe_2$ alloys.

$AgGa_{1-x}Tl_xSe_2$		E_g	m_e^*/m_0	m_h^*/m_0	C_{ii}	E_{CBM}	E_{VBM}	μ_e	μ_h
x = 0	This work	1.834	0.091	0.193	86.58	-3.33	-5.16	713	412
	Expt.	1.83 [43], 1.80[44]	-	-	-	-	-	-	-
	Other calc.	1.76[49] , 1.80[50]	0.17[51]	0.73[51]	-	-	-	-	-
x = 0.25		1.682	0.085	0.187	103.57	-3.40	-5.08	475	569
x = 0.5		1.428	0.079	0.173	157	-3.53	-4.95	412	336
x = 0.75		1.276	0.073	0.169	831.3	-3.61	-4.88	436	392

IV.6. Optical properties

The optical properties such as complex dielectric function, refractive index, reflectivity, and absorption coefficient play a crucial role in designing good PV materials. In the current study, the optical properties of $AgGa_{1-x}Tl_xSe_2$ alloys were estimated using WC-GGA + TB-mBJ approximation for (x = 0) and including the SOC for (x = 0.25, 0.5 and 0.75) for incident radiation along the main crystallographic direction "xx" and "zz". Many properties mentioned above can be obtained from the dielectric function **[52]** where the imaginary part of the dielectric function is directly related to the absorption spectrum and the real part to the scattering and reflection characteristics of the material.

$$\boldsymbol{\varepsilon(\omega) = \varepsilon_1(\omega) + i\varepsilon_2(\omega)} \qquad \textbf{(IV.9)}$$

In general, the real and imaginary parts ε_1 and ε_2 are related by relations called Kramers- Kronig relations **[53]:**

$$\boldsymbol{\varepsilon_1(\omega) = 1 + \frac{2}{\pi} P \int_0^{\infty} \frac{\omega' \varepsilon_2(\omega')}{\omega'^2 - \omega^2} d\omega'} \qquad \textbf{(IV.10)}$$

$$\boldsymbol{\varepsilon_2(\omega) = 1 + \frac{2\omega}{\pi} P \int_0^{\infty} \frac{\varepsilon_1(\omega') - 1}{(\omega'^2 - \omega_{12})} d\omega'} \qquad \textbf{(IV.11)}$$

Where *P* is the main value of the integral. The real and imaginary parts of the dielectric function allow us to identify the main optical properties of solids such as the refractive index solids such as the index of refraction, the reflection coefficient and the absorption coefficient. It is stated that the dielectric function relies on the band structure of the solids **[53].** However, the values of the band gap energies of $AgGa_{1-x}Tl_xSe_2$ obtained using the TB-mBJ +So approximation are in good agreement with the experimental data **Table .IV.5**. Therefore, to determine the dielectric function of $AgGa_{1-x}Tl_xSe_2$ we used the WC-GGA+TB-mBJ approximation for x=0 and including the SOC for x=0.25, 0.5, 0.75) for an incident photon of energy $\hbar\omega$ in the range 0 eV to 14eV.

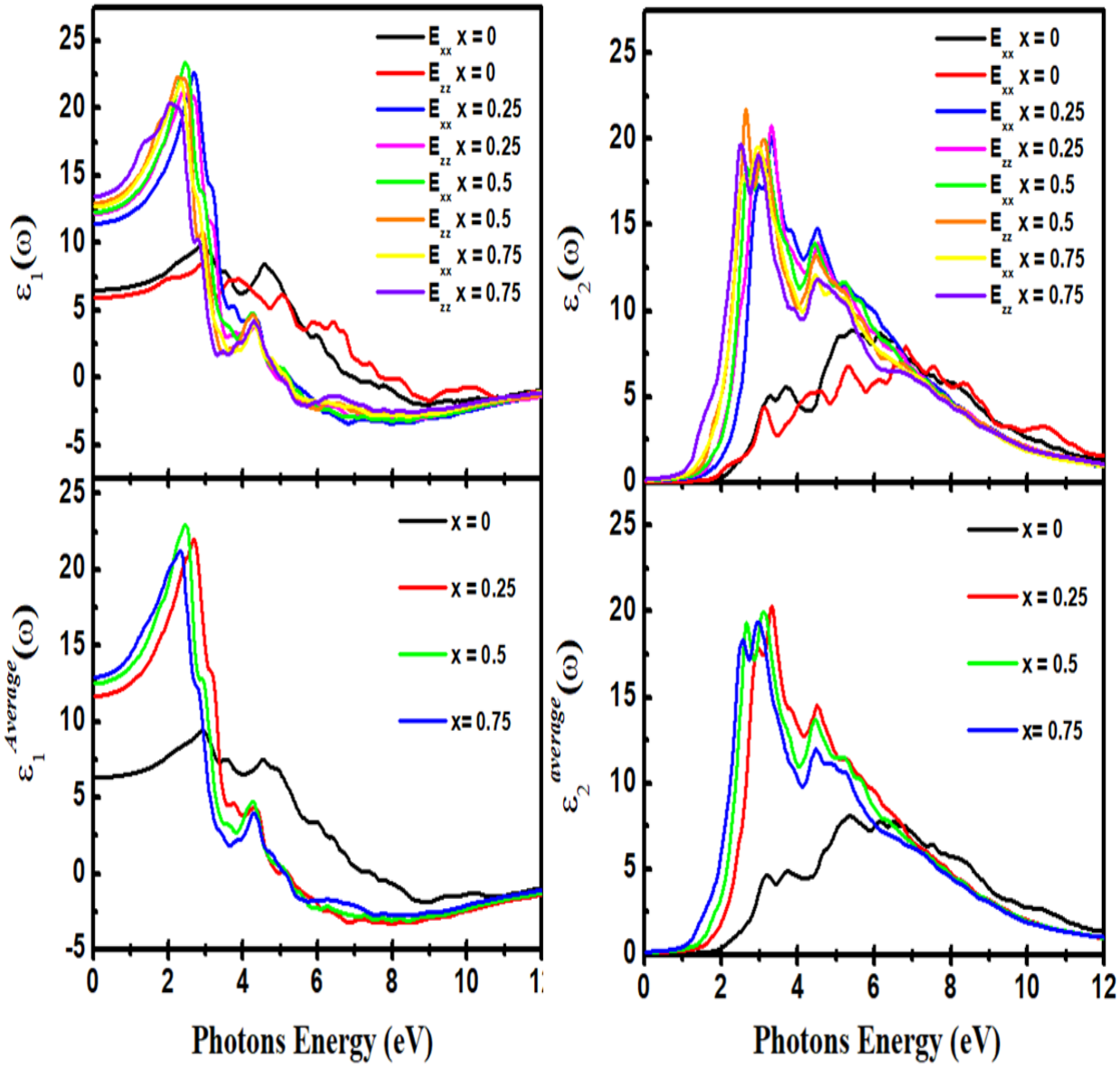

Fig.IV.5: The imaginary ε_1 (ω) (left panel) and real ε_2 (ω) (right panel) part spectra of complex dielectric function for $AgGa_{1-x}Tl_xSe_2$ materials.

Fig.IV.5 shows the calculated real (ε_{1xx} (ω), ε_{1zz} (ω)) and imaginary (ε_{2xx} (ω), ε_{2zz} (ω)) parts of the complex dielectric function of $AgGa_{1-x}Tl_xSe_2$ alloys as a function of the photon energy hν. There are two parts for dielectric function of chalcopyrite structure, ε_{2xx} and ε_{2zz}, the first term is the average of spectra for polarizations along the x and y directions and the second term is related to the z direction. The $\varepsilon^{Average}$ (ω) is the average function of both real and imaginary part calculated as follow:

$$\boldsymbol{\varepsilon}(\boldsymbol{\omega}) = (\boldsymbol{\varepsilon^x} + \boldsymbol{\varepsilon^y} + \boldsymbol{\varepsilon^z})/\mathbf{3} \qquad \textbf{(IV.12)}$$

The main peak in the calculated imaginary part ε_2 (ω) for pure $AgGaSe_2$ occurs at 5.45 eV. The increase of Tl in $AgGa_{1-x}Tl_xSe_2$ alloys results in the emergence of new peaks in the visible range. These new peaks are resulting from the photon absorption provoked by the direct interband transition from the occupied valence band to the Tl 's' states in the conduction band. These new peaks are moved toward lower energies with increasing Tl concentrations to be 3.5 eV, 3.1eV, 2.7eV for (x= 0.25, 0.5, 0.75) respectively. The main features in the spectrum of the real part ε_1 (ω) for pure $AgGaSe_2$ are a peak with a magnitude of 8.75 at around 2.93 eV , a decrease between 2.93 and 7.67 eV, after which ε_1 (ω) becomes negative , followed by a slow increase toward zero. With Tl substitution the main peak is shifted towards lower energy in the other three alloys.The most important quantity is the zero frequency limit ε_1 (0), which is the electronic part of the static dielectric constant and depends strongly on the band gap. The static dielectric constant $\varepsilon_1(0)$ values calculated at the equilibrium lattice constants, for $AgGa_{1-x}Tl_xSe_2$ alloys are listed in table **Table IV.6** and are in good agreement with the available data.

The Complex refractive index (N) has two parts, real (n) and imaginary (k) parts that are known as refractive index and extinction coefficient:

$$\boldsymbol{N(\omega) = n(\omega) + ik(\omega)} \qquad \textbf{(IV.13)}$$

The compounds with high refractive index have high optical nonlinearity.The n (ω) spectrum in **Fig.IV.6** records a maximum value in the visible light region for 0%, 25%, 50% and 75% of Tl. The average value of the static refractive index n(0) of $AgGa_{1-x}Tl_xS_2$ alloys is listed in the **table IV.6** and is in good agreement with the found data**.** Besides, the value of extinction coefficient k (ω) is zero up to 2.6 eV for $AgGaS_2$ which means it will not attenuate most of the incident visible light . The extinction coefficient is highest at 8.96 eV for $AgGaSe_2$ this implies that absorption is also prominent at about 8.96 eV, as the absorption coefficient α (ω) is related to the extinction coefficient k (ω) through the following relation:

$$\boldsymbol{\alpha = \frac{4\pi k}{\lambda}} \qquad \textbf{(IV.14)}$$

However, a new peak comes in to view when the Ga atom is replaced by the 75% Tl atom improving the optical response of $AgGaS_2$. The reflectivity $R(\omega)$ is also displayed in **Fig.IV.6**. the average reflection R average at E=0 eV are around 19.6 %, 28.1%, 30.4% and 31.6%, for 0, 25%, 50%, and 75% of Tl concentration, respectively. The R (ω) spectra show a maximum in the ultraviolet (UV) region which is enhanced with the increased Tl concentration.

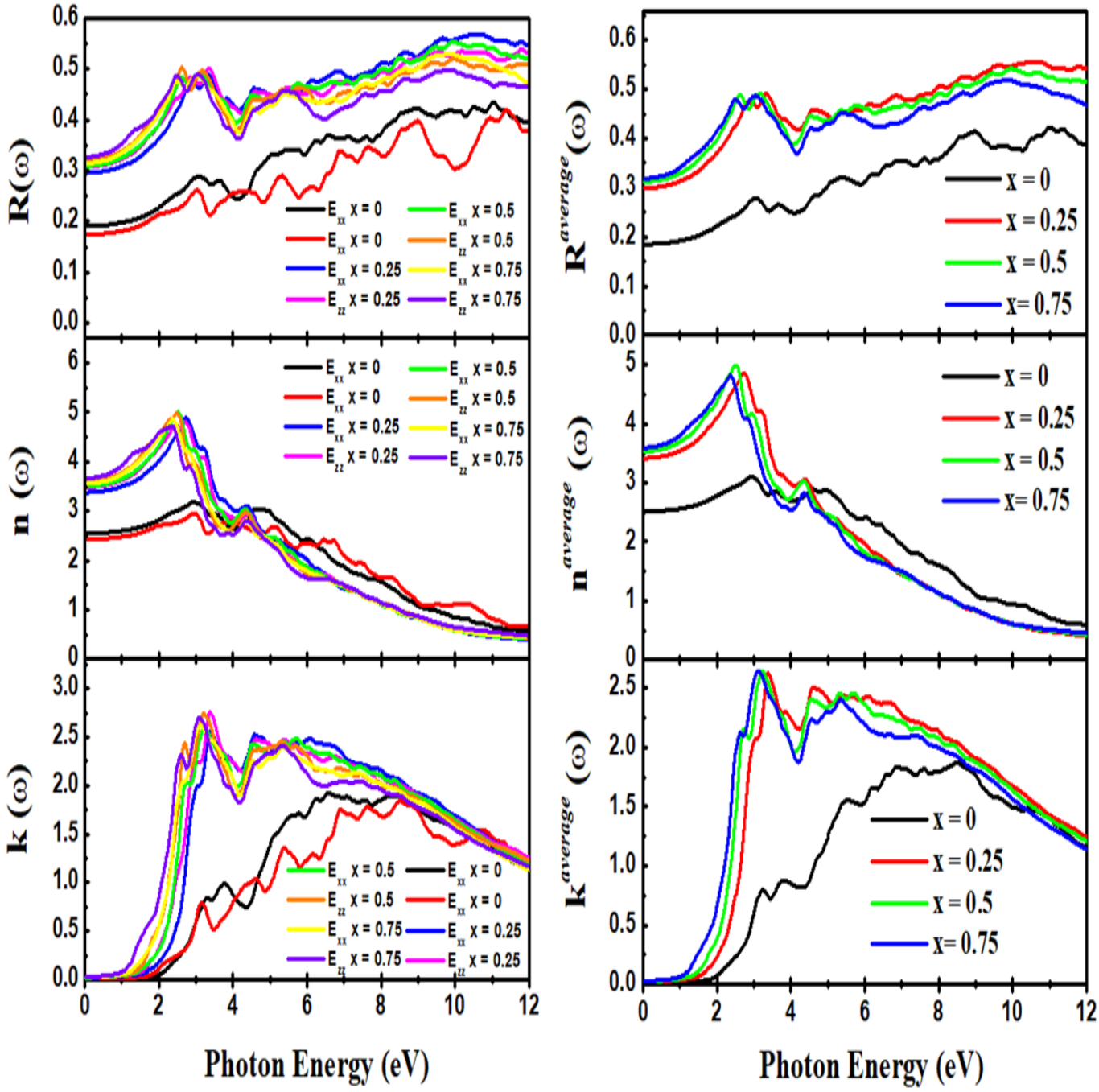

Fig.IV.6: The calculated refractive index n (ω), extinction coefficient k (ω), and reflectivity coefficient R (ω) of $AgGa_{1-x}Tl_xSe_2$ alloys along xx and zz-direction (left panel), average (right panel).

Table IV.5: The calculated optical dielectric constant, static reflectivity and static refractive index of $AgGaSe_2$

$AgGa_{1-x}Tl_xSe_2$		$\varepsilon_1(0)$	n(0)	R(0)
x = 0	This work	6.36	2.51	0.187
	Other calc.	7.2[55], 6.64[54]	2.8[55], 2.58[54]	0.198[56]
x = 0.25	This work	11.67	3.42	0.296
x = 0.5	This work	12.43	3.51	0.314
x = 0.75	This work	12.82	3.63	0.325

Fig.IV.7 illustrates the absorption coefficient α (ω) against the photon energy of $AgGa_{1-x}Tl_xSe_2$ alloys. it is apparent that the Tl substitution increases the absorption coefficient in the visible range significantly. The α (ω) value is about 0.3x 10^5 cm^{-1} for $AgGaSe_2$ and is enhanced to 2.9x10^5 cm^{-1} for $AgGa_{0.25}Tl_{0.75}Se_2$, suggesting that this alloy displays high absorption of solar light in the visible range, and acts as an optimum solar absorber. In addition, the square of absorption versus photon energy is plotted (i.e.,$(\alpha h\nu)^2$ versus hν for $AgGa_{1-x}Tl_xS_2$ alloys in **Fig.IV.8** Using a linear fitting a direct optical band gap is estimated to be 1.83 eV, 1.68 eV, 1.42 eV, and 1.27 eV for $AgGaSe_2$, $AgGa_{0.75}Tl_{0.25}Se_2$, $AgGa_{0.5}Tl_{0.5}Se_2$ and $AgGa_{0.25}Tl_{0.75}Se_2$, respectively. Evaluating the obtained results of α for $AgGa_{1-x}Tl_xSe_2$ alloys with other experimental results for established absorber materials such as $AgGaS_2$,GICS, CZTS, GaAs, CdTe, and $CH_3NH_3PbI_3$ **Fig.IV.9**, we observed that the absorption coefficient of $AgGa_{0.5}Tl_{0.5}Se_2$ is comparable to that of CdTe and CZTS, whereas the $AgGa_{0.25}Tl_{0.75}S_2$ shows a good absorption coefficient as GaAs and CIGS compound. Hence, $AgGa_{1-x}Tl_xSe_2$ alloys may be candidates for photovoltaic and solar cell usage.

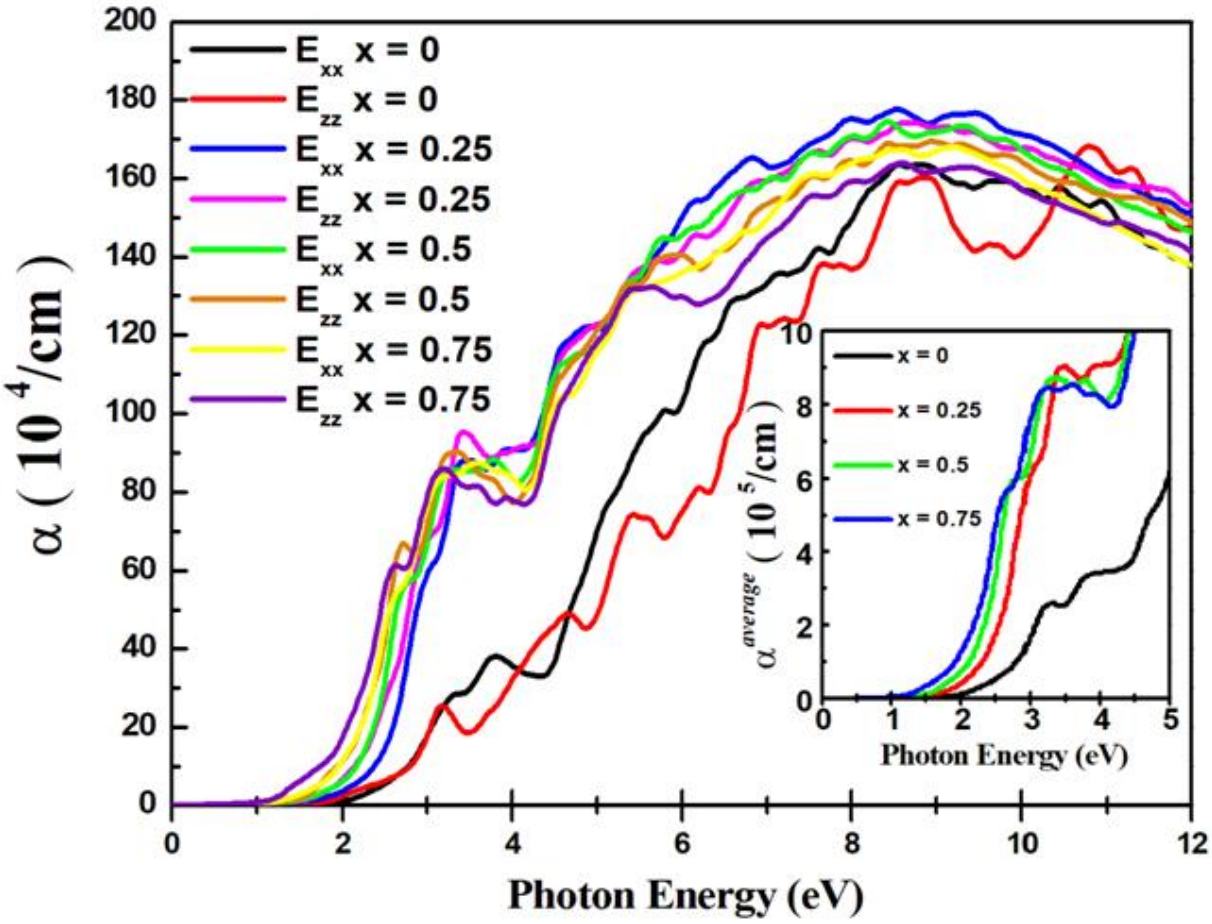

Fig.IV.7: The calculated absorption coefficient α (ω) of $AgGa_{1-x}Tl_xS_2$ alloys

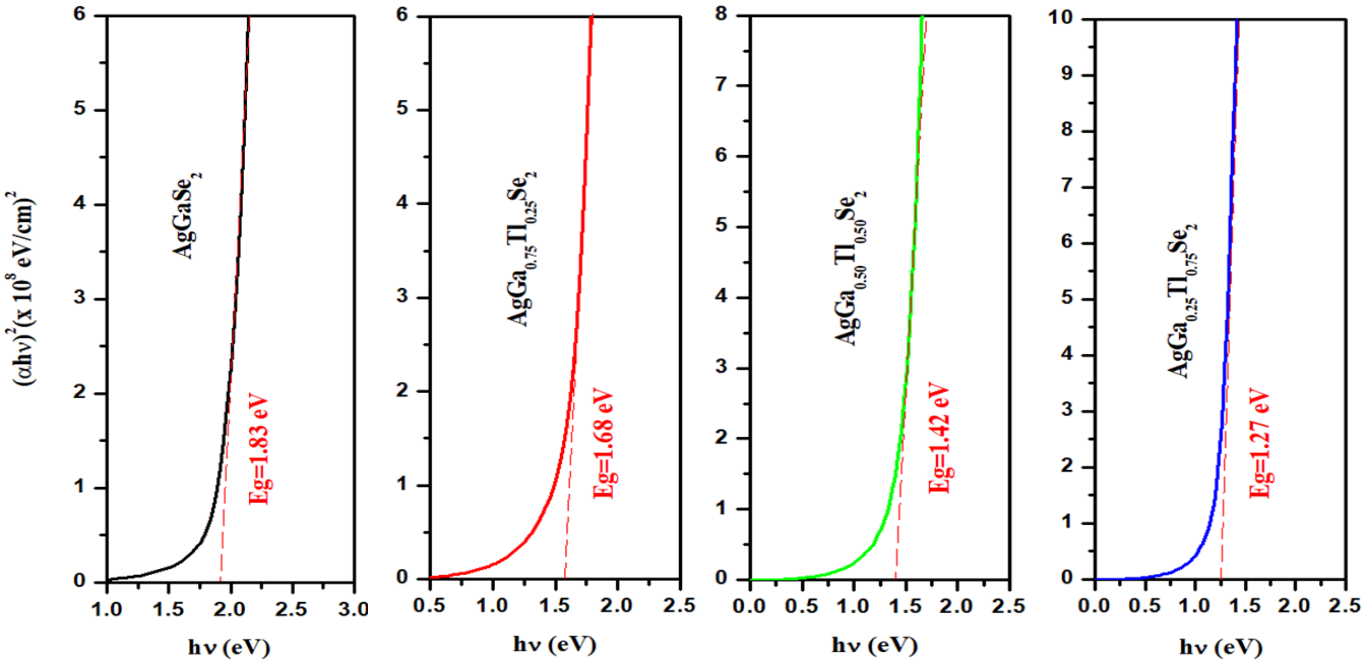

Fig.IV.8: Optical band gap of $AgGa_{1-x}Tl_xSe_2$ alloys.

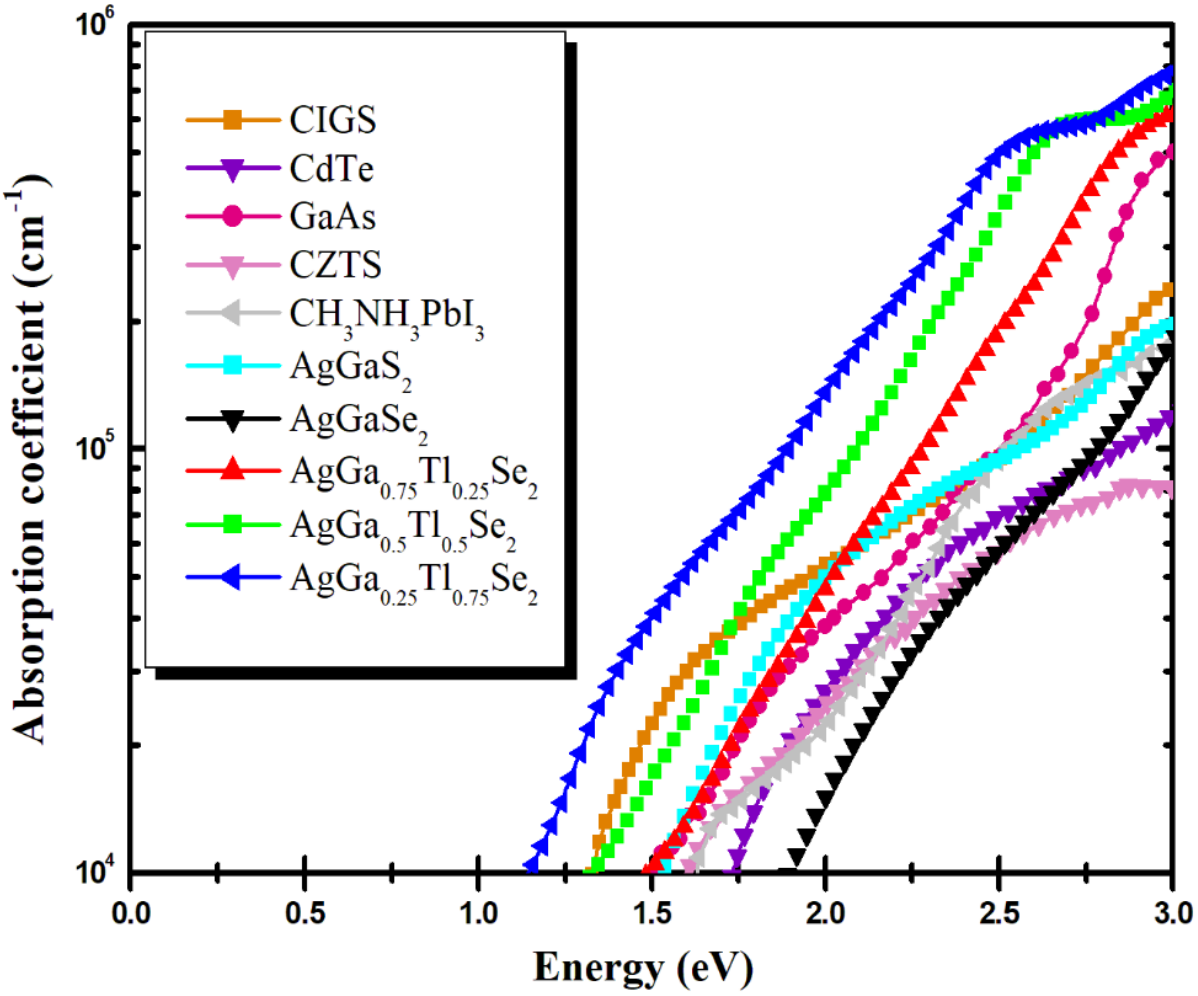

Fig.IV.9: The calculated absorption coefficient α (ω) of $AgGa_{1-x}Tl_xSe_2$ alloys compared with other materials such as CdTe [58], GaAs [59], CIGS [60], CZTS [61], $CH_3NH_3PbI_3$ [62], $AgGaS_2$ [63]

IV.7.Band alignment

The behavior of heterojunction solar cells depends crucially on the alignment of the energy bands of donor and acceptor semiconductors at the interface. Notice that these types of semiconductor heterojunction solar cells are different from that based on Schottky contacts and PN junctions consisting of semiconductor and metal heterojunctions. For donor and acceptor semiconductors used in heterojunction solar cells, there are several crucial factors for absorbing sunlight, such as a small direct band gap of roughly 1.2 - 1.6 eV to absorb wide range sunlight [67] and a high carrier mobility to facilitate efficient transport. Furthermore, the performance of

heterojunction solar cells depends ~~on~~ critically on the choice of donor and acceptor semiconductors with different VBM and CBM band positions. Here, we calculated the absolute band edges of the $AgGa_{1-x}Tl_xS_2$ according to the following equations proposed by Xu et al **[64]:**

$$E_{CBM} = \chi - (E_g/2) \quad \textbf{(IV.15)}$$

$$E_{VBM} = E_{CBM} + E_g \quad \textbf{(IV.16)}$$

where E_{VBM} and E_{CBM} represent the absolute potentials of VBM and CBM, Eg is the calculated band energy gap of present structures based on the first principles calculation and χ is the electronegativity of the semiconductors and is estimated as follows:

$$\chi(compound) = \left(\chi_1^s \chi_2^t \ldots \chi_{n-1}^p \chi_n^q\right)^{1/(s+t+p+q)} \quad \textbf{(IV.17)}$$

where χ_n and n represent the absolute electronegativities of the constituent atoms and the number of atomic species, whereas s, t, p, and q represent the number of individual atoms. Here, the atomic electronegativity is obtained from the electron affinity (I) and the first ionization energy of the atom (A) via the expression **[65]:**

$$\chi(Atom) = (I+A)/2 \quad \textbf{(IV.18)}$$

Figure IV.10 displays vacuum-aligned band diagram for $AgGa_{1-x}Tl_xSe_2$/CdS interface tacking CdS compound as n-type window layer. From this figure it is observed that the CB band edge of $AgGaSe_2$ is lying 0.95 eV upper than CB band edge of CdS, while the VB band edge is positioned 1.75 upper than that of CdS, forming type-II band alignment. This high conduction band offset (CBO = 0.95 eV) may be one of the reasons leading to a poor open circuit voltage (VOC), which in turn reduces the power conversion efficiency (PCE). It has been reported previously that the solar cell based CdS/$AgGaSe_2$ junction shows a short circuit courant J_{SC} = 12.2 $mA.cm^{-2}$, an open circuit voltage V_{OC} = 0.91 V, and a PCE = 5.8 % **[66]**. On the other hand, substituting Ga with Tl reduces the CBO to be 0.82 eV, 0.75 eV and 0.62 eV, which is a consequence of the downshift of the conduction band edge. This downshift also results in a reduction in the band gap value and an enlargement of the valence band offset (VBO) for CdS/$AgGa_{1-x}Tl_xSe_2$ junction. However, even with these new CBO values, we still believe that the PCE of CdS/$AgGa_{1-x}Tl_xSe_2$ solar cell will remain low. Therefore, we have suggesting others n-type windows layer such as ZnO **[69]**, SnO_2 **[70]**, TiO_2 **[71]**, PCMB **[72]** (see **Fig.10-b**).

Analyzing this figure it is remarked that the CBO value is reduced to be 0.57 (0.49) eV for ZnO, 0.47 (0.39) eV for SnO_2, and 0.37 (0.29) eV for both TiO_2 and PCMB in the case of $AgGa_{0.5}Tl_{0.5}Se_2$ ($AgGa_{0.25}Tl_{0.75}Se_2$) alloy. Thus, we expect that the optimal choice would be to use the TiO_2 compound as windows layer to form a $TiO_2/AgGa_{1-x}Tl_xSe_2$ solar cell, which will result in enhanced PCE.

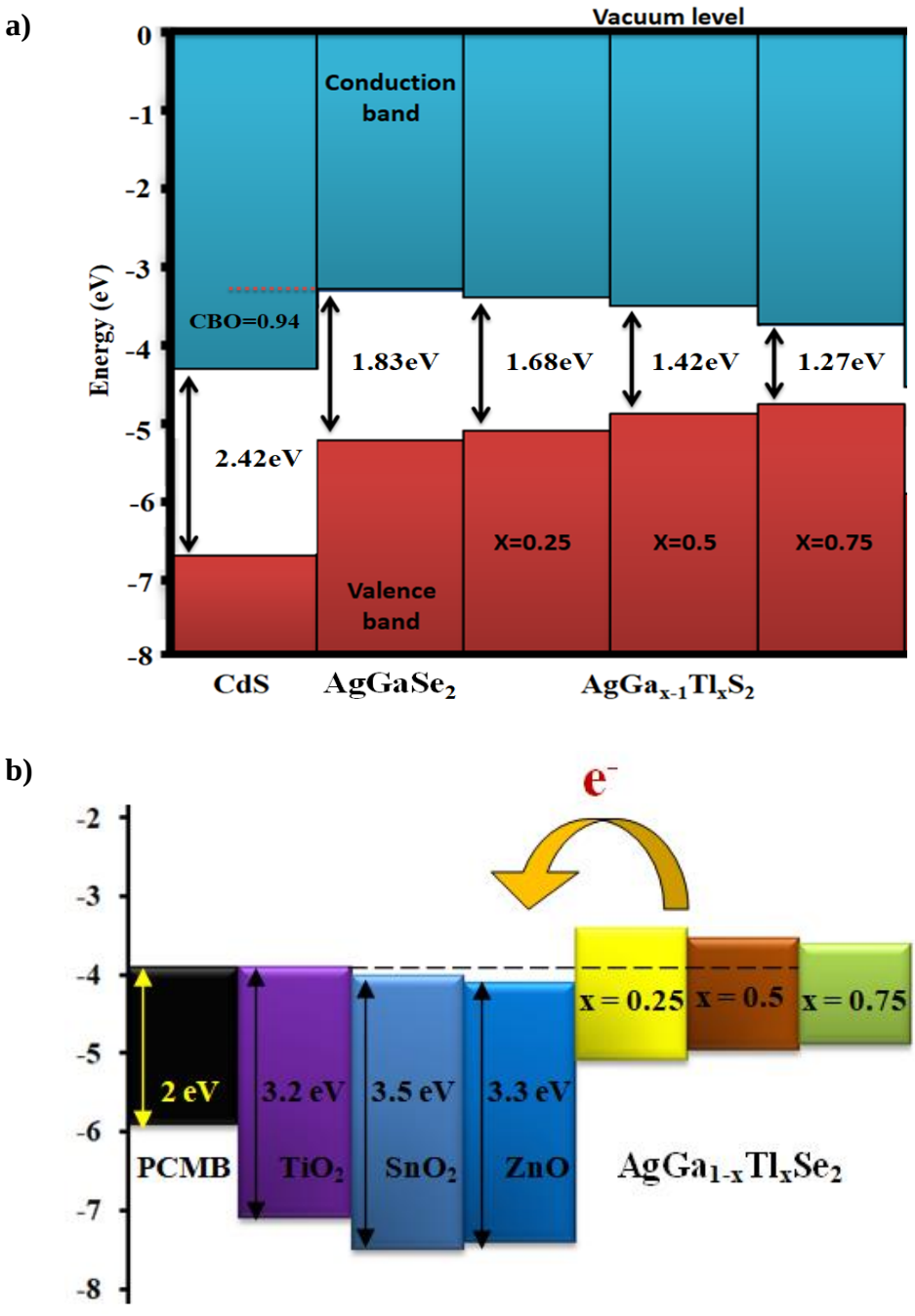

Fig.IV.10: Vacuum-aligned band diagram for $AgGa_{1-x}Tl_xS_2$ Compared with other common absorbers and the common n-type window layer material, CdS [68], ZnO [69], SnO_2 [70], TiO_2 [71], PCMB [72].

IV.8. Conclusion

In this chapter, we have carried out extensive calculations using the FP-APW+ lo method to identify the effect of Ga substitution by Tl on the structural, electronic and optical properties of the compound $AgGaSe_2$. The current DFT calculation reveals that when the gallium is replaced by the thallium, the minimum of the CB is shifted towards the Fermi level, resulting reduction of band gap from 1.86 eV for $AgGaSe_2$ pure to 1.75 eV, 1.50 eV, and 1.28 eV for $AgGa_{0.75}Tl_{0.25}Se_2$, $AgGa_{0.5}Tl_{0.5}Se_2$, and $AgGa_{0.25}Tl_{0.75}Se_2$, respectively. Besides, it is observed that both hole and electron effective masse decrease with the increase of Tl concentration, and thus both hole and electron carrier mobility is increased.

From the optical properties calculations, it is established that Tl substitution enhances the optical properties of $AgGaS_2$ by reducing the transparent region and improving the refractive index and the absorption in the visible light region. Consequently, the semiconducting nature with the appropriate direct band gap values and strong absorption ($\alpha > 10^5$ cm^{-1}) of the new $AgGa_xTl_{1-x}Se_2$ alloys in the visible light range are attractive contenders for optoelectronic and photovoltaic uses.

Analysis of the band alignments of $AgGa_{1-x}Tl_xSe_2$/CdS heterojunction reveals that when Tl is incorporated into $AgGaSe_2$, the conduction band offset is decreased. However, even with this decrease, we still believe that the PCE of CdS/$AgGa_{1-x}Tl_xSe_2$ solar cell will remain low. Therefore, others n-type windows layer such as ZnO **[69]**, SnO_2 **[70]**, TiO_2 **[71]**, PCMB **[72]** are suggested. From the analyze of the suggested band alignments we expect that the optimal choice would be to use the TiO_2 compound as windows layer to form a TiO_2/$AgGa_{1-x}Tl_xSe_2$ solar cell, which will result in enhanced PCE.

References:

[1] M. Yamaguchi, Sol. Energy Mater. Sol. Cells, , 75, 261– 269 (2003).

[2] S.A. Adonin, M.A. Bondarenko, P.A. Abramov, A.S. Novikov, P.E. Plyusnin, M.N. Sokolov, V.P. Fedin, Bromo- and polybromoantimonates(V): structural and theoretical studies of hybrid halogen-rich halometalate frameworks, Chem. Eur. J. 24, 10165 (2018).

[3] R.T. Stuart, C-W Chen, D.Manisha, Y-C Wang, Recent developments in the synthesis of nanostructured chalcopyrite materials and their applications: a review. RSC Adv, 6, 60643 (2016),

[4] R. W. Bentley, Energy Policy, , 30, 189–205 (2002).

[5] M. Z. Jacobson and M. A. Delucchi, Energy Policy., 39, 1154–1169 (2011).

[6] J.S. Jang, P.H. Borse, J.S. Lee, S.H. Choi, H.G. Kim, Indium induced band gap tailoring in AgGa1_xInxS2 chalcopyrite structure for visible light photocatalysis, Chem. Phys. 128, 154717 (2008).

[7] D. Lincota, J.F. Guillemolesa, S. Tauniera, D. Guimarda, J. Sicx-Kurdia, A. Chaumonta, O. Roussela, O. Ramdania, C. Huberta, J.P. Fauvarquea, N. Bodereaua, L. Parissia, P. Panheleuxa, P. Fanouillerea, N. Naghavia, P.P. Granda, M. Benfaraha, P. Mogensenb, O. Kerreca, Chalcopyrite Thin Film Solar Cells by Electro-Deposition Solar Energy, vol. 77, pp. 725–737. (2004)

[8] T. Plirdpring, K. Kurosaki, A. Kosuga, T. Day, S. Firdosy, V. Ravi, G.T. Snyder,A. Harnwunggmoung, A. Sugahara, Y. O-hishi, H. Muta, S. Yamanaka, Chalcopyrite CuGaTe2 : a high-Efficiency bulk thermoelectric material, Adv. Mater. 24 (2012) 3622.

[9] P.C. Ricci, A. Anedda, R. Corpino, C.M. Carbonaro, M. Marceddu, I.M. Tiginyanu, V.V. Ursaki, Temperature dependence of the photoluminescence spectra in AgGaS2, J. Phys. Chem. Solid. 66, 1950–1953 (2005).

[10] Y.X. Fan, R.C. Eckardt, and R.L. Byer, in Topical Meeting on Solid State Lasers (Optical Society of America, Zig Zag, Oregon, (1986).

[11] G.J. Quarles, C.L. Marquardt, and L. Es- terowitz, in LEOS Optical Society of America, (1990).

[12] N.P. Barnes, D.J. Gettemy, J.R. Hietanen, and R.A. Iannini, in CLEO/IEEE Conf. Optical Society of America, Baltimore, MD, (1987).

[13] U. Simon, C.E. Miller, C.C. Bradley, R.G. Hulet, R.F. Curl, and F.K. Tittel, Opt. Lett. 18, p. 1062 (1993).

[14] U. Simon, F.K. Tittel, and L. Goldberg, ibid. p56 (1931).

[15]. N. B. SINGH, R. H. HOPKINS, J. D. FEICHTNER. Effect of annealing on the optical quality of AgGaS2 and AgGaSe2 single crystals Journal of Materials Science 21 837 841 (1986)

[16] N.B. Singh, R.H. Hopkins, J.D. Feichtner, J. Mater. Sci. 21, 837 (1986).

[17] G. Boyd, H.M. Kasper, J.H. Mcfee, F.G. Storz, IEEE J. Quantum Electron. QE-8, 900 (1972).

[18] G.K.H. Madsen, P. Blaha, K. Schwarz, E. Sjöstedt, L. Nordström, Phys. Rev. B 64, 195134 (2001)

[19] Z. Wu, R.E. Cohen, Phys. Rev. B 73, 235116 (2006).

[20] F. Tran, P. Blaha, Phys. Rev. Lett. 102, 226401 (2009).

[21] P. Blaha, K. Schwarz, G. K. H. Madsen, D. Kvasnicka, J. Luitz, Technische Universitat Wien, Austria (2001).

[22] J. P. Perdew, K. Burke, M. Ernzerhof, Physical Review Letters 77, 3865–3868 (1996).

[23] T. Sakuntala, A.K. Arora, Pressure-tuned resonance Raman scattering in AgGaSe2, Phys. Rev. B 53, 15667 (1996).

[24] A.Chahed,O.Benhelal,S.Laksari,B.Abbar,B.Bouhafs,N.Amrane,PhysicaB: Condens. Matter 367, 142–151 (2005).

[25] F.D. Murnaghan, Proc. Natl. Acad. Sci. U. S. A 30 (1944).

[26] J. Phys.: Condens. Matter 15, 6043–6055 (2003)

[27] H. Salehi, E. Gordanian / Materials Science in Semiconductor Processing 47, 51-56 (2016)

[28] J.L. Shay, J.H. Wernick, Ternary Chalcopyrite Semiconductors: Growth, Electronic Properties and Applications, Pergamon Press, Oxford, (1974).

[29] B.B. Karki, S.J. Clark, M.C. Warren, H.C. Hsueh, G.J. Ackland, J. Crain, J. Phys.: Condens. Matter 9, 375 (1997).

[30] H. Neumann, Phys. Stat. Sol. (A) 96, K121 (1986).

[31] R. Asokamani, R.M. Amirthakumari, R. Rita, C. Ravi, Phys. Stat. Sol. (B) 213, 349 (1999).

[32] T. Tinoco, A. Polian, J.P. Itie´ , E. Moya, J. Gonzales, J. Phys. Chem. Solids 55, 481 (1995).

[33] J.E. Jaffe, D. Zunger, Phys. Rev. B 29, 1882 (1984).

[34] T. Ouahrani, A. Otero-de-la-Roza, A.H. Reshak, R. Khenata, H.I. Faraoun, B. Amrani, M. Mebrouki, V. Luan, Physica B 405, 3658 (2010).

[35] A.S. Verma, S.R. Bhardwaj, Phys. Scr. 79, 015302 (2009).

[36] S. Sharma et al. / Materials Research Bulletin 53, 218–233 (2014)

[37]A.Chahed,O.Benhelal,S.Laksari,B.Abbar,B.Bouhafs,N.Amrane,PhysicaB:Condens.Matter 142–151 (2005).

[38] S. Chen, X.G. Gong, S.-H. Wei, Phys. Rev. B 75 (2007).

[39] H. Neumann, Cryst. Res. Technol. 18 1567 (1983).

[40] V. Kumar, B.S.R. Sastry / Journal of Physics and Chemistry of Solids 66 99–102 (2005).

[41] S.M. Hosseini, T. Movlarooy, A. Kompany, First-principle calculations of the cohesive energy and the electronic properties of PbTiO3, Physica B 391 316–321 (2007).

[42] E. Gordanian and H. Salehi, Investigation of the Structural and the Electronic Properties of AgGaX2(X = S, Se, Te) Nanolayers in the [112] Direction by using Density Functional Theory, Journal of the Korean Physical Society, Vol. 76, No. 10, , pp. 928~934 (2020).

[43] L.C. Tang, M.H. Lee, C.H. Yang, J.Y. Huang, C.S. Chang, J. Phys.: Condens. Matter 15 6043 (2003).

[44] A.S. Verma, Phys. Status Solidi B 246 192 (2009).

[45] J. Bardeen, W. Shockley, Phys. Rev. , 80, 72 (1950).

[46] Q. Y. Xue, H. J. Liu, D. D. Fan, L. Cheng, B. Y. Zhao, J. Shi, Phys. Chem. Chem. Phys. 18, 17912 (2016).

[47] Y-L.Liu, C-L.Yang, M-S.Wang, X-G.Ma, Y-G.Yi, Int J Quantum Chem, 26166 (2020).

[48] D. Huang, C. Persson, Z. Ju, M. Dou3, C. Yao and J. Guo, Investigation on AgGaSe2 for water splitting from first-principles calculations, EPL, 105, 37007 (2014)

[49] L.C. Tang, M.H. Lee, C.H. Yang, J.Y. Huang, C.S. Chang, J. Phys.: Condens. Matter 15 (2003).

[50] A.S. Verma, Phys. Status Solidi B 246 192 (2009) .

[51] Omata, N, and Otsuka-Yao-M, J. Appl. Phys. **105**, 073106 (2009).

[52] C. Ambrosch-Draxl, J. O. Sofo, Computer Physics Communications 175 , 1 1–14 (2006).

[53] W. Kin Mun, Japanese Journal of Applied Physics 48 ,8R, 085002 (2009).

[54] A.S. Verma, D. Sharma, Phys. Scr. 76, 22 (2007).

[55] A.S. Verma, S. Sharma, V.K. Jindal, Mod. Phys. Lett. B 24, 2511 (2010).

[56] S. Sharma et al. / Materials Research Bulletin 53, 218–233 (2014).

[57] Omata, N, and Otsuka-Yao-M, J. Appl. Phys. 105, 073106 (2009).

[58] G.B. Dubrovskii, Optical properties of CdTe, Sov. Phys. Solid State 3, 1305 (1961).

[59] J.O. Akinlami, A.O. Ashamu, Optical properties of GaAs, J. Semiconduct. 34,032002 (2013).

[60] S. Minoura, K. Kodera, T. Maekawa, K. Miyazaki, S. Niki, H. Fujiwara, Dielectric function of Cu(In, Ga)Se2-based polycrystalline materials, J. Appl. Phys 113,), 063505 (2013)

[61] J.S. Seol, S.Y. Lee, J.C. Lee, H.D. Nam, H.K. Kim, Electrical and optical properties of Cu2ZnSnS4 thin films prepared by rf magnetron sputtering process, Sol. Energy Mater. Sol. Cells 75, 155–162 (2003).

[62] X. Ziang, L. Shifeng, Q. Laixiang, P. Shuping, W. Wei, Y. Yu, Y. Li, C. Zhijian, W. Shufeng, D. Honglin, Y. Minghui, G.G. Qin, Refractive index and extinction coefficient of CH3NH3PbI3 studied by spectroscopic ellipsometry, Opt. Mater. Express 5, 29–43 (2015).

[63] R. Mouacher , T. Seddik , B. Rezini , Bakhtiar Ul Haq , M. Batouche , G. Ugur , S. Ugur , A. Belfedal , Journal of Solid State Chemistry 309, 122996 (2022)

[64] Y. Xu, M. A. A. Schoonen, Am. Mineral, 85, 543 (2000).

[65] R. S. Mulliken, J. Chem. Phys, 2, 782 (1934).

[66] J. K. Larsen, O. Donzel-Gargand, K. V. Sopiha, J. Keller, K. Lindgren,C. Platzer-Bjorkman, and M. EdoffACS Appl. Energy Mater. 4, 1805−1814, (2021).

[67] W. Shockley and H. J. Queisser, J. Appl. Phys, 32, 510–519 (1961).

[68] Y. Satyanarayana Mm-thy, 0. Mahammad Hussain, B. Srinivasulu Naidu and P. Jayarama Reddy, Characterization of p-AgGaSe2/n-CdS thin film heterojunction, Materials letters, Volume 10, number 11,12(1991).

[69] N.H. Nickel and E. Terukov (eds.), Zinc Oxide – A Material for Micro- and Optoelectronic Applications, 197–209. (2005)

[70] F. Mohamadkhania , S.Javadpoura, N.Taghavinia. Improvement of planar perovskite solar cells by using solution processed SnO2/CdS as electron transport layer Solar Energy 191 647–653 (2019)

[71] J.Löckinger , S.Nishiwaki, T.P. Weiss, B.Bissig, Y.E. Romanyuk, S. Buecheler, A. N. Tiwari. TiO2 as intermediate buffer layer in Cu(In,Ga)Se2 solar cells. Solar Energy Materials and Solar Cells 174 397–404 (2018)

[72] O.M. Ntwaeaborwa, R.Zhou , L. Qian ,S. Pitale, J. Xue, H.C. Swart , P.H. Holloway. Post-fabrication annealing effects on the performance of P3HT:PCBM solar cells with/without ZnO nanoparticles. / Physica B 407 1631–1633 (2012)

General conclusion

In the present work the electronic and optical properties of $AgGaS_2$ and $AgGaSe_2$ using band convergence strategy by substitution of Thallium (Tl) into the gallium (Ga) site were investigated. All calculations were carried out using the full potential augmented plane waves plus local orbital's (FP-APW+lo) method based on Density Functional Theory (DFT). Starting with the question: what effect will Tl substitution will have on these properties? We firstly formed the $AgGa_{1-x}Tl_xS_2$ and $AgGa_{1-x}Tl_xSe_2$ alloys for x = 0.25, 0.5, and 0.75.

From stability view, the estimated energy formation E_f values are found negative, indicating the thermodynamic stability of all $AgGa_{1-x}Tl_xS_2$ and $AgGa_{1-x}Tl_xSe_2$ Alloys. We also remarked that both ground states parameters *a* and *c* increase when Tl atoms are gradually substituted into Ga atoms in the $AgGaS_2$ and $AgGaSe_2$ unit cell. The present investigation reveals that when the gallium is replaced by the thallium, the minimum of the CB is shifted towards the Fermi level, resulting reduction of band gap from 2.59 eV to 1.91 eV, 1.61 eV, and 1.28 eV for $AgGa_{1-x}Tl_xS_2$ (x = 0. 0.25, 0.5, and 0.75) alloys, respectively, and from 1.86 eV to 1.75 eV, 1.50 eV, and 1.28 eV for $AgGa_{1-x}Tl_xS_2$ (x = 0. 0.25, 0.5, and 0.75) alloys, respectively. Besides, it is observed that both hole and electron effective masse decrease with the increase of Tl concentration, and thus both hole and electron carrier mobility is increased. Moreover, from the optical properties calculations, it is established that Tl substitution enhances the optical properties of $AgGaS_2$ and $AgGaSe_2$ by improving the refractive index and the absorption in the visible light region ($\alpha > 10^5$ cm^{-1}). These results making these news alloys attractive materials for optoelectronic applications.

Analysis of the band alignments of $AgGaX_2$ (X = S , Se)/CdS heterojunction reveals that both p-n junction posses high conduction band offset CBO = 0.78 eV, and 0.95 eV, respectively, which may be one of the reasons leading to a poor open circuit voltage (VOC), which in turn reduces the power conversion efficiency (PCE). In addition, when Ga is substituted by Tl atoms the conduction band offset is decreased, and thus the open-circuit voltage can be improved. In fact this conclusion may be true for $AgGaS_2$/CdS heterojunction, however is not the case of $AgGaSe_2$/CdS interface. Therefore, others n-type windows layer such as ZnO, SnO_2, TiO_2, PCMB were suggested. From the analyze of the suggested band

alignments we expect that the optimal choice would be to use the TiO_2 compound as windows layer to form a $TiO_2/AgGa_{1-x}Tl_xSe_2$ solar cell, which will result in enhanced PCE.

Overall, Tl substituted into Ga sites of $AgGaS_2$ and $AgGaSe_2$ chalcopyrite leads to new alloys that can be promising materials for solar cell applications, and we expect that these finding help scientist to experimentally investigate these new suggested alloys.

Journal of Solid State Chemistry 309 (2022) 122996

Contents lists available at ScienceDirect

Journal of Solid State Chemistry

journal homepage: www.elsevier.com/locate/jssc

First-principles calculations of electronic and optical properties of $AgGa_{1-x}Tl_xS_2$ alloys: Analyses and design for solar cell applications

R. Mouacher [a], T. Seddik [a,*], B. Rezini [a], Bakhtiar Ul Haq [b], M. Batouche [a], G. Uğur [c], S. Uğur [c], A. Belfedal [d]

[a] Laboratory of Quantum Physics of Matter and Mathematical Modeling (LPQ3M), Mascara University, Algeria
[b] Department of Physics, Faculty of Science, King Khalid University, P.O. Box 9004, Abha, Saudi Arabia
[c] Department of Physics, Faculty of Science, Gazi University, 06500, Ankara, Turkey
[d] Laboratoire de Chimie Physique des Macromolécules et Interfaces Biologiques, Université de Mascara, Algeria

ARTICLE INFO

Keywords:
AgGaS2 chalcopyrite
VBO
Electronic properties
Optical properties
Photovoltaic applications
First-principles approaches

ABSTRACT

The thallium substitution effect on structural, electronic, and optical properties of chalcopyrite-type material $AgGaS_2$ is investigated via first-principles approaches. The computed band gap energy of pure $AgGaS_2$ is about 2.59 eV using Tran-Blaha (TB)-modified Becke Johnson (mBJ) exchange potential, which is in good accord with experimental measurements. This band gap value was observed to decrease to be 1.91 eV, 1.61 eV, and 1.28 eV when Tl is substituted into Ga site, respectively, for 25%, 50%, and 75% concentrations. Besides, the $AgTlS_2$ band gap was also calculated and found to be 0.61 eV. This investigation establishes that Tl substitution increases both hole and electron carrier mobility of the pure $AgGaS_2$ compound. By analyzing the band alignment diagram, it was observed that the Tl substitution increases the valence band offset (VBO) and decreases the conduction band offset (CBO), which can lead to the improvement of open-circuit voltage V_{OC}. Moreover, the optical analysis reveals that Tl substitution enhances the optical properties of $AgGaS_2$ by reducing the transparency and improving the refractive index and the absorption in the visible light region. Based on obtained results, it is predicted that the band gap and the optical properties of the $AgGaS_2$ chalcopyrite can be effectively tuned by Tl substitution over the Ga sites, making $AgGa_{1-x}Tl_xS_2$ alloys promising candidates for optoelectronic and photovoltaic applications.

1. Introduction

To deal with the diminishing fossil fuel resources and to satisfy the ever-growing need for clean energy, the production of photovoltaic energy has taken on great importance as solar cells do not emit any unwanted emissions. The actual market for solar cells is mainly based on monocrystalline silicon or III-V semiconductors which have demonstrated a very high efficiency [1], but many low-cost solar cells are needed for general and wider applications. Therefore, designing and developing new solar cell materials with desired electronic, optical, and photovoltaic properties is an important step. For example, inorganic materials based on transition metal and chalcogenides or halide materials have recently been investigated which show promising optoelectronic properties [2,3]. Besides, mixed organic-inorganic materials have also been suggested as promising candidates for solar cell applications due to their ideal optical properties as well as relatively low-cost preparation methods [4–6].

Among these materials the chalcopyrite-based compounds of the general formula I-III-VI_2, where I is usually copper (Cu) or silver (Ag), have been receiving high attention in the last decade due to its usage in detectors, light-emitting diodes (LEDs), thermoelectric, photocatalysts, nonlinear optics (NLO) applications and solar energy conversion [7–12]. The major characteristic of chalcopyrite semiconductors is that they possess unique electronic and optical properties, direct band gap, transparent behavior against visible and infrared radiation, a high absorption coefficient and a lifetime in outer space longer compared to that of Si and III-V compounds [13]. Recently the copper (Cu-III–VI_2) based chalcopyrites have proven their efficiency for solar cell applications. For example the $CuGaSe_2$ shows efficiency of about 11.2% [8] while $CuInSe_2$ realizes 14.5% efficiency [14] via a tandem cell of ZnO/CdS/$CuInSe_2$. However, $Cu(InGa)Se_2$ (CIGS) have recorded the highest power conversion efficiency (PCE) of about 23.4% (cells), 17.4% (module) [15–19] which make it promising absorber materials for solar cell applications. Conversely, the silver (Ag-III–VI_2) based chalcopyrites receive much

* Corresponding author. LPQ3M-Laboratory, Faculty of Science and Technology, Mascara University, 29000, Mascara, Algeria.
E-mail addresses: seddik.taib@univ-mascara.dz, sedik_t@yahoo.fr (T. Seddik).

https://doi.org/10.1016/j.jssc.2022.122996
Received 10 November 2021; Received in revised form 13 February 2022; Accepted 15 February 2022
Available online 17 February 2022

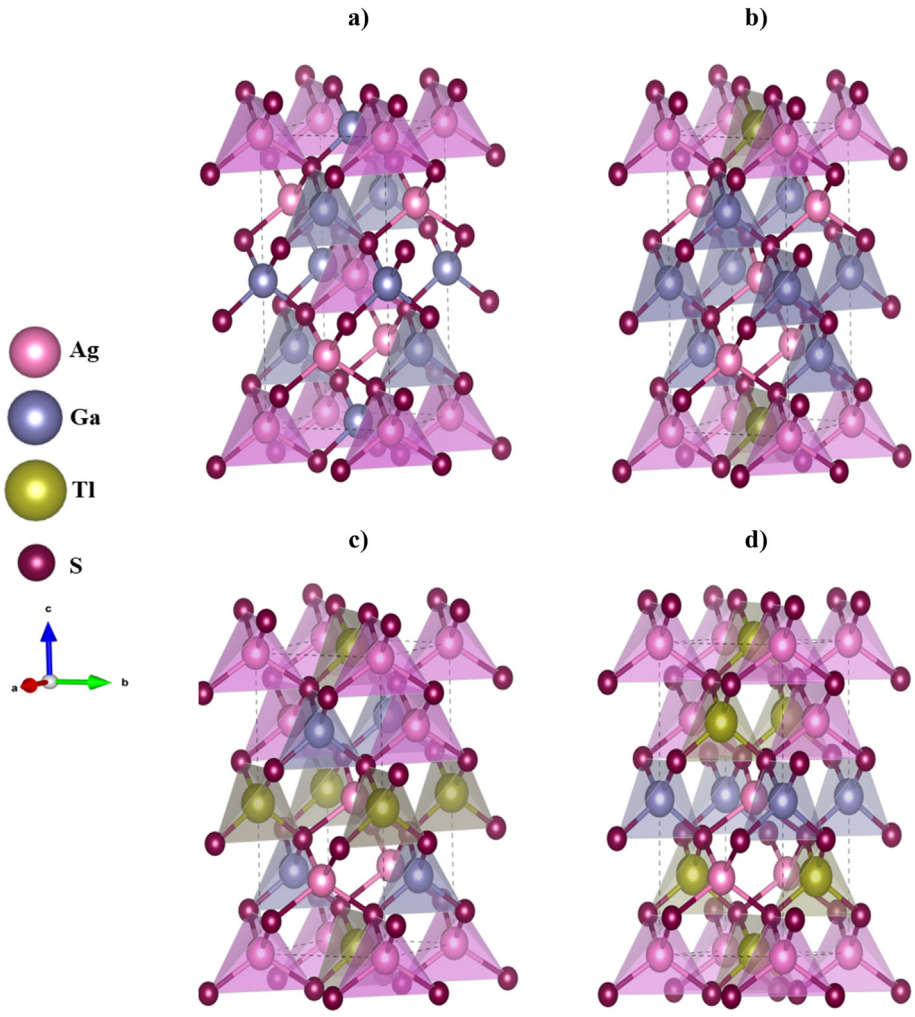

Fig. 1. Visualization of crystal structure of $AgGaS_2$ (a), and $AgGa_{0.75}Tl_{0.25}S_2$ (b), $AgGa_{0.5}Tl_{0.5}S_2$ (c), $AgGa_{0.25}Tl_{0.75}S_2$ alloy (d) obtained using VESTA software [37].

attention due to their suitability for non-linear optical and photonic applications [20].

The $AgGaS_2$ is known as part of the chalcopyrite family with a direct band gap of about (2.48–2.75) eV [21–24]. This compound is used as commercial material for NLO applications due to its large NLO coefficient d_{36} = 39 p.m./V and excellent transparency in the mid-IR range (1–18 μm) [25]. Besides, the $AgGaS_2$ compound was proposed as a promising candidate for X-ray dosimetry [26]. However, its band gap value and weak absorption in the visible light region limit its use as absorber material for photovoltaic solar cells. Very recently, the best efficiency of 5.85% was reported using $AgGaS_2$ chalcopyrite as an absorbing layer [27]. Therefore, the main goal of the present work is to improve the optical and electronic properties of $AgGaS_2$ using band convergence strategy by substitution of Thallium (Tl) into the gallium (Ga) site in the $AgGaS_2$ compound for the building of $AgGa_{1-x}Tl_xS_2$ alloy. From an experimental and theoretical point of view, it has already been reported that tailoring the band gap value of $AgGaS_2$ leads to interesting optoelectronic and photocatalytic properties [9,28–30]. The current work deals with the study of the structural, electronic, and optical properties of the Tl-doped $AgGaS_2$ chalcopyrite through the full potential augmented plane wave plus local orbital's method.

2. Calculations detail

In the present investigations, all calculations are done using the FP-APW + lo method [31,32], implemented in the WIEN2k code [33]. In this technique, the system space is divided into two regions the interstitial one and the muffin-tin spheres with muffin-tin radius (R_{Mt}) are chosen in a manner that the MT spheres do not overlap. The RMT values are adjusted to be 2.5, 2.3, 2.41, and 1.88 a.u for Ag, Ga, Tl, and S, respectively, with the following electronic configuration Ag: [Kr] $4d^{10}5s^1$, Ga: [Ar] $4s^23d^{10}4p^1$, S: [Ne] $3s^23p^4$, Tl: [Xe] $4f^{14}5d^{10}6s^26p^1$. The electronic wave functions are expanded up to l_{max} equal to 4 and 10 outside and inside the MT sphere, respectively. Besides, the expansion of the wave functions and charge density were cut off by the $R_{MT}K_{max}$ = 7.5 and G_{max} = 12 parameters. The exchange-correlation potential is treated by the generalized gradient approximation performed by Wu and Cohen (GGA-WC) [34]. However, since the GGA approximation yields an underestimated band gap value, the Tran-Blaha modified Becke-Johnson (mBJ) exchange potential is employed [35,36]. Besides, the $AgGa_{1-x}Tl_xS_2$ alloys are modeled using 1 × 1 × 2 periodic supercells with 16 atoms in the primitive cell. The gallium atoms are substituted by thallium atoms to adopt all the possible configurations with Ga and Tl mixed atoms to generate $AgGa_{1-x}Tl_xS_2$ alloys with x = 0.25, 0.50, and 0.75 (see Fig. 1).

3. Results and discussion

3.1. Structural properties

At ambient conditions, the $AgGaS_2$ material is reported to crystallize in chalcopyrite type-structure (space group I-42d) [38] (see Fig. 1). In this structure, the Ag atoms are situated at 4a (0, 0, 0), the Ga atoms at (0,

Table 1
The calculated lattice constant (a and c) (Å), the anion displacement parameter u, bulk modulus (GPa) and its pressure derivative, and formation energy (KJ/mol) for $AgGa_{1-x}T_xS_2$ Alloys.

$AgGa_{1-x}Tl_xS_2$		a	c	u	B	B'	E_f
x = 0	This work	5.746	10.266	0.287	75.08	4.88	−328.05
	Expt.	5.755 [23]	10.278 [23]	0.282 [23]	77.6 [40]	4 [41]	
	Other calc.	5.587 [42]	10.408 [42]	0.288 [43]	67.15 [44]	4.744 [42]	−386.5 [48]
		5.742 [45]	10.26 [45]	0.2844 [46]	72.62 [45]	4.7 [46]	−359.4 [48]
		5.75 [47]	10.299 [47]	0.281 [47]	76.2 [47]	5 [47]	
x = 0.25	This work	5.868	10.493	0.268	68.82	4.56	−275.948
x = 0.5	This work	5.98	10.67	0.257	61.45	4.63	−300.069
x = 0.75	This work	6.09	10.86	0.244	56.95	4.73	−262.44
x = 1	This work Other calc.	6.22	11.12	0.239	59.95	4.77	−246.92
		5.882 [43]		0.257 [43]			

Table 2
Interatomic distance for $AgGa_{1-x}Tl_xS_2$ alloys.

$AgGa_{1-x}Tl_xS_2$		Ag–S	Ga–S	Tl–S
x = 0	This work Expt [23].	2.524	2.293	–
		2.556 ± 1	2.276 ± 1	–
x = 0.25	This work	2.577	2.342	2.342
x = 0.5	This work	2.625	2.385	2.385
x = 0.75	This work	2.673	2.429	2.429
x = 1	This work	2.565	–	2.644

0, 1/2) and the S atoms at (0.28, 1/4, 1/8). Regarding this structure, we first optimized the anion displacement parameter u_S with 1×10^{-4} Ry/a.u. force convergence criteria, and then calculated the total energy as a function of volume and c/a ratio for each alloy. After that, the ground-state properties such as lattice parameters (a and c), bulk modulus B and its first pressure derivative B' are determined through the Murnaghan equation [39] fitting of the energy vs. volume optimization curves. The results of the estimated structural properties (a, c, B and B') of $AgGa_{1-x}Tl_xS_2$ alloys are reported in Table 1 along with experimental [23,40,41] and theoretical results [43–47]. The resulting values are in reasonable agreement when compared to the experimental values. The difference in values between the calculated unit cell parameters and the experimental values is less than 0.2%. From Table 1, one can observe that both a and c increase when Tl atoms are gradually substituted into Ga atoms in the $AgGaS_2$ unit cell. Conversely, the bulk modulus was found to decrease with increase in Tl concentration owing to increase in the interatomic distance in the $AgGa_{1-x}Tl_xS_2$ alloys from x = 0 to x = 1 (see Table 2).

In the aim of analyzing the stability and formation of $AgGa_{1-x}Tl_xS_2$ alloys, the formation energy E_f is predicted as below:

Table 3
The total energy E_T of $AgGa_{1-x}Tl_xS_2$ alloys and the energies of Ag, Ga, Tl and S atoms in (eV).

E_T ($AgGaS_2$)	E_T ($AgGa_{0.75}Tl_{0.25}S_2$)	E_T ($AgGa_{0.5}Tl_{0.5}S_2$)	E_T ($AgGa_{0.5}Tl_{0.75}S_2$)	E_T ($AgTlS_2$)
$-4.385\ 517 \times 10^5$	$-1.376\ 255 \times 10^9$	$-1.875\ 427 \times 10^6$	$-2.374\ 59 \times 10^6$	-1.056085×10^5
E_{Ag}	E_{Ga}	E_{Tl}	E_S	
$-5.288\ 679 \times 10^4$	$-1.446\ 705 \times 10^5$	$-1.085\ 236 \times 10^4$	$-5.520\ 529 \times 10^5$	

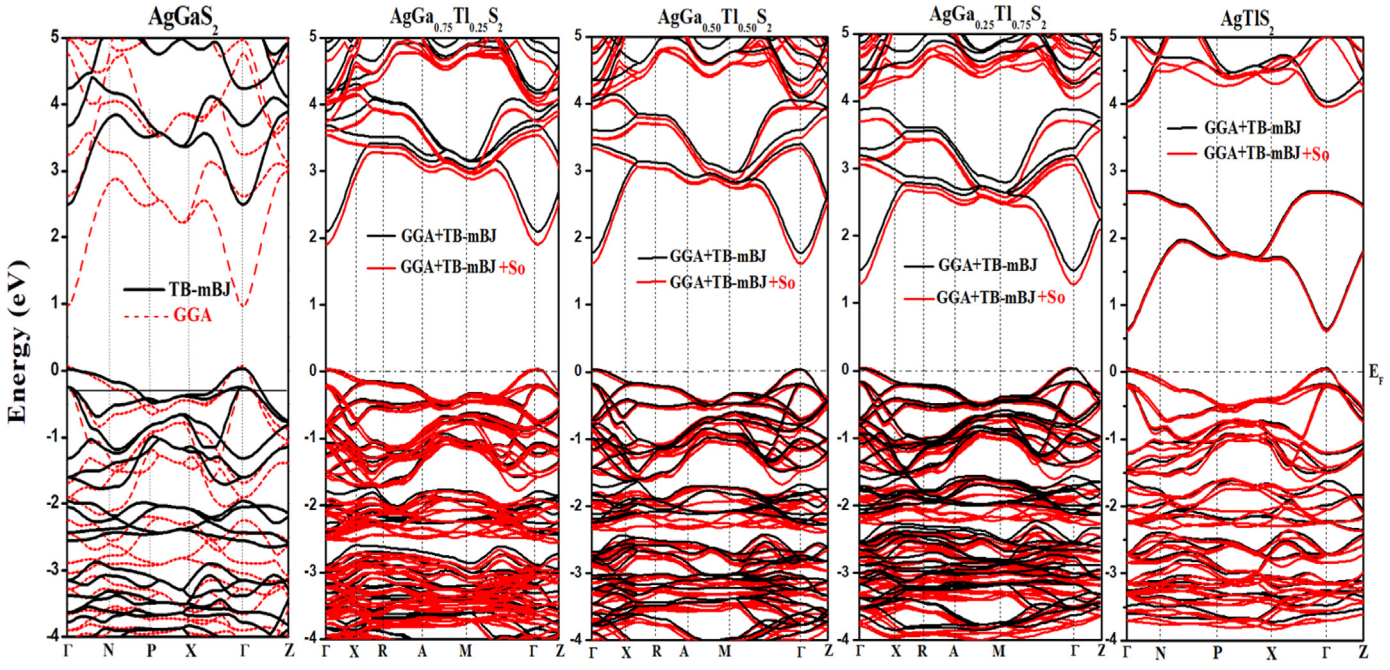

Fig. 2. The calculated band structure of $AgGa_{1-x}Tl_xS_2$ alloys.

Table 4
The calculated band gap values and the effective mass of electron and hole, m_e^*, m_h^*, elastic constant C_{ii} (Kbar), deformation potential constants E_{CBM} (eV) and E_{VBM} (eV), and carrier mobility μ ($\times 10^3$ cm^2 V^{-1} s^{-1}) of $AgGa_{1-x}Tl_xS_2$ alloys.

$AgGa_{1-x}Tl_xS_2$		*Eg*	m_e^*/m_0	m_h^*/m_0	C_{ii}	E_{CBM}	E_{VBM}	μ_e	μ_h
x = 0	This work	2.59	0.196	0.388	322.8	−3.5	−6.09	0.946	0.119
	Exp.	2.63 [23], 2.7 [21,24] 2.48 [22], 2.75 [22]	0.230	0.72	–	–	–	–	–
	Other calc.	2.4 [47]	0.137	0.383	–	–	–	–	–
x = 0.25	This work	1.91	0.115	0.331	681.59	−3.98	−5.88	2.06	0.181
x = 0.5	This work	1.61	0.110	0.296	721.3	−4.11	−5.72	2.45	0.264
x = 0.75	This work	1.28	0.107	0.283	831.3	−4.29	−5.57	2.93	0.379
x = 1	This work Other calc.	0.61 1.1 [43,53]	0.151	0.328	364.49	−4.48	−5.09	1.48	0.127

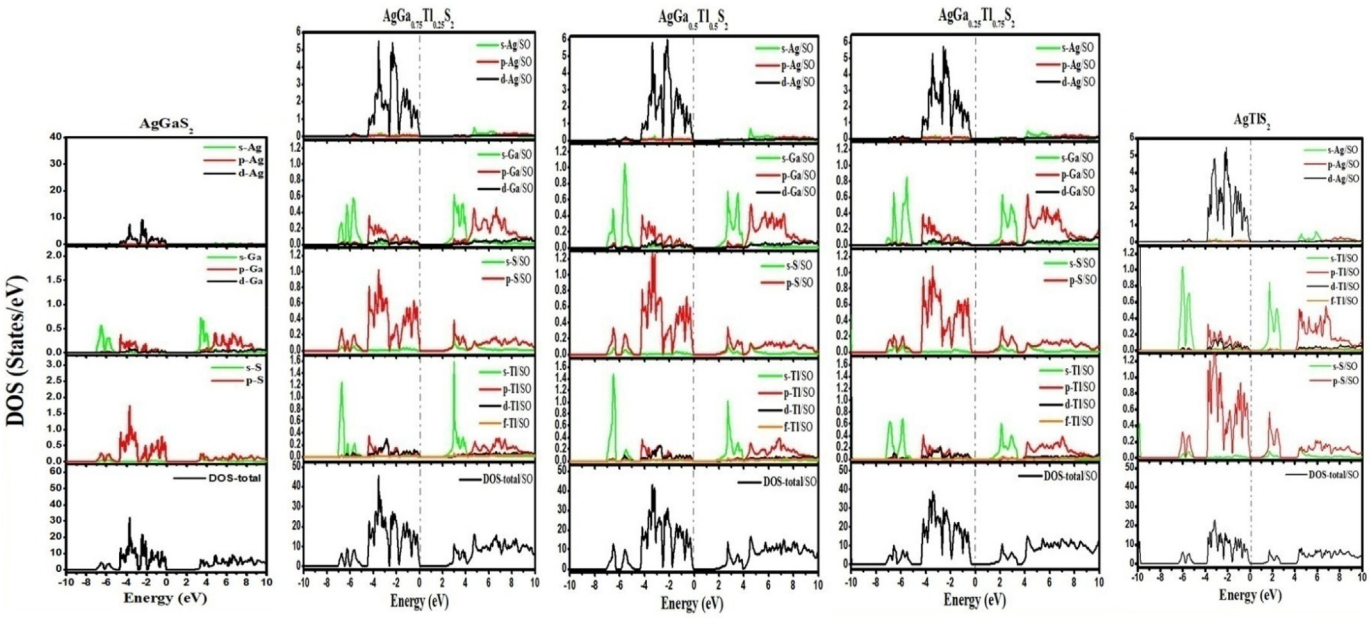

Fig. 3. Total and partial density of states (DOS) of $AgGa_{1-x}Tl_xS_2$ alloys.

$$E_f(AgGa_{1-x}Tl_xS_2) = 1/N\left(E_T(AgGa_{1-x}Tl_xS_2) - \left[E_{Ag} + (1-x)E_{Ga} + xE_{Tl} + 2E_S\right]\right) \quad (1)$$

where, E_T ($AgGa_{1-x}Tl_xS_2$) is the total energy and E_{Ag}, E_{Ga}, E_{Tl} and E_S are the energies of Ag, Ga, Tl and S atoms, respectively (see Table 3). From Table 1 it is remarked that the estimated E_f is negative suggesting thermodynamic stability of all $AgGa_{1-x}Tl_xS_2$ alloys. It is also noticed that the current calculated Ef of pure $AgGaS_2$ is in good agreement with that estimated by Kumar et al. [48].

3.2. Electronic properties

To give an exhaustive understanding of the electronic properties of $AgGa_{1-x}Tl_xS_2$ alloys, the band structure and both total and partial density of state are calculated. Fig. 2 shows the calculated band structure of $AgGaS_2$ and $AgGa_{1-x}Tl_xS_2$ alloys, respectively. This figure demonstrates clearly that both the top of the valence band (VB) and bottom of the conduction band (CB) are located at the same high symmetry point (Γ), without overlapping between them. Thus, $AgGaS_2$ is a semiconductor material with a direct band gap of about 0.96 eV with GGA-WC. This band gap value is significantly lower than the experimental measurement (see Table 4) which is due to the well-known shortcoming of the GGA approximation. Hence, the band structure is also estimated employing the WC-GGA + TB-mBJ where the band gap value found is equal to 2.59 eV, which agrees well with the experimental values [21–24]. Moreover, using WC-GGA + TB-mBJ, the band structure of $AgGa_{1-x}Tl_xS_2$ alloys is calculated Fig. 1. We remarked that when the Ga atom is substituted by the Tl atom the nature of the band gap and the semiconducting character is retained, however the minimum of the CB is shifted towards the Fermi level resulting in a reduction of the band gap value to be 2.17 eV, 1.84 eV, 1.53 eV, 0.65 eV for $AgGa_{0.75}Tl_{0.25}S_2$, $AgGa_{0.5}Tl_{0.5}S_2$, $AgGa_{0.25}Tl_{0.75}S_2$, and $AgTlS_2$, respectively. This behavior is mainly coming from the increase of the atomic size from Ga to Tl atom. In addition, due to the presence of the heavy atom (Tl) the spin-orbit coupling (SOC) is included Fig. 2. It is well observed that SOC influences the band structures causing reduction of the energy band gap to be 1.91 eV, 1.61 eV, 1.28 eV, and 0.61 eV for $AgGa_{0.75}Tl_{0.25}S_2$, $AgGa_{0.5}Tl_{0.5}S_2$, $AgGa_{0.25}Tl_{0.75}S_2$, and $AgTlS_2$, respectively. This spin-orbit coupling also increases the degeneracy of the bands near VBM in Γ-point. We note here that the band gap values of $AgGa_{0.75}Tl_{0.25}S_2$, $AgGa_{0.5}Tl_{0.5}S_2$, and $AgGa_{0.25}Tl_{0.75}S_2$ are quite similar to the established absorbent materials such as Cu_2ZnSnS_4 [49], GaAs [50], CdTe [51], and $CH_3NH_3PbI_3$ [52], which proving their promising candidates for photovoltaic (PV) applications.

The calculated density of states (DOS) of $AgGa_{1-x}Tl_xS_2$ alloys through the WC-GGA + TB-mBJ approximation for (x = 0) and including the SOC for (x = 0.25, 0.5, 0.75, and 1) are displayed in Fig. 3. From Fig. 3 one can remark that the valence band of $AgGaS_2$ is divided into two sub-bands. The first one is starting from the top (zero energy) to −5 eV labeled as VB1 and the second one from −5 eV to −8 eV labeled as VB2. The VB1 is mostly originated from the cation Ag '4*d*' states hybridized with S '3*p*' states suggesting covalent character for Ag–S bond. While in VB2 the bands are derived from a combination of Ga '4s' states and anion S '3p'

states. Whereas, the conduction band of $AgGaS_2$ mainly comes from Ga '4*s*, 4*p*' states hybridized with the anion S '3*p*' states, the bottom of the conduction band has a dominant contribution from Ga '4*s*' states. However, when Gallium is replaced by thallium, the valence band structure of $AgGa_{1-x}Tl_xS_2$ (x = 0.25, 0.5, 0.75, and 1) alloys remains unchanged except near the Fermi level where a small contribution of Tl 'd' state is observed. However, with increasing Tl content the S′3p′-Ag'4d′ hybridization state is pushed up towards higher energy to become between −3.8 eV and E_F level in the case of $AgTlS_2$ compound. Inversely the substitution of Tl atoms into Ga sites highly affects the conduction band. This Tl substitution leads to the formation of new states in the CB minimum, which mainly comes from the Tl '6s′ states. These Tl '6s′ states are hybridized with Ga '4s′ states for $AgGa_{1-x}Tl_xS_2$ (x = 0.25, 0.5, and 0.75) alloys and lowered the CBM and thus the band gap value is diminished. In contrast, for $AgTlS_2$ the CB minimum is derived from a combination of Tl '6s' states and anion S '3p' states. It is previously reported that the anion displacement affected the band gap value of the $AgGaX_2$ chalcopyrite [46]. Hence the band gap reduction can be explained by the increase of the atomic size from Ga to Tl and the decrease in the internal parameter *u* (see Table 1) as the Tl concentration increase.

3.3. Carrier effective mass and mobility

Using the calculated band structure we have calculated the effective mass of holes (m_h^*) from the maximum VB and the electrons effective mass (m_e^*) from the minimum CB for $AgGa_{1-x}Tl_xS_2$ alloys using the following Equation:

$$m^* = \hbar^2 \left(\frac{\partial^2 E}{\partial^2 k} \right)^{-1} \quad (2)$$

The results are summarized in Table 3. It is remarked that the electron effective mass is lower than the hole effective mass for pure $AgGaS_2$, which agrees reasonably with the previous finding [54,55]. Besides, as this mass is linked to the band gap and this later is tuning after Tl substitution, it is also expected that this mass will be affected. Therefore, we have also calculated both hole and electron effective mass of $AgGa_{1-x}Tl_xS_2$ alloys (Table 4). One can see that both hole and electron effective masses decrease when Ga is substituted by the Tl atom.

Relying on the deformation potential theory [56], the carrier mobility for this compound is determined using the following relation:

$$\mu = \frac{(8\pi)^{1/2} \hbar^4 e C_{ii}}{3(m^*)^{5/2} (k_B T)^{3/2} E_\alpha^2} \quad (3)$$

where $\hbar$, C_{ii}, e, m^*, k_B, T, E_α are respectively, the reduced Planck constant, elastic modulus, the element charge, effective mass (of a hole (m_h^*) or electron (m_e^*)), Boltzmann constant, temperature, and deformation potential constant of the CB minimum for electron or VB maximum for the hole [57]. The calculated electron and hole carrier mobility are listed in Table 4. We noticed that the electron carrier mobility of the pure $AgGaS_2$ is much larger than hole carrier mobility. After Ga substitution by Tl, both hole and electron carrier mobility increases with the increase of Tl concentration, where the increase is about 70% for electron and 66% for hole after 75% Tl substitution. This carrier mobility augmentation is principally owing to increased elastic constant and reduced carrier effective masses after doping. Besides, when Ga is replaced by Tl the carrier mobility is slightly reduced compared to the other concentration especially in the case of hole carrier mobility. It is noteworthy to say that the high mobility value is one of the most wanted properties for a superior photovoltaic response since it will help to separate efficiently the photo-generated carriers without giving way to recombination.

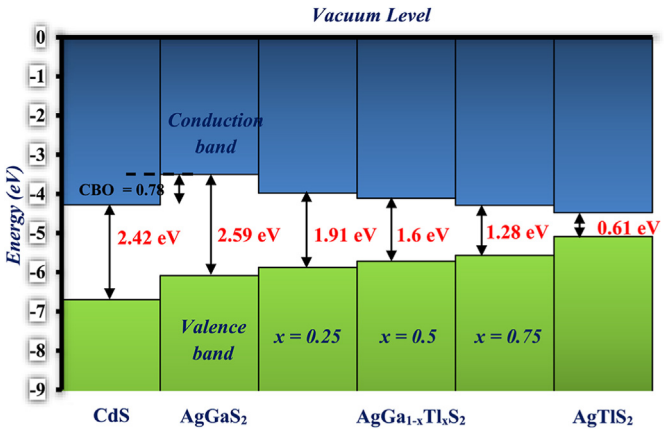

Fig. 4. Vacuum-aligned band diagram for $AgGa_{1-x}Tl_xS_2$ alloys compared with n-type window layer material CdS.

3.4. Band alignment

In the designing of a solar cell it is very important to consider the band edge position between the p-type absorber materials and the n-type window layer (p-n junction), because the electron charge carrier transport can be affected by the band misalignments from incompatible cell architecture design. Here we discuss the band alignments of $AgGa_{1-x}Tl_xS_2$/CdS heterojunction taking the CdS compounds as n-type window layer (Fig. 4). The positions of the conduction and valence bands (E_{CBM} and E_{VBM}) with respect to the vacuum level of $AgGa_{1-x}Tl_xS_2$ alloys are calculated using the method described in Ref. [58], however, those of CdS compound are taken from the literature [59].

From Fig. 4 it is observed that the $AgGaS_2$/CdS heterojunction forms a type-II band alignment, with the conduction band edge of $AgGaS_2$ positioning 0.78 higher than that of CdS compound. This conduction band offset (CBO) could be one of the reasons which reduce their PCE. Recently, using $AgGaS_2$ as p-type absorber materials and CdS as n-type window layer the $AgGaS_2$/CdS solar cell shows an open circuit voltage V_{OC} = 0.60 V, short circuit courant J_{SC} = 7.5 mA cm^{-2}, and a PCE of about 5.85% [27]. On the other hand, the valence band offset (VBO) is about 0.61 eV. When Tl is substituted into Ga site of $AgGaS_2$ the CBO is decreased to be 0.3 eV, and 0.17 eV, for $AgGa_{0.75}Tl_{0.25}S_2$, and $AgGa_{0.5}Tl_{0.5}S_2$, respectively Fig. 4. Conversely, for x = 0.75 and 1, the $AgGa_{1-x}Tl_xS_2$/CdS heterojunction forms a type-I band alignment, with the conduction band edge of $AgGa_{0.25}Tl_{0.75}S_2$ and $AgTlS_2$ positioning 0.01 and 0.2 lower than that of CdS compound, respectively. This decrease in CBO is resulting from the downshift of the conduction band edge which also leads to a reduction of the band gap value and then to the VBO enlargement. Consequently, one can conclude that the band gap and the band alignment of the $AgGa_{1-x}Tl_xS_2$/CdS heterojunction can be tuned by controlling Tl content.

3.5. Optical properties

The optical properties such as complex dielectric function, refractive index, reflectivity, and absorption coefficient play a crucial role in designing good PV materials. In the current study, the optical properties of $AgGa_{1-x}Tl_xS_2$ alloys were estimated using WC-GGA + TB-mBJ approximation for (x = 0) and including the SOC for (x = 0.25, 0.5, 0.75, and 1) for incident radiation along the main crystallographic direction "*xx*" and "*zz*". Fig. 5 illustrate the real ε_2 (ω) and imaginary ε_1 (ω) part of complex dielectric function for $AgGa_{1-x}Tl_xS_2$ materials.

We remarked that both imaginary ε_1 (ω) and real ε_2 (ω) spectra

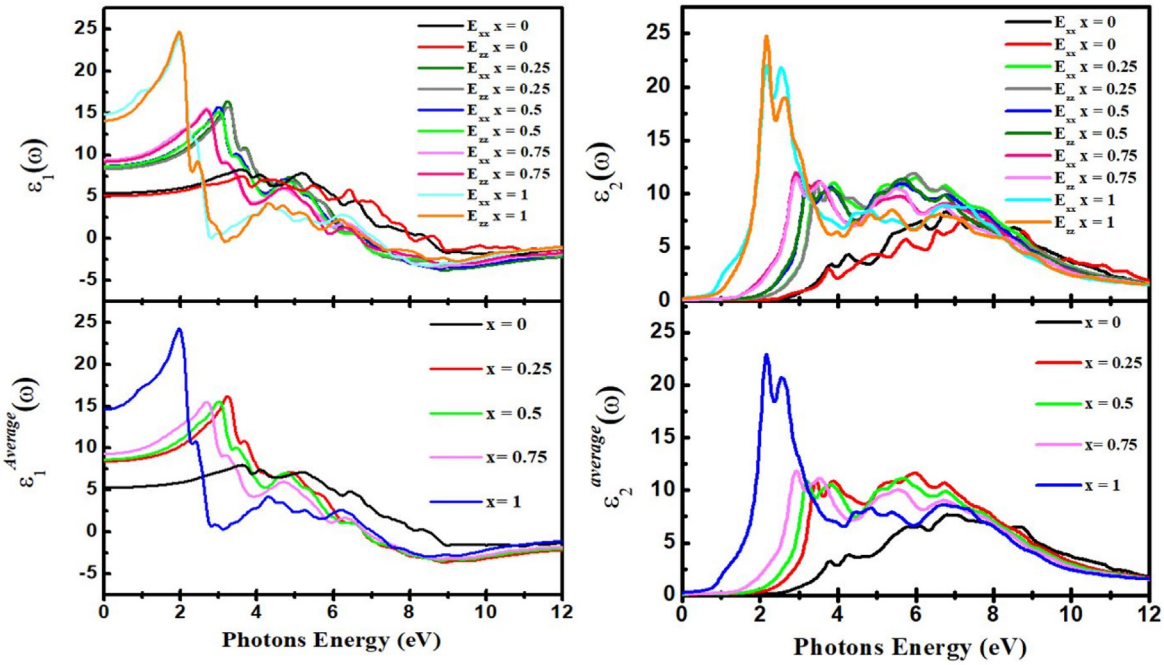

Fig. 5. The imaginary ε_1 (ω) (left panel) and real ε_2 (ω) (right panel) part spectra of complex dielectric function for $AgGa_{1-x}Tl_xS_2$ materials.

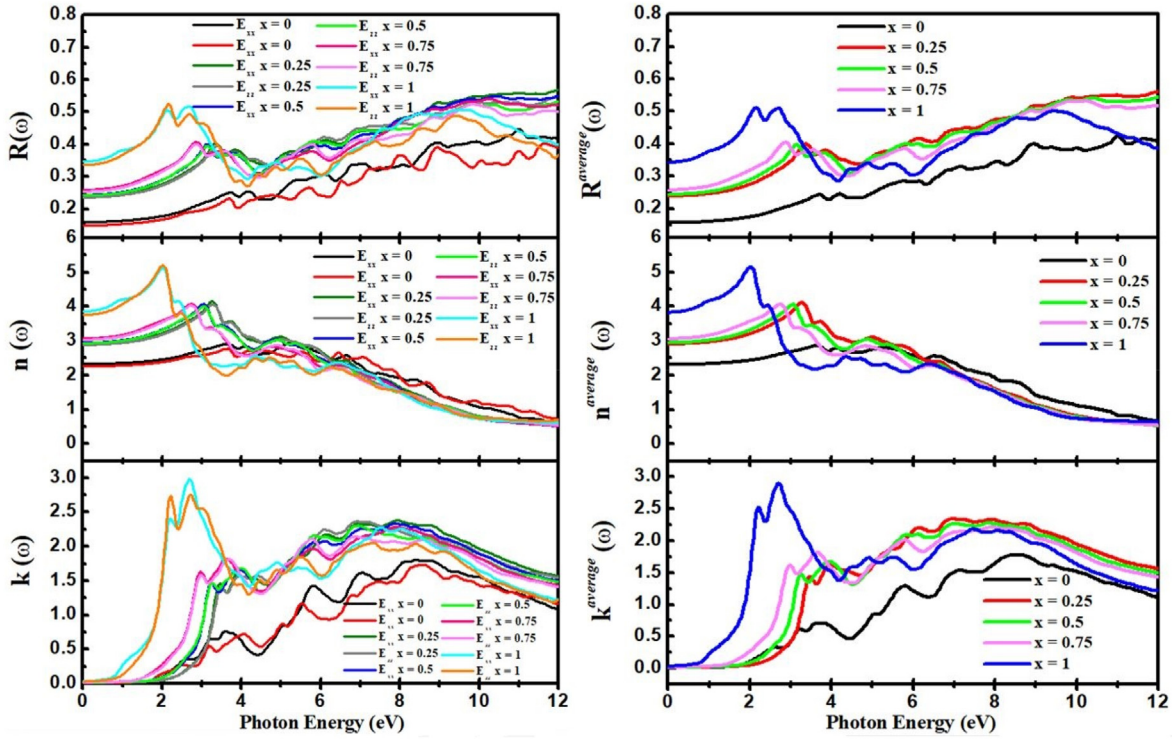

Fig. 6. The calculated refractive index *n* (ω), extinction coefficient *k* (ω), and reflectivity coefficient *R* (ω) of $AgGa_{1-x}Tl_xS_2$ alloys along *xx* and *zz*-direction (left panel), average (right panel).

display strong anisotropy for all alloys. As shown in Fig. 5, the ε_1 (ω) spectra of pure $AgGaS_2$ reveal the main peak around 3.6 eV which is shifted towards lower energy in the other four alloys due to the Tl atom substitution. Besides, the average static dielectric value $\varepsilon_1^{average}$ (0) is increased from 5.14 for $AgGaS_2$ pure to 9.34 for $AgGa_{0.25}Tl_{0.75}S_2$ alloy, and 14.62 for $AgTlS_2$ which is consistent with the decrease of the band gap value (Table 3). On the other hand, as can be seen from Fig. 5, doping $AgGaS_2$ by 25% Tl leads to appearing of new peaks in the visible region. These new peaks are resulting from the photon absorption provoked by the direct interband transition from the occupied VB to the Tl 's' states in the MCB. Interestingly, these novel peaks are red-shifted along with the increased Tl concentrations from 3.42 eV for $AgGa_{0.75}Tl_{0.25}S_2$ to 2.12 eV for $AgTlS_2$ compound.

Furthermore, using the real and imaginary part of the complex dielectric function, we have estimated the refractive index *n* (ω), extinction coefficient *k* (ω), reflectivity coefficient *R* (ω) and the

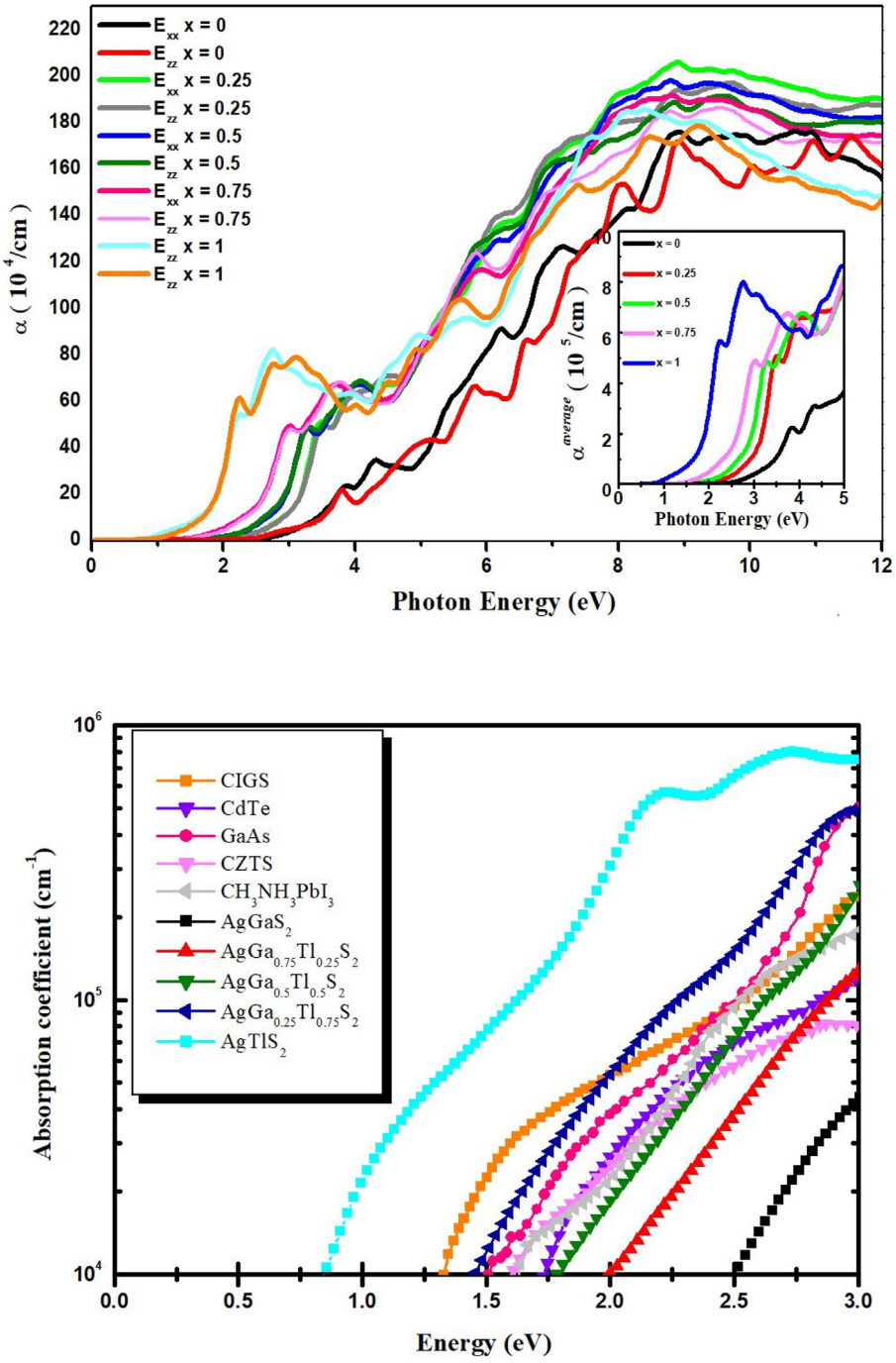

Fig. 7. The calculated absorption coefficient α (ω) of $AgGa_{1-x}Tl_xS_2$ alloys (top panel) compared with other materials (bottom panel) such as CdTe [61], GaAs [62], CIGS [63], CZTS [64], $CH_3NH_3PbI_3$ [65].

absorption coefficient α (ω) of $AgGa_{1-x}Tl_xS_2$ alloys shown in Fig. 6. As follows from Fig. 6, the average reflection $R^{average}$ at E = 0 eV are around 15.5%, 23.8%, 24.2%, 25.6%, and 34.2% for 0, 25%, 50%, 75% and 100% of Tl concentration, respectively. The R (ω) spectra show a maximum in the ultraviolet (UV) region which is enhanced with the increased Tl concentration. The dependence of the real and imaginary parts (n (ω), k (ω)) of the complex refractive index $\tilde{n}$ (ω) = n (ω) + i k (ω) along xx, and zz direction are given in Fig. 6. The average value of the static refractive index $n(0)$ of pure $AgGaS_2$ is 2.25 which is in reasonable agreement with the measured one (2.405) [60]. This value is augmented to be 2.9, 2.94, 3.05, and 3.82 for $AgGa_{0.75}Tl_{0.25}S_2$, $AgGa_{0.5}Tl_{0.5}S_2$, $AgGa_{0.25}Tl_{0.75}S_2$, and $AgTlS_2$, respectively. Apparently, the n (ω) spectrum records a maximum value in the visible light region for 25%, 50%, 75% and 100% of Tl concentration whereas this maximum is observed in the UV region for pure $AgGaS_2$. Besides, the value of extinction coefficient k (ω) is zero up to 2.6 eV for $AgGaS_2$ which means it will not attenuate most of the incident visible light. However, a new peak comes in to view when the Ga atom is replaced by the 75% Tl atom improving the optical response of $AgGaS_2$ Fig. 6.

Consider Fig. 7 (top panel), which plots the absorption coefficient α (ω) against the photon energy of $AgGa_{1-x}Tl_xS_2$ alloys; it is obviously observed that the Tl substitution strongly enhances the absorption coefficient in the visible region. The α (ω) value is about 0.4×10^5 cm^{-1} for $AgGaS_2$ and is augmented to be 4.8×10^5 cm^{-1} for $AgGa_{0.25}Tl_{0.75}S_2$.

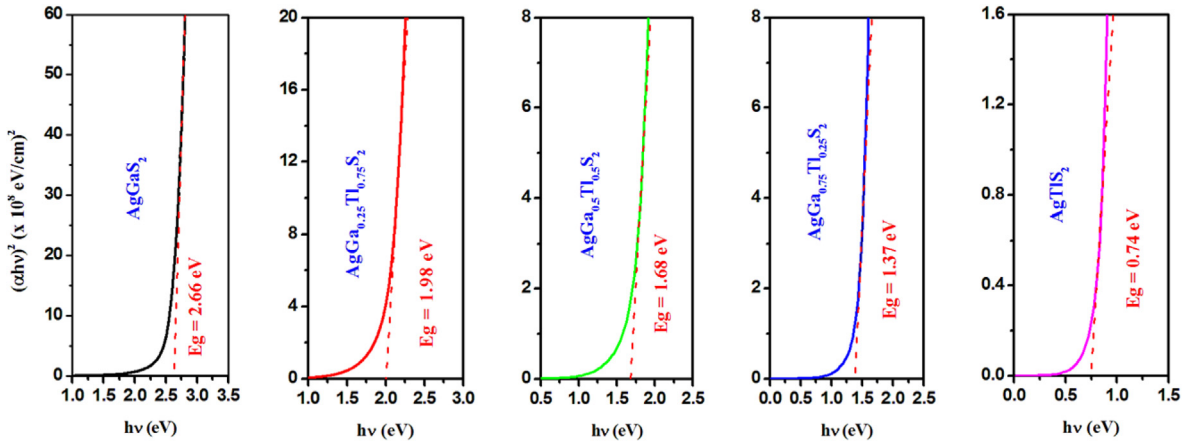

Fig. 8. Optical band gap of $AgGa_{1-x}Tl_xS_2$ alloys.

Suggesting that this alloy would display high absorption of sunlight in the visible region, and behave as ideal solar absorber. In addition, the square of absorption versus photon energy is plotted (i.e., $(\alpha h\nu)^2$ versus $h\nu$) for $AgGa_{1-x}Tl_xS_2$ alloys in Fig. 8. Using a linear fitting a direct optical band gap is estimated to be 2.66 eV, 1.98 eV, 1.68 eV, 1.37 eV, and 0.74 eV for $AgGaS_2$, $AgGa_{0.75}Tl_{0.25}S_2$, $AgGa_{0.5}Tl_{0.5}S_2$, $AgGa_{0.25}Tl_{0.75}S_2$, and $AgTlS_2$, respectively. Evaluating the obtained results of α for $AgGa_{1-x}Tl_xS_2$ alloys with other experimental results for established absorber materials such as GICS, CZTS, GaAs, CdTe, and $CH_3NH_3PbI_3$ Fig. 7 (bottom panel), we observed that the absorption coefficient of $AgGa_{0.5}Tl_{0.5}S_2$ is comparable to that of CdTe and CZTS, whereas the $AgGa_{0.25}Tl_{0.57}S_2$ shows a good absorption coefficient as GaAs and CIGS compound. Consequently, $AgGa_{1-x}Tl_xS_2$ alloys could be considered as potential materials for photovoltaic and solar cells utilization.

4. Conclusion

In the present study, the impact of the thallium substitution effect on tuning the band gap energy and optical properties of $AgGaS_2$ chalcopyrite was investigated. The current DFT calculation reveals that when the gallium is replaced by the thallium, the minimum of the CB is shifted towards the Fermi level, resulting reduction of band gap from 2.59 eV for $AgGaS_2$ pure to 1.91 eV, 1.61 eV, and 1.28 eV for $AgGa_{0.75}Tl_{0.25}S_2$, $AgGa_{0.5}Tl_{0.5}S_2$, and $AgGa_{0.25}Tl_{0.75}S_2$, respectively. Besides, it is observed that both hole and electron effective masse decrease with the increase of Tl concentration, and thus both hole and electron carrier mobility is increased. Analysis of the band alignments of $AgGa_{1-x}Tl_xS_2$/CdS heterojunction reveals that when Tl is incorporated into $AgGaS_2$, the conduction band offset is decreased, and thus the open-circuit voltage can be improved. From the optical properties calculations, it is established that Tl substitution enhances the optical properties of $AgGaS_2$ by reducing the transparent region and improving the refractive index and the absorption in the visible light region. Consequently, the semiconducting nature with the appropriate direct band gap values and strong absorption ($\alpha > 10^5$ cm^{-1}) of the new $AgGa_xTl_{1-x}S_2$ alloys in the visible light region make them promising candidates for optoelectronic and photovoltaic applications, especially in solar cells.

CRediT authorship contribution statement

R. Mouacher: Conceptualization, Investigation, Methodology, Data curation, Formal analysis, Software, Writing – original draft. **T. Seddik:** Conceptualization, Supervision, Investigation, Validation, Writing – original draft, Writing – review & editing. **B. Rezini:** Investigation, Methodology, Software, Validation, Visualization, Funding acquisition. **Bakhtiar Ul Haq:** Conceptualization, Investigation, Validation, Writing – review & editing. **M. Batouche:** Methodology, Software, Validation. **G. Uğur:** Conceptualization, Investigation, Validation, Writing – review & editing. **S. Uğur:** Conceptualization, Investigation, Validation. **A. Belfedal:** Conceptualization, Supervision, Investigation, Validation.

Declaration of competing interest

The authors declare that they have no known competing financial interests or personal relationships that could have appeared to influence the work reported in this paper.

Acknowledgment

The authors T. Seddik, B. Rezini, and M. Batouche acknowledge support from the Algerian National Research project P.R.F.U under number B00L02UN290120220001. The author (Bakhtiar Ul Haq) extends his appreciation to the Deanship of Scientific Research at King Khalid University for funding his work through the Research Groups Program under Grant No. R.G.P1/121/43.

Appendix A. Supplementary data

Supplementary data to this article can be found online at https://doi.org/10.1016/j.jssc.2022.122996.

References

[1] M.A. Green, K. Emery, Y. Hishikawa, W. Warta, Solar cell efficiency tables (version 36), Prog. Photovoltaics Res. Appl. 18 (2010) 346–352, https://doi.org/10.1002/pip.2404.
[2] M. Buffiere, Dattatray S. Dhawale, F. El-Mellouhi, Chalcogenide materials and derivatives for photovoltaic applications, Energy Technol. (2019) 1900819, https://doi.org/10.1002/ente.201900819.
[3] M. Faizan, S.H. Khan, H. Khachai, T. Seddik, S.B. Omran, R. Khenata, J. Xie, M.M. Al-Anazy, Electronic, optical, and thermoelectric properties of perovskite variants A_2BX_6: insight and design via first-principles calculations, Int. J. Energy Res. 45 (3) (2021) 4495–4507.
[4] A.N. Usoltsev, S.A. Adonin, A.S. Novikov, D.G. Samsonenko, M.N. Sokolova, V.P. Fedin, One-dimensional polymeric polybromotellurates (IV): structural and theoretical insights into halogen···halogen contacts, CrystEngComm (2017), https://doi.org/10.1039/C7CE01487B.
[5] S.A. Adonin, M.A. Bondarenko, P.A. Abramov, A.S. Novikov, P.E. Plyusnin, M.N. Sokolov, V.P. Fedin, Bromo- and polybromoantimonates(V): structural and theoretical studies of hybrid halogen-rich halometalate frameworks, Chem. Eur. J. 24 (2018) 10165, https://doi.org/10.1002/chem.201801338.
[6] S.A. Adonin, I.D. Gorokh, A.S. Novikov, D.G. Samsonenko, P.E. Plyusnin, M.N. Sokolov, V.P. Fedin, Bromine-rich complexes of bismuth: experimental and theoretical studies, Dalton Trans. 47 (2018) 2683–2689, https://doi.org/10.1039/C7DT04779G.
[7] S.F. Chichibu, T. Ohmori, N. Shibata, T. Koyama, T. Onuma, Greenish-white electroluminescence from p-type $CuGaS_2$ heterojunction diodes using n-type ZnO as an electron injector, Appl. Phys. Lett. 85 (2004) 4403, https://doi.org/10.1063/1.1818333.
[8] S. Ishizuka, A. Yamada, P.J. Fons, H. Shibata, S. Niki, Structural tuning of wide-gap chalcopyrite $CuGaSe_2$ thin films and highly efficient solar cells: differences from

narrow-gap Cu(In,Ga)Se_2, Prog. Photovolt. 22 (2014) 821–829, https://doi.org/10.1002/pip.2464.
[9] J.S. Jang, P.H. Borse, J.S. Lee, S.H. Choi, H.G. Kim, Indium induced band gap tailoring in $AgGa_{1-x}In_xS_2$ chalcopyrite structure for visible light photocatalysis, Chem. Phys. 128 (2008) 154717, https://doi.org/10.1063/1.2900984.
[10] D. Lincota, J.F. Guillemolesa, S. Tauniera, D. Guimarda, J. Sicx-Kurdia, A. Chaumonta, O. Roussela, O. Ramdania, C. Huberta, J.P. Fauvarquea, N. Bodereaua, L. Parissia, P. Panheleuxa, P. Fanouillerea, N. Naghavia, P.P. Granda, M. Benfaraha, P. Mogensenb, O. Kerreca, Chalcopyrite Thin Film Solar Cells by Electro-Deposition Solar Energy, vol. 77, 2004, pp. 725–737, https://doi.org/10.4313/JKEM.2010.23.11.911, 6.
[11] T. Plirdpring, K. Kurosaki, A. Kosuga, T. Day, S. Firdosy, V. Ravi, G.T. Snyder, A. Harnwunggmoung, A. Sugahara, Y. O-hishi, H. Muta, S. Yamanaka, Chalcopyrite $CuGaTe_2$: a high-Efficiency bulk thermoelectric material, Adv. Mater. 24 (2012) 3622.
[12] P.C. Ricci, A. Anedda, R. Corpino, C.M. Carbonaro, M. Marceddu, I.M. Tiginyanu, V.V. Ursaki, Temperature dependence of the photoluminescence spectra in $AgGaS_2$, J. Phys. Chem. Solid. 66 (2005) 1950–1953, https://doi.org/10.1016/j.jpcs.2005.09.034.
[13] M.V. Yakushev, R.W. Martin, Semiconductor spectroscopy and devices. https://ssd.phys.strath.ac.uk/research-areas/chalcopyrites-for-solar-cells/, 2020.
[14] J.A.M. Abu Shama, S. Johnston, T. Moriarty, G. Teeter, K. Ramanathan, R. Noufi, Properties of ZnO/CdS/$CuInSe_2$ solar cells with improved performance, Prog. Photovolt. 12 (2004) 39–45, https://doi.org/10.1002/pip.537.
[15] P. Chirila, F. Reinhard, P. Pianezzi, A.R. Bloesch, C. Uhl, L. Fella, D. Kranz, C. Keller, H. Gretener, D. Hagendorfer, R. Jaeger, S. Erni, S. Nishiwaki, S. Buecheler, A.N. Tiwari, Potassium-induced surface modification of Cu(In,Ga)Se_2 thin films for high-efficiency solar cells, Nat. Mater. 12 (2013) 1107–1111, https://doi.org/10.1038/nmat3789.
[16] M.A. Contreras, J. Tuttle, A. Gabor, A. Tennant, K. Ramanathan, S. Asher, A. Franz, J. Keane, L. Wang, R. Noufi, High efficiency Cu(In,Ga)Se_2 based solar cells: processing of novel absorber structures, Sol. Energy Mater. Sol. Cells 119 (2013) 296.
[17] A. Jäger-Waldau, PV Status Report EUR 28817 EN, Publications Office of the European Union, Luxembourg, 2017, https://doi.org/10.2760/452611,JRC108105.
[18] P. Reinhard, F. Pianezzi, L. Kranz, S. Nishiwaki, A. Chirila, S. Buecheler, A.N. Tiwari, Flexible Cu(In,Ga)Se_2 solar cells with reduced absorber thickness, Prog. Photovoltaics Res. Appl. 23 (2015) 281, https://doi.org/10.1002/pip.2420.
[19] Solar Frontier, Achieves world record thin-film solar cell efficiency of 23.35%. https://www.solar-frontier.com/eng/news/2019/0117press.html, 2019.
[20] P.C. Ricci, A. Anedda, R. Corpino, C.M. Carbonaro, M. Marceddu, I.M. Tiginyanu, V.V. Ursaki, Temperature dependence of the photoluminescence spectra in $AgGaS_2$, J. Phys. Chem. Solid. 66 (2015) 1950–1953, https://doi.org/10.1016/j.jpcs.2005.09.034.
[21] H.C. Hsu, H. Chen, S.Y. Kuo, C.S. Chang, W.F. Hsieh, Effect of annealing on the structural and optical properties of $AgGaS_2$ thin films prepared by pulsed laser deposition, Thin Solid Films 419 (2002) 237–241.
[22] H. Karaagac, M. Parlak, The investigation of structural, electrical, and optical properties of thermal evaporated $AgGaS_2$ thin films, Thin Solid Films 519 (2011) 2055–2061, https://doi.org/10.1016/j.tsf.2010.10.027.
[23] J.L. Shay, J.H. Wernick, Ternary Chalcopyrite Semiconductors: Growth, Electronic Properties, and Applications, Pergamon Press, Oxford; New York, 1975.
[24] H. Xiao, J. Tahir-Kheli, W.A. Goddard, Accurate band gaps for semiconductors from density functional theory, Phys. Chem. Lett. 2 (2011) 212–217, https://doi.org/10.1021/jz101565j.
[25] J.J. Zondy, D. Touahri, O. Acef, Absolute value of the d36 nonlinear coefficient of $AgGaS_2$: prospect for a low-threshold doubly resonant oscillator-based 3:1 frequency divider, J. Opt. Soc. Am. B 14 (10) (1997) 2481–2497, https://doi.org/10.1364/JOSAB.14.002481.
[26] M.M. Asadov, S.N. Mustafaeva, Xray dosimetry of an AgGaS2 single crystal, Bull. Russ. Acad. Sci. Phys. 79 (9) (2015) 1113–1117, https://doi.org/10.3103/S106287381509004X.
[27] M. Thirumoorthy, K. Ramesh, Materials Today: Proceedings, (2021) Characteristics of pulse electrodeposited AgGaS2 thin films for photovoltaic application https://doi.org/10.1016/j.matpr.2021.03.410.
[28] N. Karunagaran, P. Ramasamy, Investigation on synthesis, growth, structure and physical properties of $AgGa_{0.5}In_{0.5}S_2$ single crystals for Mid-IR application, J. Cryst. Growth 483 (2018) 169–174, https://doi.org/10.1016/j.jcrysgro.2017.11.030.
[29] M. Purohit, S.K. Meena, A. Dashora, B.L. Ahuja, Bandgap engineering of AgGaS2 for optoelectronic devices: first-principles computational technique, Intellig. Comput. Techniq. Smart Energy Syst. (2020) 67–74, https://doi.org/10.1007/978-981-15-0214-9_9.
[30] L.C. Tang, M.H. Lee, C.H. Yang, J.Y. Huang, C.S. Chang, Cation substitution effects on structural, electronic and optical properties of nonlinear optical $AgGa(S_xSe_{1-x})_2$ crystals, J. Phys. Condens. Matter 15 (2003) 6043–6055, 10.1088/0953-8984/15/35/312.
[31] G.K.H. Madsen, P. Blaha, K. Schwarz, E. Sjöstedt, L. Nordström, Efficient linearization of the augmented plane-wave method, Phys. Rev. B 64 (2001) 195134, https://doi.org/10.1103/PhysRevB.64.195134.
[32] K. Schwarz, P. Blaha, G.K.H. Madsen, Electronic structure calculations of solids using the WIEN2k package for material sciences, Comput. Phys. Commun. 147 (2002) 71, https://doi.org/10.1016/S0010-4655(02)00206-0.
[33] P. Blaha, K. Schwarz, F. Tran, R. Laskowski, G.K.H. Madsen, L.D. Marks, WIEN2k: an APW+lo program for calculating the properties of solids, J. Chem. Phys. 152 (2020), 074101, https://doi.org/10.1063/1.5143061.
[34] Z. Wu, R.E. Cohen, More accurate generalized gradient approximation for solids, Phys. Rev. B 73 (2006) 235116, https://doi.org/10.1103/PhysRevB.73.235116.
[35] D. Koller, F. Tran, F. Blaha, Merits and limits of the modified Becke-Johnson exchange potential, Phys. Rev. B 83 (2011) 195134, https://doi.org/10.1103/PhysRevB.83.195134.
[36] F. Tran, F. Blaha, Accurate band gaps of semiconductors and insulators with a semilocal exchange-correlation potential, Phys. Rev. Lett. 102 (2009) 226401, https://doi.org/10.1103/PhysRevLett.102.226401.
[37] K. Momma, F. Izumi, VESTA 3 for three-dimensional visualization of crystal, volumetric and morphology data, J. Appl. Crystallogr. 44 (2011) 1272–1276.
[38] T. Sakuntala, A.K. Arora, Pressure-tuned resonance Raman scattering in $AgGaSe_2$, Phys. Rev. B 53 (1996) 15667, https://doi.org/10.1103/PhysRevB.53.15667.
[39] F.D. Murnaghan, The compressibility of media under extreme pressures, Proc. Natl. Acad. Sci. U.S.A. 30 (1944) 244, https://doi.org/10.1073/pnas.30.9.244.
[40] H. Neumann, Bulk modulus-volume relationship in ternary chalcopyrite compounds, Phys. Status Solidi 96 (1986) K121, https://doi.org/10.1002/pssa.2210960245.
[41] T. Tinoco, A. Polian, J.P. Itie, E. Moya, J. Gonzales, Equation of state and phase transitions in $AgGaS_2$ and $AgGaSe_2$, J. Phys. Chem. Solid. 56 (1995) 481–484, https://doi.org/10.1016/0022-3697(94)00239-8.
[42] A. Chahed, O. Benhelal, S. Laksari, B. Abbar, B. Bouhafs, N. Amrane, First-principles calculations of the structural, electronic and optical properties of $AgGaS_2$ and $AgGaSe_2$, Physica B 367 (2005) 142–151, https://doi.org/10.1016/j.physb.2005.06.007.
[43] J.E. Jaffe, A. Zunger, Theory of the band-gap anomaly in ABC_2 chalcopyrite semiconductors, Phys. Rev. B 29 (1882) 1882, https://doi.org/10.1103/PhysRevB.29.1882.
[44] R. Asokamani, R.M. Amirthakumari, R. Rita, C. Ravi, Electronic structure calculations and physical properties of ABX_2 (A = Cu, Ag; B = Ga, In; X = S, Se, Te) Ternary Chalcopyrite Systems, Phys. Status Solidi B 213 (1999) 349, https://doi.org/10.1002/(SICI)1521-3951(199906)213:2<349::AID-PSSB349>3.0.CO;2-8.
[45] A.H. Reshak, Linear, nonlinear optical properties and birefringence of AgGaX2 (X=S, Se, Te) compounds, Phys. B Condens. Matter 369 (2005) 243–253, https://doi.org/10.1016/j.physb.2005.08.038.
[46] S. Chen, X.G. Gong, S.H. Wei, Band-structure anomalies of the chalcopyrite semiconductors $CuGaX_2$ versus $AgGaX_2$ (X=S and Se) and their alloys, Phys. Rev. B 75 (2007) 205–209, https://doi.org/10.1103/PhysRevB.75.205209.
[47] S. Ullah, H. Ud Din, G. Murtaza, T. Ouahrani, R. Khenata, Naeemullah, S. Bin Omran, Structural, electronic and optical properties of $AgXY_2$ (X = Al, Ga, In and Y = S, Se, Te), J. Alloys Compd. 617 (2014) 575–583, https://doi.org/10.1016/j.jallcom.2014.08.058.
[48] V. Kumar, B.S.R. Sastry, Heat of formation of ternary chalcopyrite semiconductors, J. Phys. Chem. Solid. 66 (2005) 99–102, https://doi.org/10.1016/j.jpcs.2004.08.034.
[49] S. Ahmed, K.B. Reuter, O. Gunawan, L. Guo, L.T. Romankiw, H. Deligianni, A high efficiency electrodeposited Cu_2ZnSnS_4 solar cell, Adv. Energy Mater. 2 (2012) 253, https://doi.org/10.1002/aenm.201100526.
[50] P. Kusch, S. Breuer, M. Ramsteiner, L. Geelhaar, H. Riechert, S. Reich, Band gap of wurtzite GaAs: a resonant Raman study, Phys. Rev. B 86 (2012), 075317, https://doi.org/10.1103/PhysRevB.86.075317.
[51] S. Lalitha, S.Z. Karazhanov, P. Ravindran, S. Senthilarasu, R. Sathyamoorthy, J. Janabergenov, Electronic structure, structural and optical properties of thermally evaporated CdTe thin films, Physica B 387 (2007) 227–238, https://doi.org/10.1016/j.physb.2006.04.008.
[52] B.A. Al-Asbahi, S.M.H. Qaid, M. Hezam, I. Bedja, H.M. Ghaithan, A.S. Aldwayyan, Effect of deposition method on the structural and optical properties of $CH_3NH_3PbI_3$ perovskite thin films, Opt. Mater. 103 (2020) 109836, https://doi.org/10.1016/j.optmat.2020.109836.
[53] Z. Zhaochun, P. Ruiwu, C. Nianyi, Artificial neural network prediction of the band gap and melting point of binary and ternary compound semiconductors, Mater. Sci. Eng. B 54 (1998) 149–152.
[54] T. Omata, K. Nose, S. Otsuka-Yao-Matsuo, Size dependent optical band gap of ternary I-III-VI_2 semiconductor nanocrystals, J. Appl. Phys. 105 (2009), 073106, https://doi.org/10.1063/1.3103768.
[55] C. Rincón, J. González, Acoustic deformation potentials in $A^IB^{III}C^{VI}_2$ chalcopyrite semiconductors, Phys. Rev. B 40 (1989) 8552, https://doi.org/10.1103/PhysRevB.40.8552.
[56] I. Chung, J.H. Song, J. Im, J. Androulakis, C.D. Malliakas, H. Li, A.J. Freeman, J.T. Kenney, M.G. Kanatzidis, $CsSnI_3$: semiconductor or metal? high electrical conductivity and strong near-infrared photoluminescence from a single material. High hole mobility and phase-transitions, J. Am. Chem. Soc. 134 (2012) 8579, https://doi.org/10.1021/ja301539s.
[57] S.H. Wei, A. Zunger, Predicted band-gap pressure coefficients of all diamond and zinc-blende semiconductors: chemical trends, Phys. Rev. B 60 (1998) 5404, https://doi.org/10.1103/PhysRevB.60.5404.
[58] M. Batouche, T. Seddik, V. Vu Tuan, D. Vo Dat, H.D. Tong, D.M. Hoat, O.Y. Khyzhun, Ternary sulfides $BaLa_2S_4$ and $CaLa_2S_4$ as promising photocatalytic water splitting and thermoelectric materials: first-principles DFT calculations, Int. J. Hydrogen Energy 45 (2020) 22600–22612, https://doi.org/10.1016/j.ijhydene.2019.06.124.
[59] T.J. Whittles, T.D. Veal, C.N. Savory, A.W. Welch, F.W.L. de Souza, J.T. Gibbon, M. Birkett, R.J. Potter, D.O. Scanlon, A. Zakutayev, V.R. Dhanak, Core levels, band alignments, and valence-band states in $CuSbS_2$ for solar cell applications, ACS Appl. Mater. Interfaces 9 (48) (2017) 41916–41926, https://doi.org/10.1021/acsami.7b14208.

[60] C. Gary, Catella, D. Burlage, Crystal growth and optical properties of $AgGaS_2$ and $AgGaSe_2$, MRS Bull. 23 (1998) 28–36, https://doi.org/10.1557/S0883769400029055.
[61] G.B. Dubrovskii, Optical properties of CdTe, Sov. Phys. Solid State 3 (1961) 1305.
[62] J.O. Akinlami, A.O. Ashamu, Optical properties of GaAs, J. Semiconduct. 34 (2013), 032002, https://doi.org/10.1088/1674-4926/34/3/032002.
[63] S. Minoura, K. Kodera, T. Maekawa, K. Miyazaki, S. Niki, H. Fujiwara, Dielectric function of Cu(In, Ga)Se_2-based polycrystalline materials, J. Appl. Phys. 113 (2013), 063505, https://doi.org/10.1063/1.4790174.
[64] J.S. Seol, S.Y. Lee, J.C. Lee, H.D. Nam, H.K. Kim, Electrical and optical properties of Cu_2ZnSnS_4 thin films prepared by rf magnetron sputtering process, Sol. Energy Mater. Sol. Cells 75 (2003) 155–162, https://doi.org/10.1016/S0927-0248(02)00127-7.
[65] X. Ziang, L. Shifeng, Q. Laixiang, P. Shuping, W. Wei, Y. Yu, Y. Li, C. Zhijian, W. Shufeng, D. Honglin, Y. Minghui, G.G. Qin, Refractive index and extinction coefficient of $CH_3NH_3PbI_3$ studied by spectroscopic ellipsometry, Opt. Mater. Express 5 (2015) 29–43, https://doi.org/10.1364/OME.5.000029.